INFORMATION TO USERS

The most advanced technology has been used to photograph and reproduce this manuscript from the microfilm master. UMI films the original text directly from the copy submitted. Thus, some dissertation copies are in typewriter face, while others may be from a computer printer.

In the unlikely event that the author did not send UMI a complete manuscript and there are missing pages, these will be noted. Also, if unauthorized copyrighted material had to be removed, a note will indicate the deletion.

Oversize materials (e.g., maps, drawings, charts) are reproduced by sectioning the original, beginning at the upper left-hand corner and continuing from left to right in equal sections with small overlaps. Each oversize page is available as one exposure on a standard 35 mm slide or as a 17″ × 23″ black and white photographic print for an additional charge.

Photographs included in the original manuscript have been reproduced xerographically in this copy. 35 mm slides or 6″ × 9″ black and white photographic prints are available for any photographs or illustrations appearing in this copy for an additional charge. Contact UMI directly to order.

Accessing the World's Information since 1938

300 North Zeeb Road, Ann Arbor, MI 48106-1346 USA

Order Number 8801777

Investigation of trans-1,4 polyisoprene crystals from solution: Morphologies and quantitative characterization

Xu, Jia-Rui, Ph.D.

City University of New York, 1987

U·M·I
300 N. Zeeb Rd.
Ann Arbor, MI 48106

PLEASE NOTE:

In all cases this material has been filmed in the best possible way from the available copy. Problems encountered with this document have been identified here with a check mark __✓__.

1. Glossy photographs or pages __✓__
2. Colored illustrations, paper or print _____
3. Photographs with dark background __✓__
4. Illustrations are poor copy _____
5. Pages with black marks, not original copy __✓__
6. Print shows through as there is text on both sides of page _____
7. Indistinct, broken or small print on several pages __✓__
8. Print exceeds margin requirements _____
9. Tightly bound copy with print lost in spine _____
10. Computer printout pages with indistinct print _____
11. Page(s) _____ lacking when material received, and not available from school or author.
12. Page(s) _____ seem to be missing in numbering only as text follows.
13. Two pages numbered _____. Text follows.
14. Curling and wrinkled pages _____
15. Dissertation contains pages with print at a slant, filmed as received _____
16. Other _____

_____

_____

INVESTIGATION OF TRANS-1,4 POLYISOPRENE CRYSTALS FROM SOLUTION: MORPHOLOGIES AND QUANTITATIVE CHARACTERIZATION

by

JIA-RUI XU

A dissertation submitted to the Graduate Faculty in Chemistry in partial fulfillment of the requirements for the degree of Doctor of Philosophy, The City University of New York

1987

This manuscript has been read and accepted for the Graduate Faculty in Chemistry in satisfaction of the dissertation requirement for the degree of Doctor of Philosophy.

9/17/87
date

Arthur E Woodward
Chairman of Examining Committee

9/17/87
date

A. M.
Executive Officer

Theodore Cuccuzzella

Supervisory Committee

The City University of New York

Abstract

INVESTIGATION OF TRANS-1,4 POLYISOPRENE CRYSTALS
FROM SOLUTION:
MORPHOLOGIES AND QUANTITATIVE CHARACTERIZATION

by

Jia-Rui Xu

Adviser: Professor Arthur E. Woodward

Trans-1,4 polyisoprene (TPI) structures in the α and β crystalline forms with various morphologies were prepared using different crystallization procedures. Optical microscopy and scanning electron microscopy were used to investigate these preparations after treatment in suspension with OsO_4. Changes in morphology with molecular weight, crystallization temperature and time were followed; curved lamellae, lamellar stacks and spherulites were found. Scanning electron microscopy revealed features, such as lamellar interpenetration and curvature, branching, and twisting, either not seen or not seen clearly with optical microscopy. The effects of molecular weight, crystallization temperature and annealing treatment on the length of the crystalline stem and the noncrystalline traverse for these TPI structures were quantitatively characterized using epoxidation followed by ^{13}C NMR analysis in solution. Preliminary studies were carried out to determine the optimum conditions for quantitative reaction of the double bonds at the lamellar surfaces. Results were obtained suggesting that for many liquids penetration of partially reacted lamellae can take place from the lateral surfaces; reac-

tant concentration and time were also shown to be important and conditions were found that gave agreement between the fraction reacted and the noncrystalline content from infrared and density measurements. An epoxidation mechanism based on the experimental results was proposed. The results of ^{13}C NMR analysis showed that the fold surfaces of these TPI lamellae were loose with an average fold length of 9 monomer units. For the multilamellar structures, interlamellar traverses were detected with the amount increasing with increasing molecular weight. The nature of chain folding in these structures and in the trans polydienes is discussed.

Acknowledgements

I would like to express, first of all, my sincere thanks to my mentor, Professor Arthur E. Woodward, in appreciation for his excellent guidance and valuable time throughout my graduate study; without his untiring direction and assistance this dissertation would not have been possible.

I would like to thank my supervising committee members, Professors Nan-Loh Yang and Theodore Axenrod, for their precious time and helpful suggestions and discussions.

I should also extend my acknowledgement to the Zhongshan University , Guangzhou, China for providing me the opportunity to pursue my further academic study.

My grateful thanks are due to my parents, Mr. and Mrs. Ying-guang Xu, and my parent-in-law, Mrs. Xian Cheng, and all of my family members for their continuous encouragement and supports.

Finally, I feel that it is hard to find words to properly express my indebtedness to my wife, Yafei, and my son, Yanming. Only with their love, understanding and willing supports during these years, can the completion of this dissertation be possible.

TABLE OF CONTENTS

	Page
Abstract	iii
List of Tables	viii
List of Figures	ix
1. Introduction	1
1.1 Morphologies of Polymer Crystallized from Solution	1
1.2 Organization of Semicrystalline Polymer Structures	6
1.3 Quantitative Characterization of Polymer Crystals	9
1.4 Objectives of This Study	14
2. Experimental	16
2.1 Samples	16
2.2 Fractionation	16
2.3 Molecular Weight Determination	18
2.4 Crystallization Techniques	18
2.5 DSC and X-ray Experiments	20
2.6 Crystallinity Measurements	20
2.7 Morphological Studies	22
2.8 Epoxidation	23
2.9 ^{13}C NMR Measurements	24
3. Results	28
3.1 Morphologies of TPI Crystals from solution	28
3.1.1 Single Crystals	28
3.1.2 Multilamellas	28

Page

3.2 Epoxidation of TPI Crystals in Suspension 67

3.2.1 Calculation of <A>, <B> and Fe from ^{13}C NMR Analysis 67

3.2.2 Effects of Reaction Medium, MCPBA Concentration and Reaction Time 68

3.2.3 Completion of the Epoxidation Reaction 74

3.3 Quantitative Characterization of the Amorphous and Crystalline Components in TPI Structures from Solution 78

4. Discussion 88

4.1 The Morphology 88

4.2 The Effects on Reaction and the Epoxidation Mechanism 93

4.3 Quantitative Investigations of Chain Folding and Crystalline Stem Length 98

5. Conclusions 113

6. Appendix 115

7. References 119

LIST OF TABLES

Table	Caption	Page
2.1	^{13}C NMR Assignments used for analysis of TPI and epoxidized TPI block copolymers	27
3.1	<A>, <B> and Fe of Epoxidized β-TPI lamellas at different [M]/[D] ratios	71
3.2	The heat of fusion of β-TPI and epoxidized-TPI at different reaction levels by DSC	73
3.3	<A>, <B> and Fe of TPI structures by ^{13}C NMR	80
3.4	Effects of annealing treatment and crystallization concentration on TPI structures	84
3.5	Fraction of noncrystalline portion of TPI structures by ^{13}C NMR, FTIR and density	85
3.6	Density of TPI lamellas for pressured and unpressured samples	87
4.1	Estimation of the average thickness of amorphous interlamellar layers	107
4.2	Fraction of noncrystalline TPI units in interlamellar traverses	109

LIST OF FIGURES

Figure	Caption	Page
2.1	Trans-1,4-polyisoprene fractionation scheme	17
2.2	A typical DSC curve of β-TPI lamellas	21
2.3	A typical ^{13}C NMR spectrum of surface epoxidized TPI sample	25
3.1	Transmission electron micrograph of TPI single crystals. (a) β-lamella crystallized (T_R =34°C) from 0.1% amyl acetate solution at 20°C; (b) α-lamella crystallized (T_R = 38°C) from 0.1% hexane solution at 25°C.	29
3.2	Interference contrast optical micrograph of TPI with $\bar{M}_v$=1.4×10^5 crystallized from 1% amyl acetate solution at 20°C, observed in suspension. (a) Before treated with OsO_4; (b) after treated with OsO_4.	30
3.3	Scanning electron micrograph of TPI with $\bar{M}_v$=1.4×10^5 crystallized from 1% amyl acetate solution at 20°C for 24 hours, (a) without treated with OsO_4; (b) treated in suspension with OsO_4.	31
3.4	Scanning electron micrograph of TPI with $\bar{M}_v$=1.4×10^5 crystallized from 1% amyl acetate solution at 20°C for 3 hours, treated in suspension with OsO_4.	35
3.5	Scanning electron micrograph of TPI with $\bar{M}_v$=1.4×10^5 crystallized from 1% amyl acetate solution at 20°C for 3 hours, treated in suspension with OsO_4.	36

Figure	Caption	Page
3.6	Same as Figure 3.5, but a higher magnification.	37
3.7	Scanning electron micrograph of TPI with $\bar{M}_v=1.4\times10^5$ crystallized from 1% amyl acetate solution at 20°C for 5 hours, treated in suspension with OsO_4.	38
3.8	Scanning electron micrograph of TPI with $\bar{M}_v=1.4\times10^5$ crystallized from 1% amyl acetate solution at 20°C for 24 hours, treated in suspension with OsO_4.	39
3.9	Same as Figure 3.8, but a different field.	40
3.10	Same as Figure 3.8, but a different field.	41
3.11	Scanning electron micrograph of TPI with $\bar{M}_v=1.4\times10^5$ crystallized from 1% amyl acetate solution at 20°C for 24 hours, ultrasonically vibrated for 3 minutes, treated with OsO_4.	42
3.12	Scanning electron micrograph of TPI with $\bar{M}_v=1.4\times10^5$ crystallized from 1% amyl acetate solution at 20°C for 24 hours, ultrasonically vibrated for 3 minutes, treated in suspension with OsO_4.	43
3.13	Scanning electron micrograph of TPI with $\bar{M}_v=1.4\times10^5$ crystallized from 1% amyl acetate solution at 20°C, etched by HNO_3 for 5 minutes, treated with OsO_4.	44
3.14	Scanning electron micrograph of TPI with $\bar{M}_v=2.6\times10^5$ crystallized from 1% amyl acetate solution at 20°C for 3 hours, treated in suspension with OsO_4.	45

Figure	Caption	Page
3.15	Scanning electron micrograph of TPI with $\bar{M}_v=2.6\times10^5$ crystallized from 1% amyl acetate solution at 20°C for 24 hours, treated in suspension with OsO_4.	46
3.16	Scanning electron micrograph of TPI with $\bar{M}_v=2.6\times10^5$ crystallized from 1% amyl acetate solution at 20°C for two days, treated in suspension with OsO_4, viewed from the sides of the ribbons.	47
3.17	Scanning electron micrograph of TPI with $\bar{M}_v=2.6\times10^5$ crystallized from 1% amyl acetate solution at 20°C for two days, treated in suspension with OsO_4, viewed from the ends of the ribbons.	48
3.18	Scanning electron micrograph of TPI with $\bar{M}_v=2.6\times10^5$ crystallized from 1% amyl acetate solution at 20°C for 24 hours, ultrasonically vibrated for 3 minutes, treated in suspension with OsO_4.	49
3.19	Scanning electron micrograph of TPI with $\bar{M}_v=2.6\times10^5$ crystallized from 1% amyl acetate solution at 20°C for 24 hours, ultrasonically vibrated for 3 minutes, treated in suspension with OsO_4.	50
3.20	Scanning electron micrograph of TPI with $\bar{M}_v=2.6\times10^5$ crystallized from 0.1% amyl acetate solution at 20°C for 2 days, treated with OsO_4.	51
3.21	Scanning electron micrograph of TPI with $\bar{M}_v=5.9\times10^5$ crystallized from 1% amyl acetate solution at 20°C for 3 hours, treated in suspension with OsO_4.	52

Figure	Caption	Page
3.22	Scanning electron micrograph of TPI with $\bar{M}_v=5.9\times10^5$ crystallized from 1% amyl acetate solution at 20°C for 3 hours, treated in suspension with OsO_4.	53
3.23	Scanning electron micrograph of TPI with $\bar{M}_v=5.9\times10^5$ crystallized from 1% amyl acetate solution at 20°C for 24 hours, treated in suspension with OsO_4, minor structures (30-40%).	54
3.24	Interference contrast optical micrograph of TPI with $\bar{M}_v=5.9\times10^5$ crystallized from 1% amyl acetate solution at 20°C for 24 hours. (a) Before treated with OsO_4, observed in suspension; (b) after treated in suspension with OsO_4.	55
3.25	Scanning electron micrograph of TPI with $\bar{M}_v=5.9\times10^5$ crystallized from 1% amyl acetate solution at 20°C for 24 hours, treated in suspension with OsO_4.	56
3.26	Scanning electron micrograph of TPI with $\bar{M}_v=2.6\times10^5$ crystallized from 1% amyl acetate solution at 25°C for 4 days, treated with OsO_4.	57
3.27	Same as Figure 3.26, but a higher magnification.	58
3.28	Scanning electron micrograph of unfractionated TPI crystallized from 1% amyl acetate solution at 30°C for 4 days, treated in suspension with OsO_4.	59

Figure	Caption	Page
3.29	Scanning electron micrograph of unfractionated crystallized from 1% amyl acetate solution at 30°C for 4 days, treated in suspension with OsO_4.	60
3.30	Scanning electron micrograph of TPI with $\bar{M}_v=2.6\times10^5$ precooling crystallized (T_R=31.7°C) from 1% amyl acetate solution at 30°C for 4 days, treated in suspension with OsO_4.	61
3.31	Scanning electron micrograph of TPI with $\bar{M}_v=2.6\times10^5$ precooling crystallized (T_R=31.7°C) from 1% amyl acetate solution at 30°C for 4 days, treated in suspension with OsO_4.	62
3.32	Same as Figure 3.31, but a higher magnification.	63
3.33	Scanning electron micrograph of TPI with $\bar{M}_v=2.6\times10^5$ crystallized from 1% amyl acetate solution at 0°C followed by annealing at 30°C, treated in suspension with OsO_4.	64
3.34	Scanning electron micrograph of balata crystallized from 1% amyl acetate solution at 0°C followed by annealing at 30°C, treated in suspension with OsO_4.	65
3.35	The sequences of block copolymer by epoxidation of TPI lamellas in suspension	67
3.36	Effects of reaction medium on epoxidation of TPI lamellas	70
3.37	Effects of MCPBA concentration on epoxidation of TPI lamellas	72

Figure	Caption	Page
3.38	Epoxidation of TPI lamellas at different reaction time	75
3.39	FTIR spectra of TPI lamellas before and after epoxidation	77
3.40	The unreacted block length <A> vsrsus molecular weight for single and multilamellar TPI structures	81
3.41	The reacted block length <B> versus molecular weight for single and multilamellar TPI structures	82
4.1	The mechanism of suspension medium effect on epoxidation	94
4.2	Epoxidation of TPI lamella assuming random chain reentry	97
4.3	Structure of β-form TPI crystal	101
4.4	Models of possible chain folding manner for TPI lamella	103
4.5	Epoxidation of TPI lamella assuming adjacent reentry with physically adsorbed molecules on the surface	104
4.6	Illustration of chain structures for TPI multilamellas	111

1. Introduction

1.1 Morphologies of Polymers Crystallized from Solution

It has been known for many years[1,2] that a large number of natural and synthetic polymers can form crystals. The studies on the morphology of crystalline polymers have been carried out by many researchers and are well summaried by the books of Geil[3] and Wunderlich[4] and by numerous shorter reviews[5–10].

Polymers exhibit various habits when they are crystallized from solution. The degrees of morphological complexity depend on the particular polymer and the crystallization conditions. The simplest structure which can be obtained from dilute solution is the single lamella which is a thin "chain-folded" platelet[11] of about 5-20 nm thick. The size, shape and regularity of these single lamellas vary with the nature of polymers and their growth conditions, and can be directly examined under a transmission electron microscope. A refinement in crystallization technique has been introduced by Keller et al[12,13], termed the "self-seeding method", to grow uniform sized single crystals of polyethylene from solution. One of the most important features of the self-seeded crystals is that any one lamella is approximately representative of the whole preparation, which should be very useful in the quantitative characterization of these structures.

The growth of polymer crystals is not restricted to lateral propagation. Thus the formation of overgrown crystals consisting of more than one superposed lamellas is also frequently observed in dilute solution crystallization at low supercoolings. A number of studies on po-

lyethylene[14–16], polyoxymethylene[15,17,18] and polyethylene oxide[15] showed that the lamellar overgrowth originated from screw dislocations situated at and/or close to the center of the basal lamella, or referred to as spiral growth. At sufficiently high supercoolings, in which new screw-dislocation-like defects are generated at the periphery of the developing crystals, growth of the crystals becomes more irregular and dendritic crystals develop[19–21].

More complex crystalline morphologies such as hedrites and spherulites can be observed when polymers are crystallized from more concentrated solution and/or higher supercooling[3,22]. When crystallized from the melt, on the other hand, polymers almost always form spherulites[7,23]. During the last three decades, much has been learned about the organization of these polymer structures and the nature of their early stages of growth. Polymer spherulites do not grow in a spherically symmetric fashion from the moment of inception. The development of a sheaflike precursor is commonly observed during the early stages of the spherulites growth[24]. Subsequent studies by Bassett et al. pointed out that these sheaflike precursors were multilayered, chain-folded structures akin to the hedrites which are formed when polymers are crystallized from concentrated solutions under certain conditions as well as from the melt at low supercooling.

The understanding of polymer spherulitic growth has been due in a large measure to the work of Keith and Padden[25–28] who interpretated the mechanism of the evolution of a single crystal through the hedrite transitional stage of development to the ultimate spherulite. According to these authors, a typical polymer is to be regarded as a multicomponent system, some components of which, principally molecules of low molecu-

lar weight and stereoirregular molecules, are rejected preferentially by the growing crystal at its lateral growth fronts. The early stages of spherulitic growth are that following the genesis of a monolayered single lamella, additional chain-folded lamellas develop thereupon through screw dislocations and the constituent layers in the resulting structures fan out progressively. To be reconciled with the radiating "fibrillar" feature of the spherulites, a distinct change in the lateral growth habit of the lamellas to the eventual fibrillar habit must occur during the course of the development of the spherulites. This change has been explained as being a consequence of the manifestation of "cellulation" at the periphery of the polygonal lamellas during the early stages of crystal growth. With the establishment of the fibrillar growth habit, the ultimate spherical symmetry of these aggregates are attributed to the significant divergences in orientation and the continued proliferation of fibrils via low-angle noncrystallographic branching.

Detailed studies on crystallization have been carried out using linear polyethylene[3,4,29–31]. The factors which influence the crystal morphology include the molecular weight and molecular weight distribution, the crystallization temperature, concentration of crystallization solution, the nature of the solvent, and the crystallization method. However, most of the studies of crystal morphologies, other than that for single lamellas, are of structures from melt crystallization. One reason for the lack of detailed morphological knowledge of polymer multilamellar structures grown from solution is that this has been limited by the microscopic techniques available. As is usually the case with optical microscopy, the magnification and contrast are low and therefore few details of the lamellar organization are visible. Direct examination under the transmis-

sion electron microscope (TEM) is limited to those objects grown from dilute solution, such as single lamellas, that are thin enough to absorb only a portion of the electron beam. For the complex lamellar structures, transmission of electrons through polymers causes radiation damage and severely limits direct study. Although fine structural information can be obtained from an examination of replicas[3,22,32,33] of the exterior of the thick objects and of etched surfaces[34, 35] of the sample, the replicating techniques are usually employed only to the samples crystallized from the melt. An alternative direct approach to observe these polymer structures is scanning electron microscopy (SEM). This technique again has been mainly limited to date to bulk crystallized samples since the structures grown from solution usually shrink upon drying. However, it is possible to study the morphologies of solution-grown structures of some polymer systems, such as trans-polydienes, by combining the techniques of SEM and sample fixing.

Trans-1,4 polyisoprene (TPI) is a readily crystallizable polymer. Two crystalline forms, monoclinic (α) and orthorhombic (β), have been reported for this polymer[36–38]. The morphologies described in great detail are that of single lamellas from dilute solution[39–42] and that of spherulites from the melt[43–46]. Recently, Kuo and Woodward[47] studied the effects of molecular weight and crystallization temperature on the morphology of TPI multilamellar structures from solution. In that work, TPI (gutta percha) fractions with $\bar{M}_n=4.7\times10^3$–2.5×10^5 were crystallized from solutions by cooling directly from 100°C to a crystallization temperature of -15 to +32°C, by precooling to 0°C, redissolving, and crystallizing at Tc, and by cooling to 0°C and slowly heating to 10, 20 or 30°C. The structures obtained by direct crystallization were α- and β-hedrites, α-

and β-spherulites, and β-aggregates of cup-shaped lamellas, depending on molecular weight, crystallization temperature and solvent. The precooling method yielded overgrown lamellas in most cases; but more complex morphologies developed when the thermal history was changed. These structures were characterized, while suspended in the crystallization liquid, by interference contrast microscopy and with crossed polaroids. A preparation of curved lamellar aggregates was reacted with OsO_4 prior to drying and viewed with a transmission electron microscope at much higher magnifications. Due to the overall thickness and complexity, hedrites and spherulites are difficult to investigate by transmission electron microscopy. However, the existence of the double bond in each TPI repeat unit would make it possible to preserve the organization of these structures by treating the sample with the fixative OsO_4 prior to drying. These structures can then be viewed under scanning electron microscopy to provide clear three dimensional observation on the solution-grown structures.

Studies of polymer crystalline morphology are important in both theory and practice. For instance, the discovery of the thin platelet-shaped single lamellas led to the modern view of "chain-folded" polymer crystallization[11,48,49]. Although the lamella-like crystallite has been well established as a major morphological element for polymers crystallized either in bulk or in dilute solution, the properties which result from the different crystallization modes are quite different. These differences arise not only because of variations in the lamellar thickness but also from other structural elements of which the crystal structures are built up. Therefore an adequate knowledge of polymer lamellar and larger-scale morphologies will lead to a better understanding of many properties of

semicrystalline polymers.

1.2 Organization of Semicrystalline Polymer Structures

The first indication of polymer crystallization with a folded macroconformation was published in 1938 by Storcks[50] who made 27 nm thick films of gutta percha (TPI) and obtained electron diffraction evidence to show that the macromolecules in the crystals were folded back. The modern concept of polymer crystallization finally resulted from the work of Keller[11] in 1957. On the basis of the formation of polyethylene single crystals from dilute solution and the properties of such crystals, Keller concluded that the molecules in the crystals are folded back and forth on themselves because the chain length is much larger than the lamellar thickness. The observation of polyethylene lamellas was made simultaneously by Fischer[48] and Till[49] supporting this conclusion. It is now generally recognized that chain-folded lamellas are the elementary feature of most, perhaps all, flexible chain crystallizable polymers[3,4]. In these lamellas, the chain axes are essentially perpendicular, or nearly so, to the two wide faces of the lamella, and the upper and lower surfaces consist of chain folds. It is also known that these lamellas contain an amorphous component as determined by such methods as density[51,52], broad-line NMR[53,54] and x-ray[55,56]. For single lamellas, some of the defects may exist within the lattice, but there is a general consensus of opinion that the noncrystalline component is mainly located along the crystal surfaces which include the chain folds and the noncrystallizing chain ends or cilia.

However, the manner of stem reentry is still a matter of considerable controversy in the field of polymer crystallization[57]. Two extremes have been suggested, namely the adjacent reentry model[58–60] and the random reentry, or switchboard, model[61,62]; the former requires an array of regularly folded chains with a very smooth surface, while the latter automatically implies large amounts of fold looseness. The existence of sectors as observed on nonplanar polyethylene single lamellas[12,17,63] is evidence for a distinct preference for folding along well-defined crystal faces. A direct approach to the adjacent reentry model was due to Krimm[64–66] who used infrared spectroscopy to analyze mixed crystals of deuterated polyethylene introduced as a guest component into the protonated host. In this way the environment of the isotopically labelled guest stems can be probed by examining splitting effects arising in appropriate infrared bands that rely on interactions between isotopewise (but not symmetrywise) identical segments in the crystal core of the lamellas. The experimental results provided clear evidence that on chain-folded crystallization adjacent reentry is favored. Other evidences for this model were derived from the results of neutron scattering[67–69] using a deuterated and protonated polyethylene mixture, and selective degradation of folded polyethylene crystals with fuming nitric acid[70,71]. The evidence favoring the switchboard model includes statistical treatment of chain folding[61,72,73], the results of small angle neutron scattering[74–76] and the characterization of the amorphous content[77].

In most crystalline polymer systems, the noncrystalline portion is irreconcilable with that predicted by the regularly folded model. For instance, a wide variety of properties of linear polyethylene crystals requires about 10-50% of the units to be in disordered or nonordered con-

formation[77,78]. Some modified approaches have been therefore suggested to account for the nature of chain folding; among those are: (1) a model of adjacent reentry with surface looseness as suggested by Keller et al.[79–81], (2) a model of adjacent reentry with a physically adsorbed noncrystalline layer on the lamellar surface as suggested by Hoffman et al.[82], and (3) a model of three phases with an interfacial zone present between the crystalline and amorphous phases as suggested by Mandelkern[77,83]. Since the amount of the noncrystalline component in crystalline polymers strongly depends on the crystallization conditions and the nature of individual polymer, it is fair to say at present time that a model of chain folding that is universally applicable for all crystalline polymer systems is not yet well established; or perhaps different systems require corresponding theoretical models.

The organization of more complex semicrystalline polymer structures, such as curved lamellar aggregates, hedrites and spherulites, have also been investigated for many years. It is generally accepted that these structures consist of chain folded lamellas. In the spherulites, the polymer chain axes in lamellas are more or less perpendicular to the radius of the spherulite. Besides the arguments of the nature of chain folding in the lamellas as discussed above, many investigations have been carried out on the way by which these lamellas were held together and the nature of the phase existing between the lamellas.

Based on the deformation behavior of polymer spherulites, it was suggested that the constituent lamellas were probably held together by chain molecules, termed "tie-molecules", which were partly embedded in one lamella and partly in another[84]. Evidence for the existence of these tie molecules was provided by Keith et al.[85–87]. Two-dimensional

spherulites of polyethylene were grown using the long-chain paraffin n-$C_{32}H_{66}$ as a diluent, upon dissolution of the dotriacontane, the intercrystalline links between the lateral edges of lamellas were visible under the electron microscope. The intercrystalline links were found to be crystalline with the c axes along their long dimension. The same observations were also obtained by Geil et al. on swollen samples of poly(4-methylpentene-1)[88,89]. This view thus provides a consistent basis for the explanation of the mechanical properties of the polymers, although it was questioned that the extended chain conformation of the intercrystalline links which are crystalline was energetically unfavorable[93]. On the other hand, the measurements of physical properties[90-92], such as density, heat of fusion and mobility by broad-line NMR, suggest that crystalline polymers have a considerable amount of amorphous component which should be located between lamellas.

On the basis of lamellar features revealed, the organization of multilamellas is thus believed to consist of a crystalline portion and an amorphous portion. The amorphous component is expected to include the fold surfaces, the noncrystallizing chain ends and tie molecules connecting the lamellas.

1.3 Quantitative Characterization of Polymer Crystals

Quantitative characterization of the crystalline and the amorphous portion in polymer crystals provides knowledges for understanding many important properties. Crystallinity is one of the most important parameters to characterize the relative crystalline and amorphous content

present in a semicrystalline polymer, and is directly related to many physical properties of such a system. Crystals formed by linear polyethylene have been most extensively studied. For dilute-solution-grown crystals, the crystalline thickness is independent of molecular weight except at very low molecular weights and depends only on the crystallization temperature for a given solvent[94–96]. Properties are found to be dependent only on the crystallite thickness and thus are also independent of molecular weight. In contrast, the properties of bulk-crystallized systems are highly dependent on molecular weight under comparable crystallization conditions. Since crystallization from concentrated solution almost always leads to crystal structures other than single lamellas, a study of properties over a wide molecular weight range would enable conclusions to be reached with respect to the molecular morphology.

However, many of the physical methods, such as density, x-ray diffraction, broad-line NMR and differential scanning calorimetry, used measure only the total noncrystalline content and therefore give little direct information concerning the location of this component, the average chain dimensions at the fold surfaces and the fraction and length of the interlamellar traverses. A number of chemical methods thus have been developed to study the amorphous surface portion of polymer crystals. Williams et al.[70] used fuming nitric acid to degrade the amorphous portion of polyethylene single crystals followed by measurements of the density, heat of fusion and molecular weight distribution of the fragments as a function of reaction time. The results obtained were interpreted in terms of a high degree of adjacent reentry. Keller and Priest[97,98] used a milder reagent, ozone, to degrade the same types of samples. The

peak distribution from gel permeation chromatography showed that the undegraded fragments contained molecular lengths of single, double and higher multiple-chain traverses of the crystal layer. The results were also interpreted in terms of adjacent reentry folds terminated via random chain scission by the ozone. However, the degradation method has little selectivity between amorphous and crystalline portions, making a quantitative study of the amorphous region difficult to carry out. Other chemical modification methods, such as substitution, elimination and addition reactions, for various polymer lamellas have been carried out by various authors as summaried in a review by Woodward[99].

A non-destructive chemical method involving epoxidation reactions on the lamellar surfaces of trans-1,4 polybutadiene (TPBD) and trans- 1,4 polyisoprene (TPI) has been developed by Woodward and coworkers[100–105]. The valuable features of this method are that (1) each of the repeat unit in the chains of TPBD and TPI has a double bond available for epoxidation, (2) the reactions of the epoxidation reagent, m-chloroperbenzoic acid (MCPBA), with the double bonds are found to be mild, quantitative but highly selective, and uncomplicated by side reactions and alternative routes, and (3) TPBD and TPI are readily crystallizable polymers; various crystal morphologies such as single lamellas as well as other lamellar structures can be grown by using different crystallization conditions and techniques.

The epoxidation reaction has been applied to suspensions of dilute-solution-grown crystals of TPBD[100,101,103,104] to evaluate the amorphous fraction of the lamellas. Evidence was given to suggest that the surface component consists of chain folds and chain ends or cilia, the latter becoming of greater importance at lower molecular weight. The number

of monomer units per fold and the number per chain end were obtained from an equation[104] that relates these two parameters to the crystal thickness, the fraction of double bonds at the crystal surfaces, the repeat distance along the polymer chain and the number average molecular weight, $\bar{M}_n$. In more recent work[106], the ^{13}C NMR technique has been employed to study these lamellas. Resonances for methylene carbons within diene sequences, within epoxidized sequences and at junctions between these sequences were identified and quantitatively determined. Since the selective reaction of the double bonds at the lamellar surfaces leads to a segmented block copolymer in which the reacted blocks correspond to the chain folds and chain ends, it is possible to obtain direct information about the average length of folds and crystalline stems by analyzing the sequences of the resulting copolymer. The value of monomer units per fold ranging from three to five were found.

Epoxidation reactions on trans-1,4 polyisoprene lamellas have also received some attention[41,47]. Some α-TPI crystals grown from dilute amyl acetate solution of naturally occurring TPI (balata and gutta percha) fractions were reacted in amyl acetate suspension with MCPBA to form an epoxide. The extent of double bonds reacted was determined by ^{1}H NMR. This quantity was then combined with the lamellar thickness from electron microscopy to calculate the number of monomer units per fold. The length of folds falls in the 6 to 10 monomer units range and increases with increasing $\bar{M}_n$ and Tc.

More recently, ^{13}C NMR analysis has been extended to investigate one sample of surface epoxidized α-TPI single lamellas[107]. The ^{13}C NMR spectra of the resultant copolymer were analyzed with the aid of TPI and squalene (the model compound) epoxidized in homogeneous solution to

several levels of reaction. Epoxidation of TPI lamellas in suspension produces an (AB)x block copolymer where A represents the olefinic units in the crystalline stem and B represents the oxirane units of the crystal surface folds. With the pertinent spectra assignments, a quantitative comparison of the A block and the B block with the AB junction yields a measure of the average length of the crystal stem and the folds, respectively. The TPI preparation examined in that study is found to have an average surface fold length of 7.4 monomer units and an average stem length of 4.9 nm. The results are in agreement with an earlier estimate[41] based on the lamellar thickness given by TEM for the same TPI sample.

Using chemical reaction to quantitatively characterize the amorphous component in polymer crystal structures, one assumes that: (1) all noncrystalline portions of the structure are completely reacted; (2) the lateral surfaces are negligibly small compared to the total area; and (3) reaction does not penetrate into the crystalline core of the lamellas. It has been found, however, that penetration did take place when lamellas were epoxidized in amyl acetate[41]. Electron microscopic examination showed erosion at the edges of these lamellar; the amount of which increased with reaction time and amount of epoxidation reagent MCPBA present. In some cases, it was found that the total fraction epoxidized exceeded the noncrystalline fraction from density measurements[41,47]. These results suggest that the excessive double bond reaction takes place along the lateral surfaces during the epoxidation period. Therefore, it is considered important to explore the reaction conditions on the results of the epoxidation reaction and to chose the optimum reaction parameters.

As discussed above, a sizeable noncrystalline component is present in TPI crystal structures, the amount of which depends on the crystalliza-

tion conditions. In single lamellas, this noncrystalline component is expected to be at the lamellar surfaces as chain fold and noncrystallizing chain ends. For multilamellar structures, interlamellar chain traverses may also be present. Taking advantage of the optimum epoxidation conditions to be found and the newly developed ^{13}C NMR method, it is of interest to study the effects of molecular weight and crystallization condition on the nature of the noncrystalline component in the solution crystallized TPI structures.

1.4 Objectives of This Study

The principle objectives of this study are as follows:

(1) The combined techniques of scanning electron microscopy and sample fixing will be used to view features of solution-grown trans-1,4 polyisoprene structures that can not be well revealed by optical microscopy and transmission electron microscopy; these TPI structures will be studied as a function of molecular weight, crystallization temperature and time. The effects of mechanical (ultrasonic vibration) and chemical (etching) treatments on these structures will also be investigated. (morphological studies)

(2) The effects of suspension medium and of the relative concentrations of reactant on the epoxidation reaction of TPI structures will be explored and the optimum reaction conditions chosen for quantitative analysis. (epoxidation conditions)

(3) ^{13}C NMR will be used to study epoxidized TPI structures in the α and β crystalline forms with various morphologies as a function of

molecular weight, to quantitatively characterize these epoxidized products in terms of an average reacted block length, an average unreacted block length and a fraction of reacted double bonds, and to investigate the effects of annealing treatment on some of the TPI structures and the existence of tie-molecules between lamellas. (quantitative characterization)

(4) The quantity of noncrystalline portion of the various TPI structures obtained by ^{13}C NMR will be compared with that obtained from other independent measurements such as density and infrared spectroscopy. (other methods)

2. Experimental

2.1 Samples

Both synthetic and natural TPI were used in this study. The synthetic trans-1,4 polyisoprene (Polysciences Inc.) was found earlier[108] by gel permeation chromatography to have a number average molecular weight, $\overline{M}_n$, of 3.5×10^4 and a molecular weight distribution, $\overline{M}_w/\overline{M}_n$, of 4.8 and by ^{13}C NMR to have a trans content of 99%.

Gutta percha obtained from Gabundan Produsen Karet, Indonesia and Balata from Dunlop Sports Co. were purified first by repeated filtration and precipitation from toluene solution into methanol followed by extraction with acetone in a Soxhlet extraction column[109]. The molecular weight of the unfractionated balata is $\overline{M}_n=1.1\times10^5$ with $\overline{M}_w/\overline{M}_n=2.2$. The molecular weight of the gutta percha is $\overline{M}_n=6.3\times10^4$ with $\overline{M}_w/\overline{M}_n=4.3$. The trans content of these natural materials were determined by ^{13}C NMR to be 100%.[108]

2.2 Fractionation

Fractionation of synthetic TPI was carried out by fractional precipitation from toluene solution with methanol using the scheme shown in Figure 2.1. A 1% TPI solution containing antioxidant 2246, 2,2-methylene-bis-(4-methyl-6-tertiary-butyl phenol), of 0.2g/l was prepared at 50°C. Methanol was then added until cloudiness appeared. After heat-

ing to clarify the solution it was placed in a 29°C bath overnight for precipitation. After separation of the supernatant and the precipitate phases, more methanol was added to the former to again bring about cloudiness while the latter was dissolved in toluene, keeping the concentration at about 1%, and the fractionation procedure was repeated. The fractions of P_4, P_5, P_6 and P_{15} described in Fig.2.1 were collected by precipitation in large amount of methanol, dried under vacuum and subjected to molecular weight determination.

The same procedure was used for gutta percha and balata fractionation.

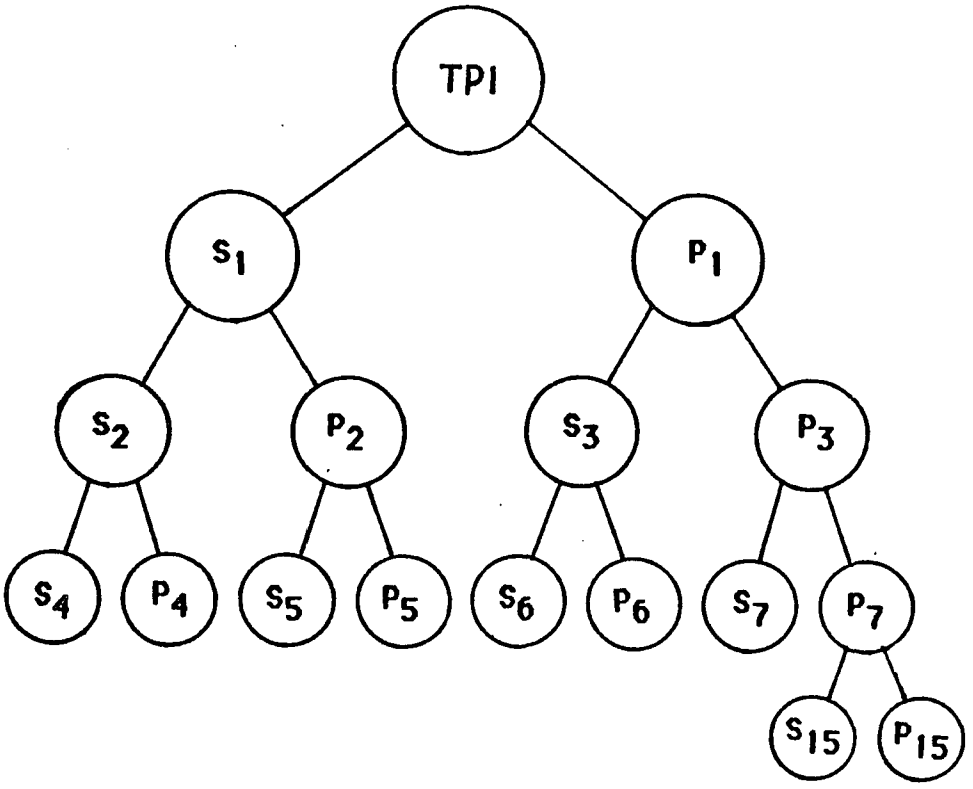

Figure 2.1 Trans-1,4 polyisoprene Fractionation Scheme

s: supernatant phase; p: precipitate phase.

2.3 Molecular Weight Determination

Viscosity-average molecular weight, $\bar{M}_v$, of the fractions was determined by solution viscosity measurements in toluene at 30°C using an Ubbelohde viscometer. The empirical relationship of $\bar{M}_v$ and intrinsic viscosity $[\eta]$ has been given by the equation of Mark, Houwink and Sakurada:

$$[\eta] = K\bar{M}_v^{\alpha} \qquad (2.1)$$

Since no K and α values for TPI in toluene solution are available in the literature, these parameters were determined by measuring the viscosity of nine TPI samples with known molecular weight values, the range of $\bar{M}_w = 1.4\times10^4 - 2.7\times10^5$ and with $\bar{M}_w/\bar{M}_n = 1.2\text{-}1.3$. These were prepared on a diatomaceous earth column and characterized by gel permeation chromatography earlier[47,108]. A least squares analysis of $\log[\eta]$ vs $\log\bar{M}$ yields an intercept, logK, equal to -1.477 ($K=3.34\times10^{-2}$) and a slope, α, of 0.686. The equation of intrinsic viscosity/molecular weight becomes:

$$[\eta] = 3.34\times10^{-2}M^{0.686} \qquad (2.2)$$

The molecular weight of fractions P_4, P_5, P_6, and P_{15} shown in Fig. 2.1 were found to be 0.5, 1.4, 2.6 and 5.9×10^5, respectively.

2.4 Crystallization Techniques

Crystallization of unfractionated TPI was carried out from 1% (w/v) amyl acetate solution heated to 90-95°C for one hour; the solution was cooled to 60°C, then placed in a 0°C bath and left undisturbed for 24

hours. The resulting suspension was heated to 20° or 30°C at an average rate of 0.06°/min., left at that temperature for 40 hours and then filtered and washed with fresh amyl acetate at the same temperature to remove any material which might not be crystallized. Preparation by this procedure is referred to below as Tc=0/20 or 0/30. A small portion was sampled for morphological studies or dried below Tc for x-ray analysis or for density measurements. The remaining part was suspended in the selected liquid for epoxidation. The x-ray pattern, DSC endotherm and IR spectrum showed the crystalline part of these preparations to be in the β form. The slow heating process did not affect the morphology or the crystal form as confirmed by microscopic studies[4,5] and DSC and IR studies.

Besides the 0/20 or 0/30 procedure stated above, two other crystallization techniques were employed with the fractionated synthetic TPI and are referred to as the precooling and the direct method, respectively. In the precooling method, a 0.1% TPI solution was heated to 90-95°C for one hour, and then cooled in a 0°C bath to bring about precipitation; the crystal-liquid mixture was heated again at a rate of 0.15°C/min. to the minimum redissolution temperature, T_R, followed by cooling to a desired crystallization temperature, Tc. By carefully controlling T_R (32-36°C depending on the molecular weight), this procedure yields uniform sized single β lamellas. In the direct method the heated TPI solution was cooled directly in a constant temperature bath at the desired Tc for crystallization. This method leads to more complex TPI structures, as shown below. The crystals were then filtered, washed and subjected to studies of morphology, crystal form identification, crystallinity measurements and epoxidation.

In all the cases antioxidant 2246 was added (0.2g/l) in the solution to prevent the polymer from possible oxidation during heating and crystallization.

2.5 DSC and X-ray Experiments

Differential scanning calorimetric measurements were made with a DuPont 1090 Thermal Analyzer using a heating rate of 10°C/min. and 2-5mg samples. Values of heat of fusion, ΔH_f , were obtained by computer integration using the Interactive DSC Data Analysis Program. The melting temperature of the samples was taken as the endotherm peak maximum and was also used for crystal form identification. A typical DSC curve is shown in Figure 2.2.

Wide-angle x-ray diffraction photographs were recorded with a 57.3 mm diameter cylindrical camera to identify the crystal form(s).

2.6 Crystallinity Measurements

Density measurements of dried TPI mats were carried out with a water-ethanol gradient column. The crystallinity of the samples was calculated by the following equation assuming a two-phases system:

$$Wc = \frac{\rho_c\ (\rho_s - \rho_a)}{\rho_s\ (\rho_c - \rho_a)} \qquad (2.3)$$

where ρ_s is the density of the sample, ρ_a equal to 0.905 is the density

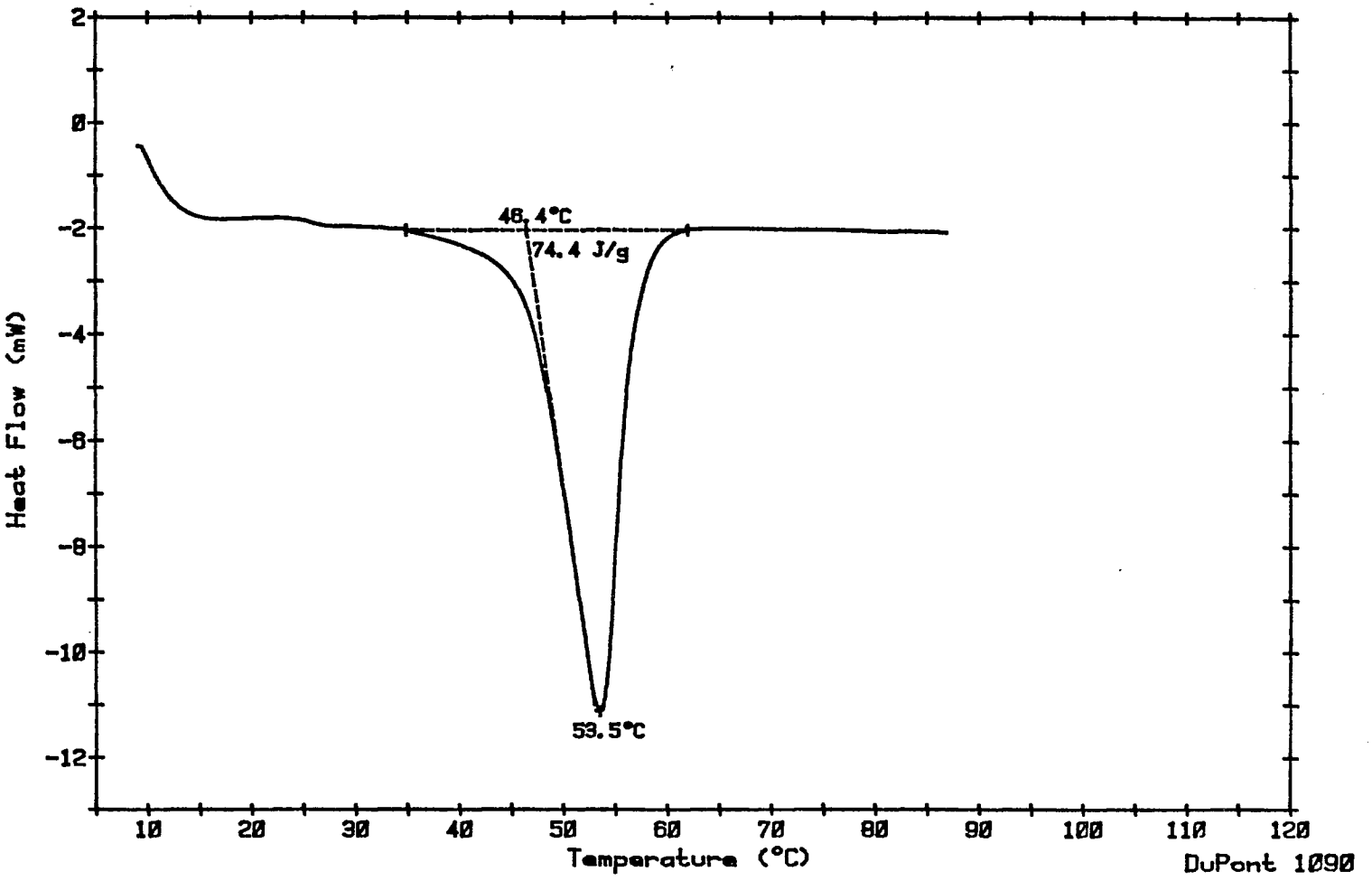

Figure 2.2 A Typical DSC Curve of β-TPI Lamellas

of the amorphous phase[44] and ρ_c is the density of 100% crystalline TPI predicted from the unit cell parameters.

Crystallinity measurements by FTIR were carried out using a Bio-Rad FTS-40 FTIR instrument. Samples were made by filtrating the suspended crystal onto a teflon membrane in a filter funnel. The IR method, developed in these laboratories[110], was employed to obtain the crystallinity of TPI preparations, using the C=C stretching band at 1663cm^{-1}. A 100% crystalline spectrum was obtained from the sample spectrum by computer subtraction of an amorphous spectrum taken at 65°C. The amorphous band at 843cm^{-1} due to the C-H out of plane bending[111] was taken as a subtracting reference. The crystallinity was then calculated from the ratio of the absorbence maximum at 1663cm^{-1} for the 100% crystalline part to that for the total sample by xeroxing, cutting and weighing the peak area. At least two subtraction determinations were made for each measurement.

2.7 Morphological Studies

Optical microscopy. After crystallization, a drop of the crystal suspension was placed on a slide with a cover glass and viewed in suspension with a Zeiss microscope having interference contrast optics.

Transmission electron microscopy. Single lamellas of TPI were placed on a grid covered with a carbon film, then dried and shadowed with Au/Pd. A Philips EM300 electron microscope was used to view these crystals.

Scanning electron microscopy. The TPI structures were first filtered

and washed at Tc with fresh liquid then resuspended in amyl acetate. The suspension was mixed with OsO_4 for about 1 hour followed by washing. A drop of the suspension was placed on the sample stage; the sample was then dried and coated with evaporated Au/Pd (80/20). For a number of the preparations, the suspension was placed in an ultrasonic vibrator for 3 minutes prior to the OsO_4 fixing. In one experiment, the crystal suspension was mixed with concentrated nitric acid, allowing the crystals to stay in contact with acid at the acid-amyl acetate interface for 5-10 minutes, followed by OsO_4 fixing. A Cambridge Stereoscan S4 scanning electron microscope was used for viewing these preparations at 20kV.

2.8 Epoxidation

Reaction of the TPI crystals, prepared as given in section 2.4, was carried out in suspension in selected liquids at 0°C with meta-chloroperbenzoic acid (MCPBA) as received from Aldrich Chemical Company, Inc.. The amount of MCPBA used is given in terms of the molar ratio of MCPBA to TPI repeat units ([M]/[D]). The reaction occurring is

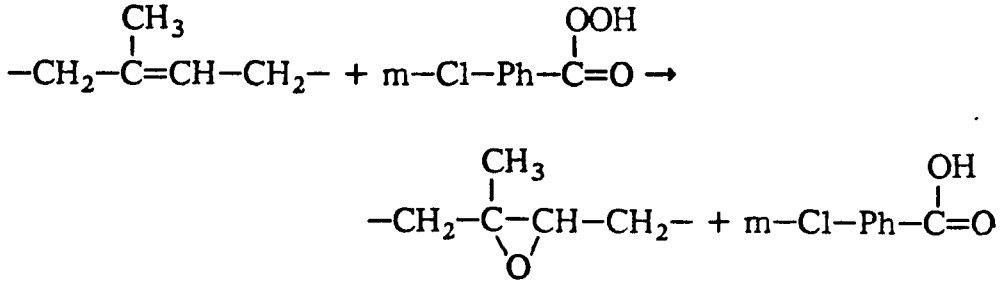

After epoxidation the reaction product was filtered and washed repeatedly with fresh suspension liquid at 0°C. Drying was carried out at 0°C for 2-3 days then at room temperature.

2.9 ^{13}C NMR Measurement

The 50.32 MHz ^{13}C NMR spectrum of each preparation was obtained with an IBM WP 200-SY NMR system on about 10% (w/v) solution in $DCCl_3$ using TMS as an internal standard and a spectral width of 8333 Hz in 32K of memory. Gated broad-band proton decoupling with NOE was used. The delay time between pulses was 20 seconds. The number of scans collected ranged from 800-10,000, but in most of cases it was 2,500-3,000. These experimental parameters were believed to be appropriate to obtain quantitative results[107]. A typical spectrum is given in Figure 2.3. The pertinent ^{13}C NMR assignments for TPI-epoxidized TPI copolymers as made in an earlier work by Woodward in a joint effort with Schilling and Bovey[107] were used in this work. Table 2.1 quotes these assignments; the numbering of the carbon atoms in the repeat unit is as follows:

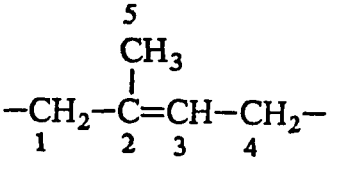

(TPI unit)

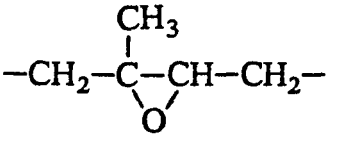

(Epoxidized-TPI unit)

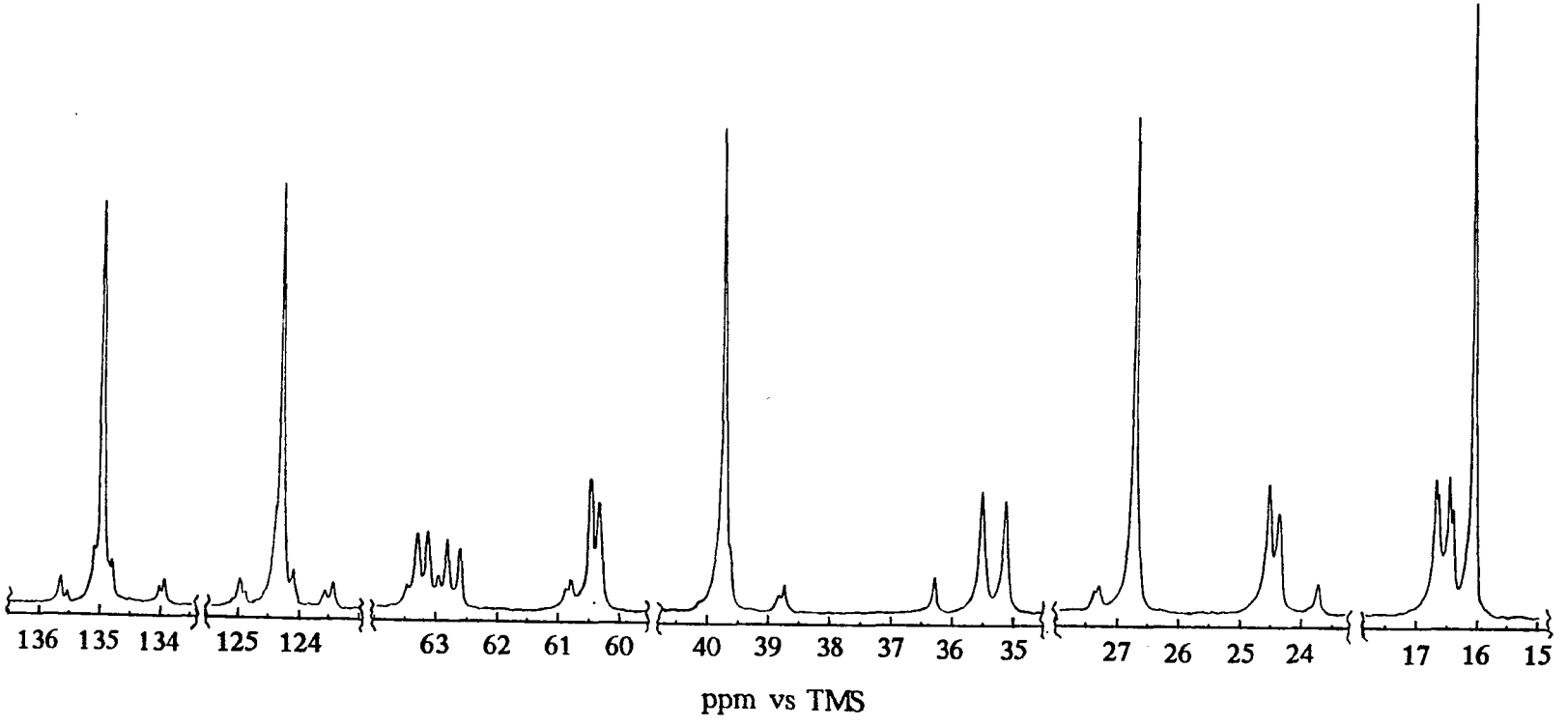

Figure 2.3 A Typical ^{13}C NMR Spectrum of Surface Epoxidized TPI Sample

Spectrum assignments and experimental parameters are given in Table 2.1 and in the text, respectively.

All quantitative measurements were made by computer intergration. The values obtained by ^{13}C NMR are the average reacted and unreacted block length and the fraction of epoxidation.

Table 2.1 ^{13}C NMR Assignments Used for Analysis of TPI and Epoxidized TPI Block Copolymers

Assignment	δ, ppm vs TMS
IIE (C4)	23.76
III&EII (C4)	26.77
IEE&EEE (C4 m,r)	24.42, 24.57
EEI (C4)	27.47
EEI&EEE (C1 m,r)	35.17, 35.54
EII (C1)	36.33
IEE (C1)	38.78
III&IIE (C1)	39.75

a. data quoted from ref.107

b. I represents an isoprene unit and E an epoxidized isoprene unit.

c. the carbon atom numbering is given in the text

3. Results

3.1 Morphologies of TPI Crystals from Solution

3.1.1 Single Crystals

Crystallization of TPI by the precooling technique at 20°C or 30°C in 0.1% solution gave single lamellas regardless of the molecular weight. When using amyl acetate as a solvent, these lamellas were rectangular-shaped as shown in Figure 3.1(a). The crystalline portion of these were found to be in the β-form as identified by DSC and FTIR, whereas crystallization using hexane as a solvent led to ellipsoidal-shaped α single lamellas as seen in Figure 3.1(b). By carefully controlling the minimum redissolution temperature (T_R), the crystal size is approximately uniform due to the simultaneous growth of the lamellas from nuclei already present in the solution.

3.1.2 Multilamellas

Figure 3.2 shows the interference contrast optical micrograph of TPI lamellar stacks observed in suspension before and after treated with OsO_4. The overall appearance of these structures is not modified by the chemical treatment. This is further evidenced by comparing them with scanning electron micrographs of similar fields taken after reaction and drying, as shown in Figure 3.3. It is also clearly seen that the fine structures of these lamellar stacks have been preserved by treating with OsO_4, while

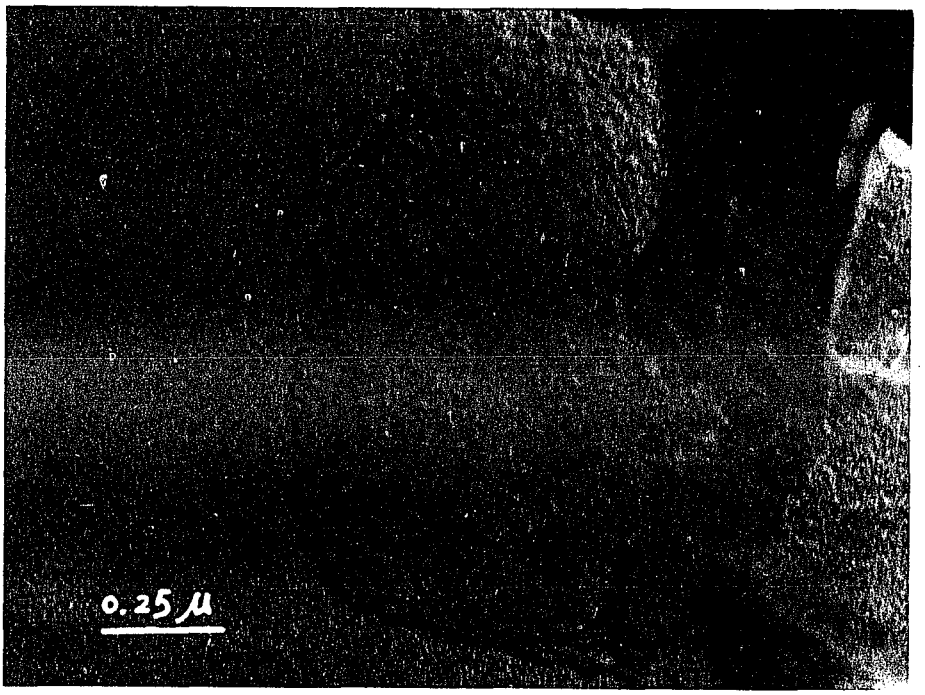

(a)

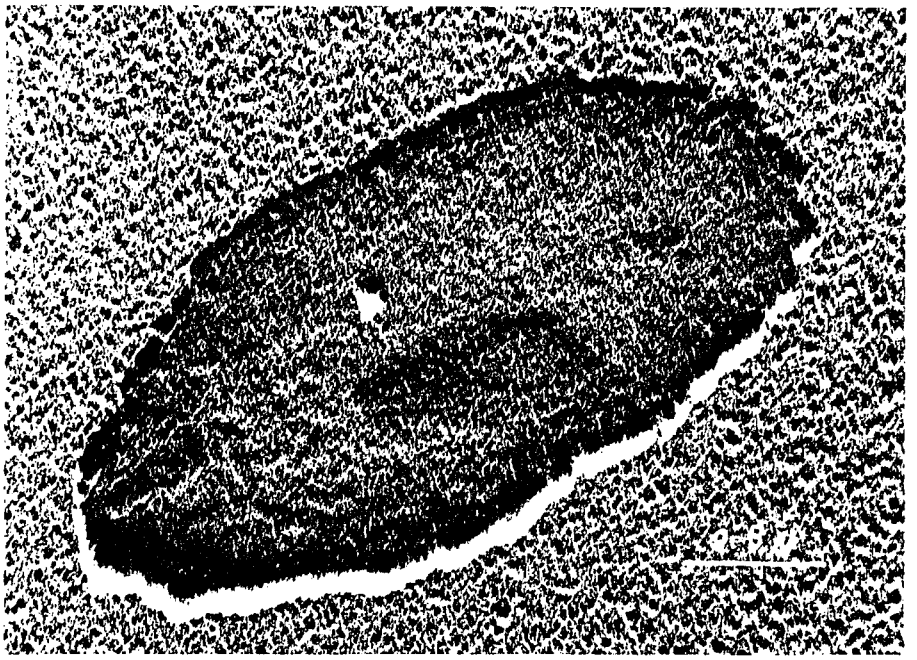

(b)

Figure 3.1 Transmission electron micrograph of TPI single crystals. (a) β-lamella crystallized (T_R =34°C) from 0.1% amyl acetate solution at 20°C; (b) α-lamella crystallized (T_R = 38°C) from 0.1% hexane solution at 25°C.

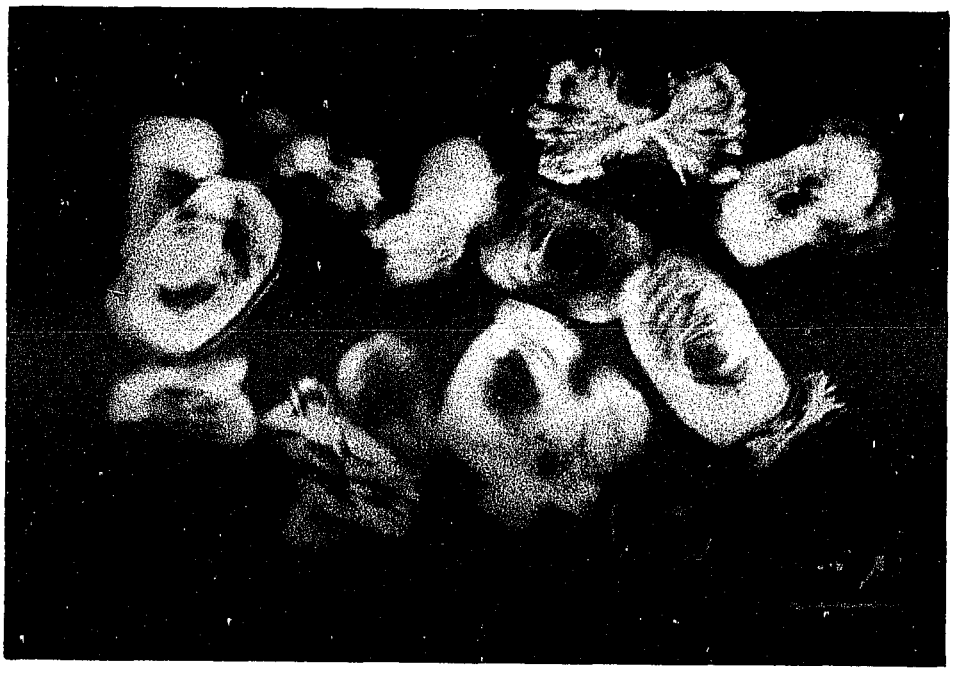

(a)

(b)

Figure 3.2 Interference contrast optical micrograph of TPI with $\overline{M}_v=1.4\times10^5$ crystallized from 1% amyl acetate solution at 20°C, observed in suspension. (a) Before treated with OsO_4; (b) after treated with OsO_4.

(a) (b)

Figure 3.3 Scanning electron micrograph of TPI with $\overline{M}_v=1.4\times10^5$ crystallized from 1% amyl acetate solution at 20°C for 24 hours, (a) without treated with OsO_4; (b) treated in suspension with OsO_4.

only poorly resolved structures are visible for the sample without treating with OsO_4, due to the sample shrinkage upon drying.

For TPI with $\bar{M}_v=1.4\times10^5$ direct crystallization at 20°C from 1% amyl acetate solution was carried out for 1, 2, 3, 5, 24 and 48 hours followed by treatment with OsO_4 before drying. For crystallization times up to 3 hours relatively little precipitation occurs. Scanning electron micrographs of the structures observed at 3 hours of crystallization are given in Figures 3.4 and 3.5. These structures consist of a large number of curved lamellar ribbons, with considerable interlamellar penetration and branching being evident. The ribbons appear in groups of approximately parallel layers and fan out upward as seen in Figure 3.4. A number of lamellar ribbons viewed edge-on in Figure 3.5 contain one or more bends, as can be better seen in a higher magnification shown in Figure 3.6. The principal structural type (>90%) found at longer crystallization time first appear at 5 hours as observed in Figure 3.7; micrographs of similar structures at 24 hours are given in Figures 3.8 and 3.9. These structures are made up of ten or more overgrown lamellar layers. The layers have some curvature along the sides and have flat or slightly rounded ends. Each layer is dished with the center depth varying from one lamellar stack to another and from one face to another in a single stack. There also is considerable branching, twisting and interlamellar penetration evident; a structure having considerable interlamellar penetration is shown in Figure 3.10. When the lamellar stacks are subjected to ultrasonic vibration for 3 minutes, breakage occurs across the center portion of all the layers, resulting in two approximately equal sized pieces, as is evident in Figure 3.11. In addition, the formation of a mosaic of cracks on the exposed layers also occurs (see Figure 3.12). From the nitric acid-

etched edges shown in Figure 3.13, sublayers as well as mosaic are also visible. Since the thickness of the lamellar layers composing the structures shown in Figures 3.4 to 3.10 is obviously much larger than a single lamella, these layers must be made up of many superposed lamellas. Crystallization from 0.1% amyl acetate solution at 20°C yields structures similar to those obtained from 1% solution.

Crystallization from amyl acetate at 20°C for 3 hours of a TPI fraction with $\bar{M}_v=2.6\times10^5$ yielded some large lamellar structures, examples of which are given in Figure 3.14. After 24 hours of crystallization, a mixture of >60% stacks and <40% of the larger rounded objects are found; a group of the latter type and a few of the former are seen in Figure 3.15. Figures 3.16 and 3.17 show the organization of the lamellas making up the larger rounded structures after 2 days of crystallization. When viewed from the sides (Figure 3.16), it appears that the ribbons fan out and develop progressively via branching. When viewed from the ends, the ribbons appear curved, twisted, irregular and interpenetrating, and grouped in different orientation. When subjected to ultrasonic vibration the rounded structures appear to fracture within the center, as shown in Figures 3.18 and 3.19. Crystallization from 0.1% amyl acetate solution at 20°C leads to large rounded structures usually with one flattened area as well as lamellar stacks. A scanning electron micrograph taken of the flattened part (the face grown at the glass wall) of one of the larger structures is given in Figure 3.20; a network of lamellar layers with branching and interpenetration is clearly evident, although the separate layers are more widely spaced than for the structures grown from 1% solution.

A TPI fraction with $\bar{M}_v=5.9\times10^5$ crystallized from 1% amyl acetate at 20°C for 3 hours yielded spherulitic structures which apparently contain

a small stack of lamellas at the center as shown in Figure 3.21. A view of part of these is given in Figure 3.22. These structures are more numerous, more spherical in shape, smaller in size and at or near the surface have more curvature and twist, leading to a looser packing than in the rounded structures found at lower molecular weight. After 24 hours crystallization curved overgrown lamellas (30-40%), as shown in Figure 3.23, are also evident. The spherical structures are evident in optical micrographs (see Figure 3.24) taken both before and after OsO_4 treatment without drying; a scanning electron micrograph of a similar structure is shown in Figure 3.25. When subjected to ultrasonic vibration, the spherulites show little change.

When the TPI fractions are crystallized from 1% amyl acetate solution at 25°C for 4 days, only the larger rounded structures are found for the fractions with $\bar{M}_v$=1.4 and 2.6×10^5 and only the spherulites are found for fraction of $\bar{M}_v$ 5.9=×10^5. One of the rounded structures is shown in Figure 3.26. The end-viewed micrograph is also given in Figure 3.27. These structures appear to be larger in size and more completely grown, as compared to that grown at 20°C (see Figures 3.16 and 3.17).

Direct crystallization of unfractionated TPI was carried out at 30°C for 4 days. Crystallization appeared to occur mainly but not exclusively at the glass surfaces and gave a number of structures with a cylindrical morphology, as shown in Figure 3.28. A curved structure grown in the solution is shown in Figure 3.29. Crystallization by a precooling procedure (Td=90-95°C → Tp=0°C → Tr=31.7°C → Tc=30°C) of the $\bar{M}_v$=2.6×10^5 fraction gave large structures as seen in Figures 3.30 and 3.31. A section of the complex lamellar stacks shown in Figure 3.31 is viewed at higher magnification; regions of relatively flat lamellar stacks grouped

Figure 3.4 Scanning electron micrograph of TPI with $\overline{M}_v=1.4\times10^5$ crystallized from 1% amyl acetate solution at 20°C for 3 hours, treated in suspension with OsO_4.

Figure 3.5 Scanning electron micrograph of TPI with $\overline{M}_v=1.4\times10^5$ crystallized from 1% amyl acetate solution at 20°C for 3 hours, treated in suspension with OsO_4.

Figure 3.6 Same as Figure 3.5, but a higher magnification.

Figure 3.7 Scanning electron micrograph of TPI with $\overline{M}_v=1.4\times10^5$ crystallized from 1% amyl acetate solution at 20°C for 5 hours, treated in suspension with OsO_4.

Figure 3.8 Scanning electron micrograph of TPI with $\bar{M}_v=1.4\times10^5$ crystallized from 1% amyl acetate solution at 20°C for 24 hours, treated in suspension with OsO_4.

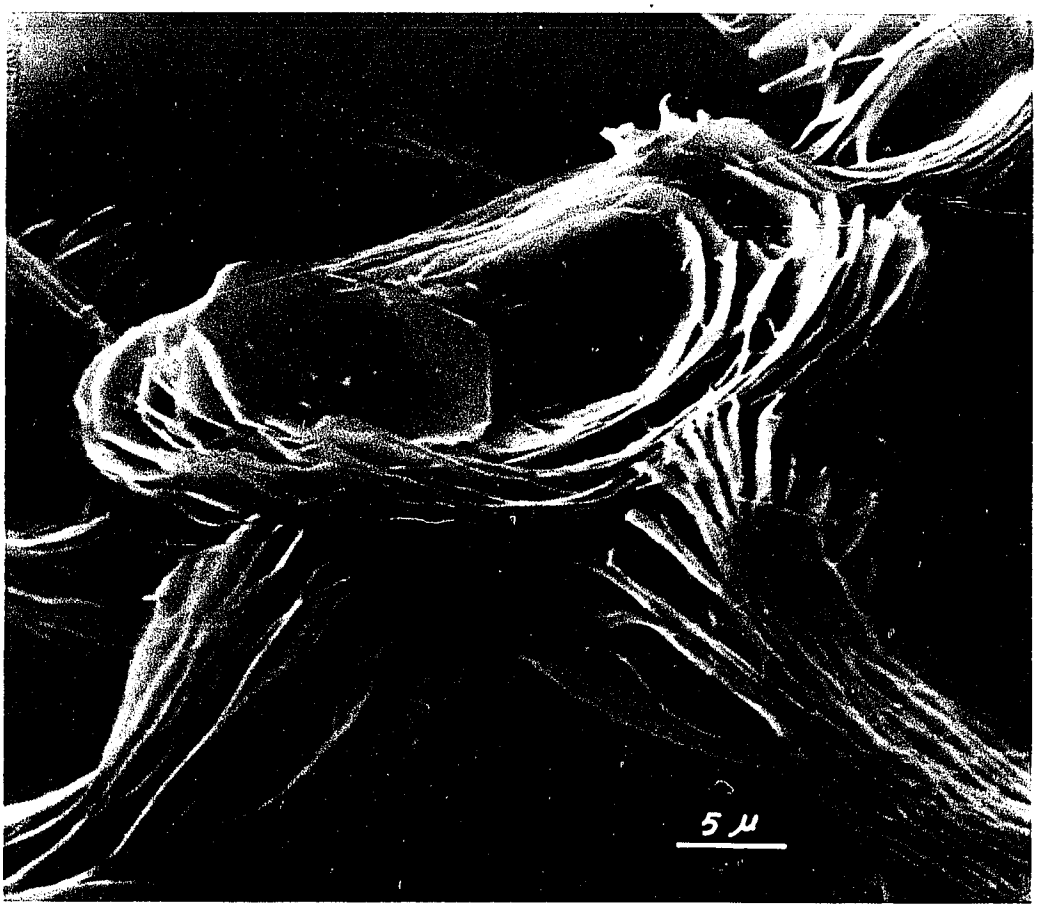

Figure 3.9 Same as Figure 3.8, but a different field.

Figure 3.10 Same as Figure 3.8, but a different field.

Figure 3.11 Scanning electron micrograph of TPI with $\overline{M}_v=1.4\times10^5$ crystallized from 1% amyl acetate solution at 20°C for 24 hours, ultrasonically vibrated for 3 minutes, treated with OsO_4.

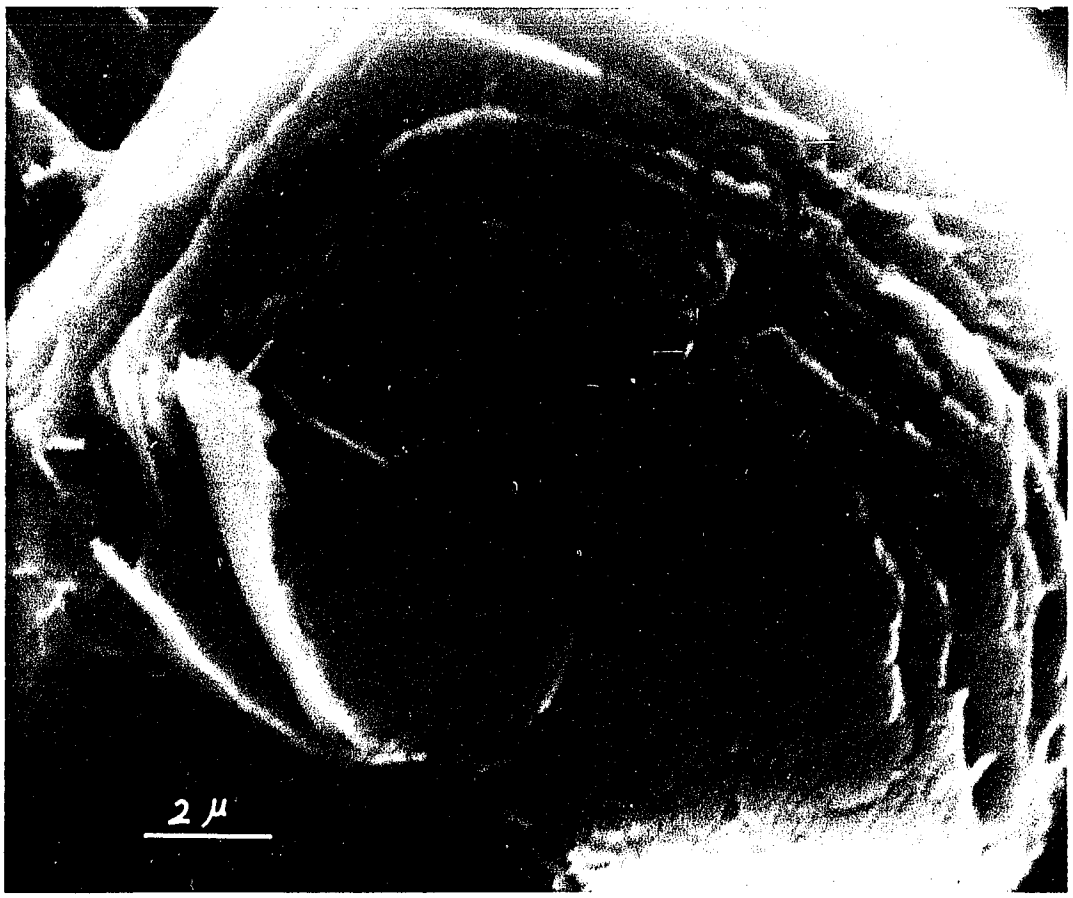

Figure 3.12 Scanning electron micrograph of TPI with $\overline{M}_v=1.4\times10^5$ crystallized from 1% amyl acetate solution at 20°C for 24 hours, ultrasonically vibrated for 3 minutes, treated in suspension with OsO_4.

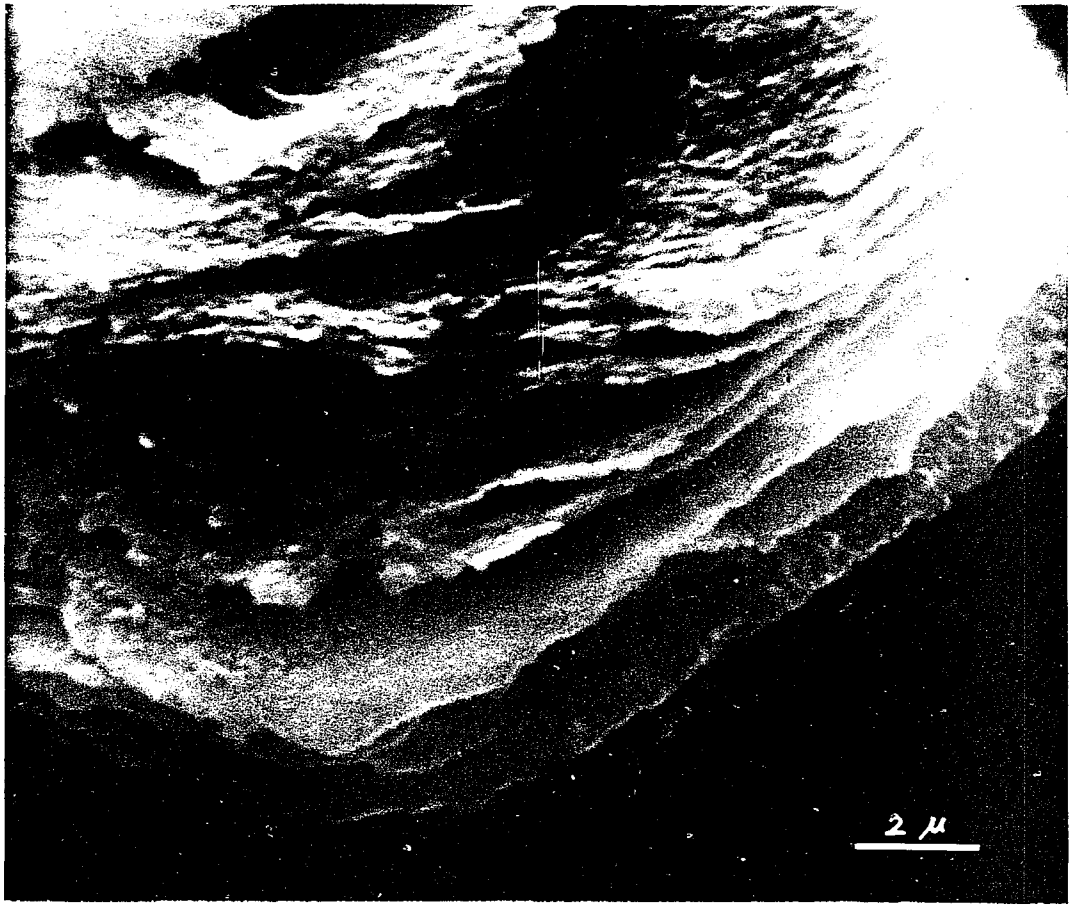

Figure 3.13 Scanning electron micrograph of TPI with $\bar{M}_v=1.4\times10^5$ crystallized from 1% amyl acetate solution at 20°C, etched by HNO_3 for 5 minutes, treated with OsO_4.

Figure 3.14 Scanning electron micrograph of TPI with $\bar{M}_v=2.6\times10^5$ crystallized from 1% amyl acetate solution at 20°C for 3 hours, treated in suspension with OsO_4.

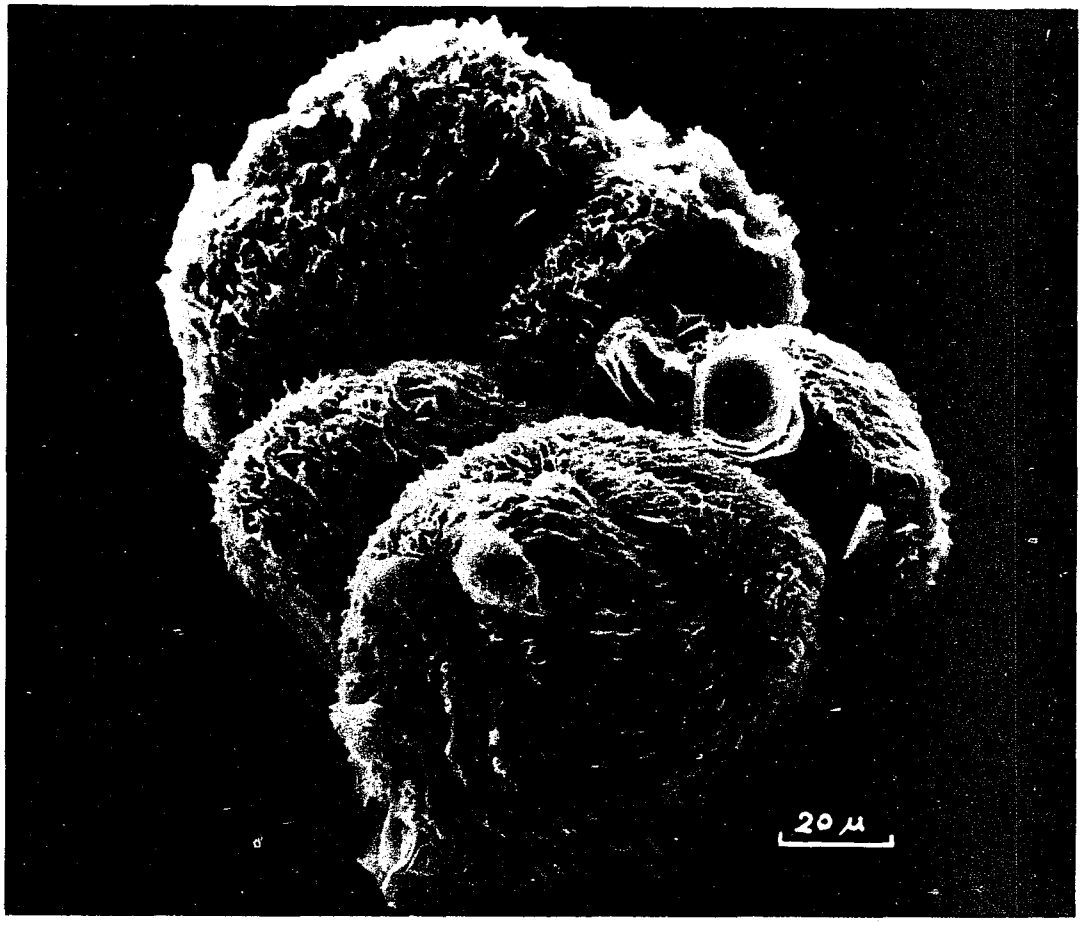

Figure 3.15 Scanning electron micrograph of TPI with $\overline{M}_v=2.6\times10^5$ crystallized from 1% amyl acetate solution at 20°C for 24 hours, treated in suspension with OsO_4.

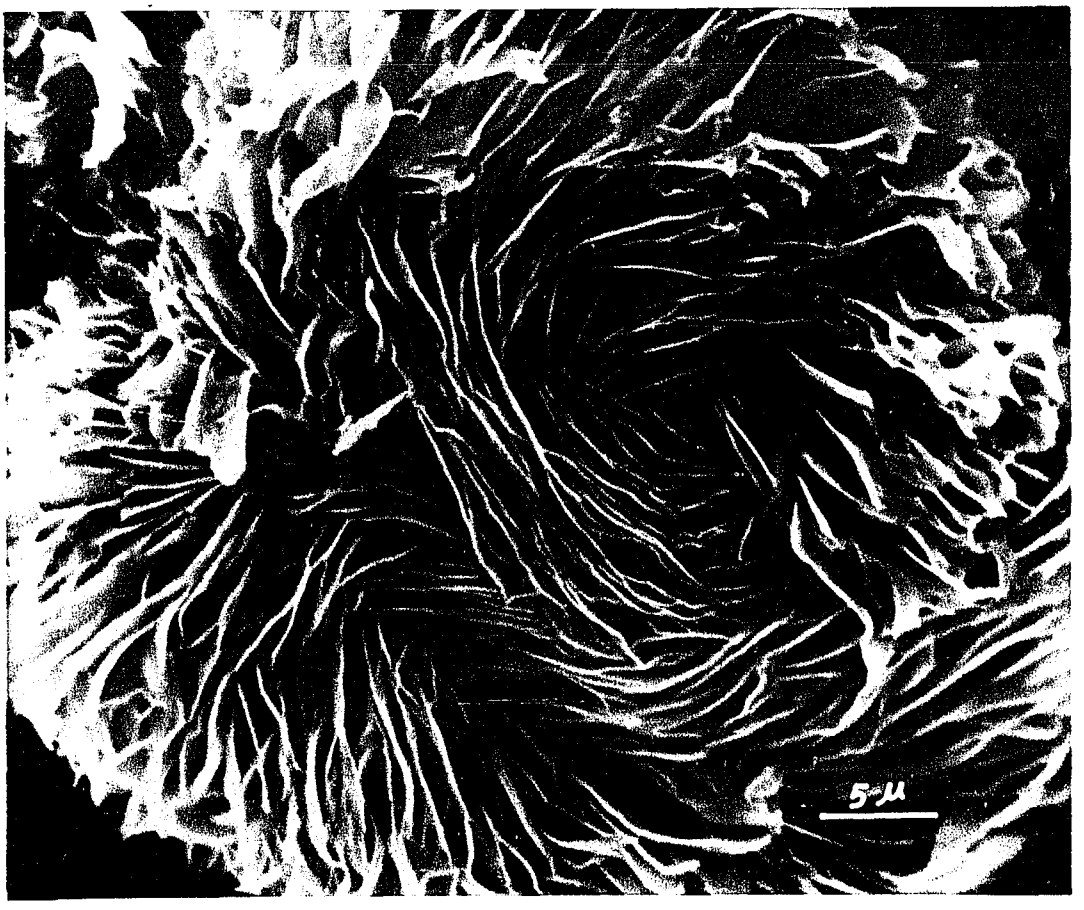

Figure 3.16 Scanning electron micrograph of TPI with $\bar{M}_v=2.6\times10^5$ crystallized from 1% amyl acetate solution at 20°C for two days, treated in suspension with OsO_4, viewed from the sides of the ribbons.

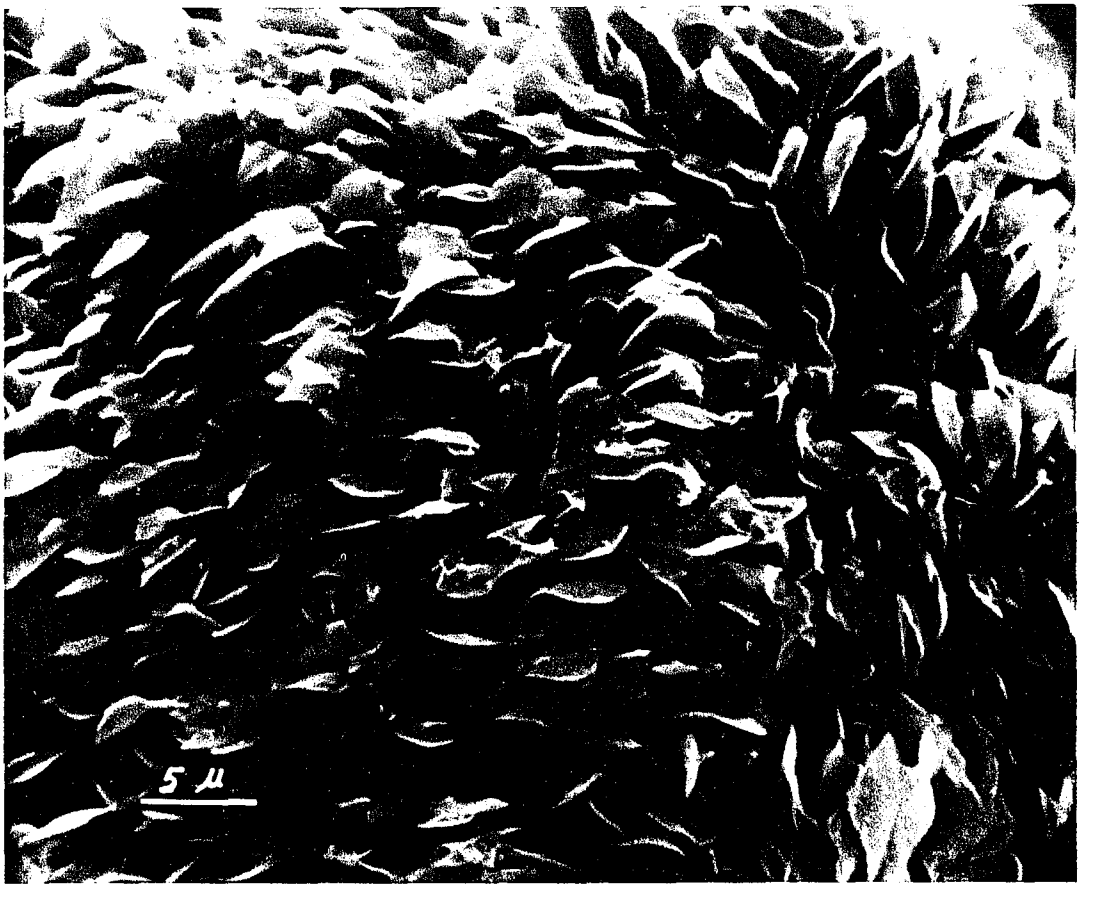

Figure 3.17 Scanning electron micrograph of TPI with $\overline{M}_v=2.6\times10^5$ crystallized from 1% amyl acetate solution at 20°C for two days, treated in suspension with OsO_4, viewed from the ends of the ribbons.

Figure 3.18 Scanning electron micrograph of TPI with $\overline{M}_v=2.6\times10^5$ crystallized from 1% amyl acetate solution at 20°C for 24 hours, ultrasonically vibrated for 3 minutes, treated in suspension with OsO_4.

Figure 3.19 Scanning electron micrograph of TPI with $\bar{M}_v=2.6\times10^5$ crystallized from 1% amyl acetate solution at 20°C for 24 hours, ultrasonically vibrated for 3 minutes, treated in suspension with OsO_4.

Figure 3.20 Scanning electron micrograph of TPI with $\bar{M}_v=2.6\times10^5$ crystallized from 0.1% amyl acetate solution at 20°C for 2 days, treated with OsO_4.

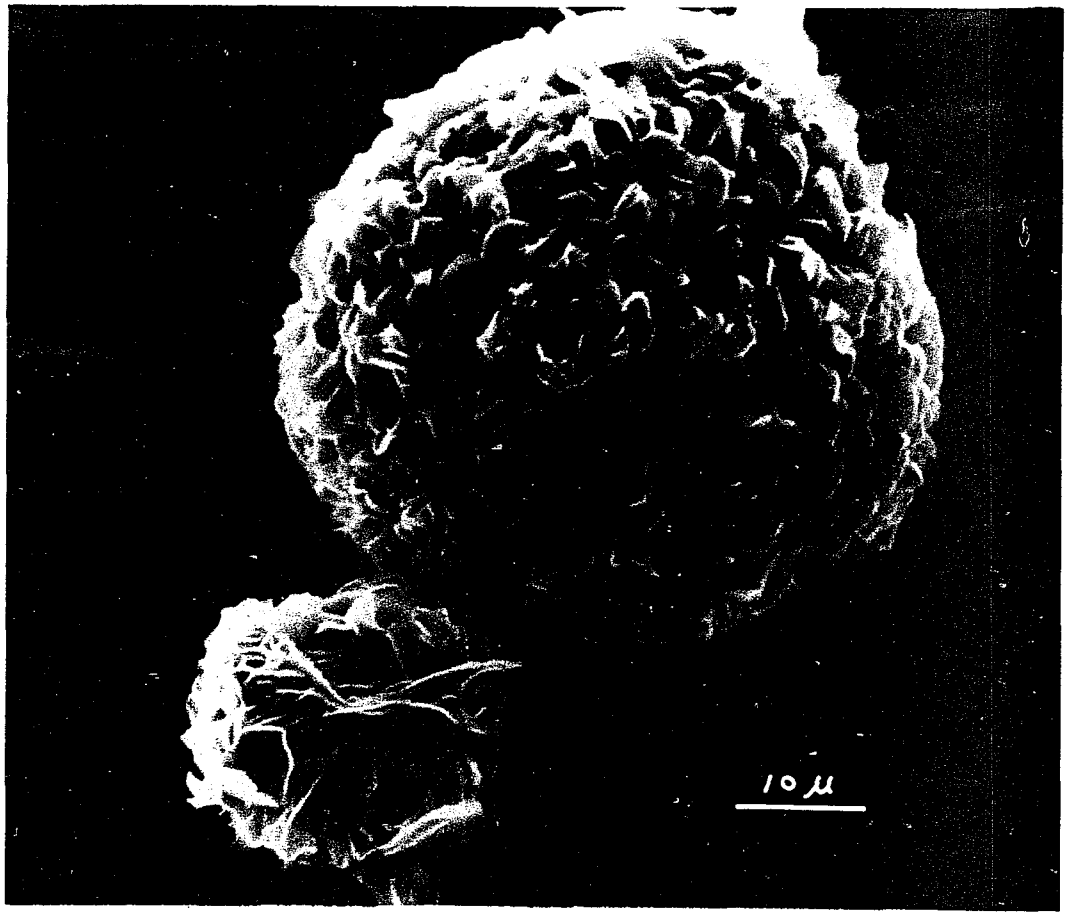

Figure 3.21 Scanning electron micrograph of TPI with $\bar{M}_v=5.9\times10^5$ crystallized from 1% amyl acetate solution at 20°C for 3 hours, treated in suspension with OsO_4.

Figure 3.22 Scanning electron micrograph of TPI with $\overline{M}_v=5.9\times10^5$ crystallized from 1% amyl acetate solution at 20°C for 3 hours, treated in suspension with OsO_4.

Figure 3.23 Scanning electron micrograph of TPI with $\bar{M}_v=5.9\times10^5$ crystallized from 1% amyl acetate solution at 20°C for 24 hours, treated in suspension with OsO_4, minor structures (30-40%).

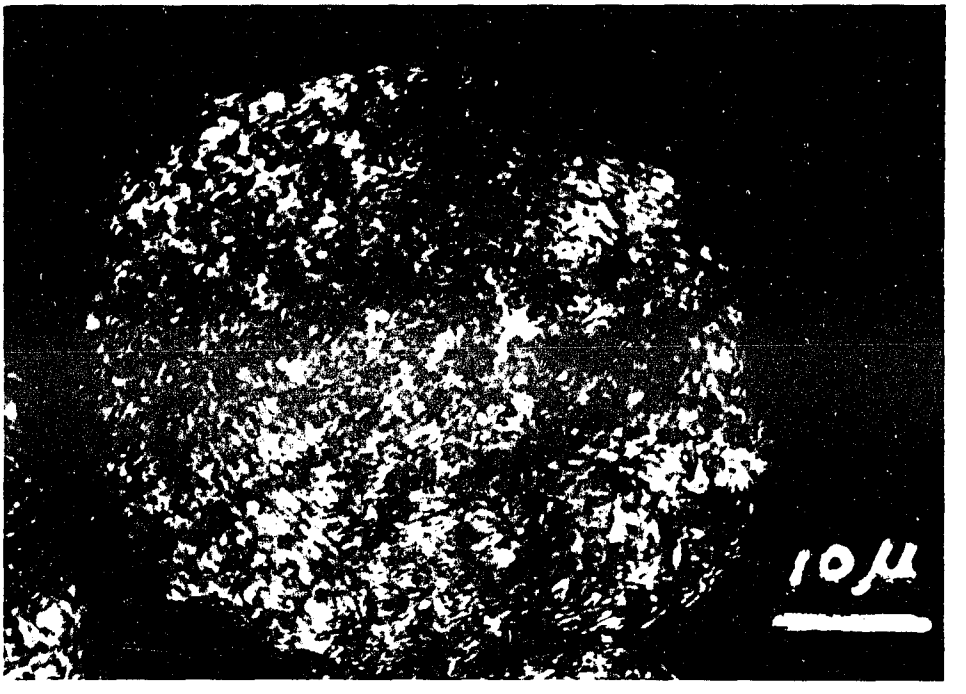

(a)

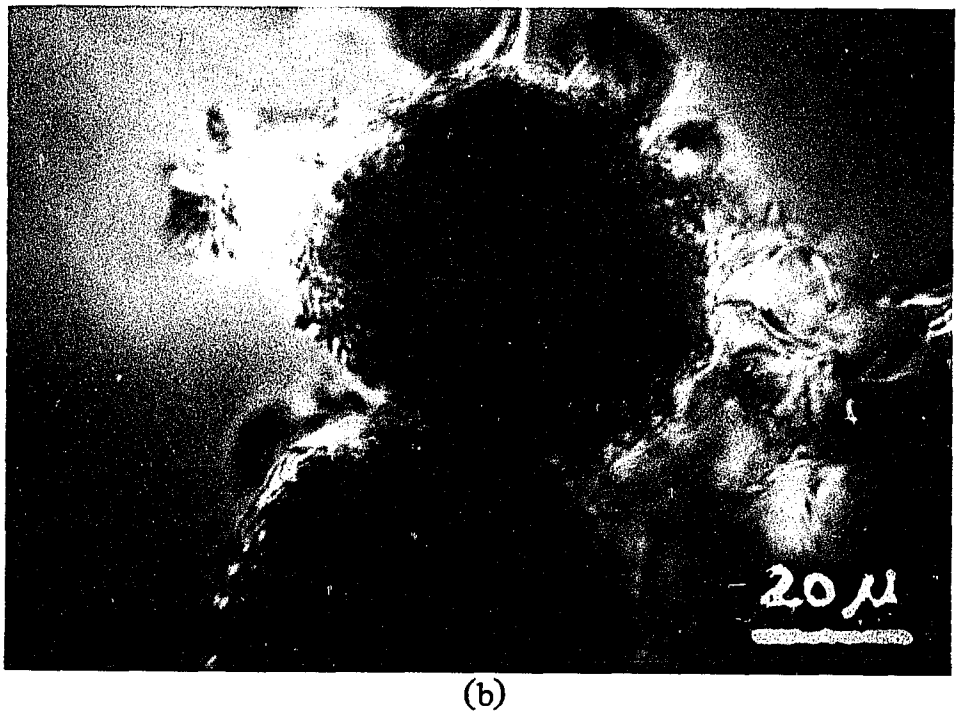

(b)

Figure 3.24 Interference contrast optical micrograph of TPI with $\overline{M}_v=5.9\times10^5$ crystallized from 1% amyl acetate solution at 20°C for 24 hours. (a) Before treated with OsO_4, observed in suspension; (b) after treated in suspension with OsO_4.

Figure 3.25 Scanning electron micrograph of TPI with $\bar{M}_v=5.9\times10^5$ crystallized from 1% amyl acetate solution at 20°C for 24 hours, treated in suspension with OsO_4.

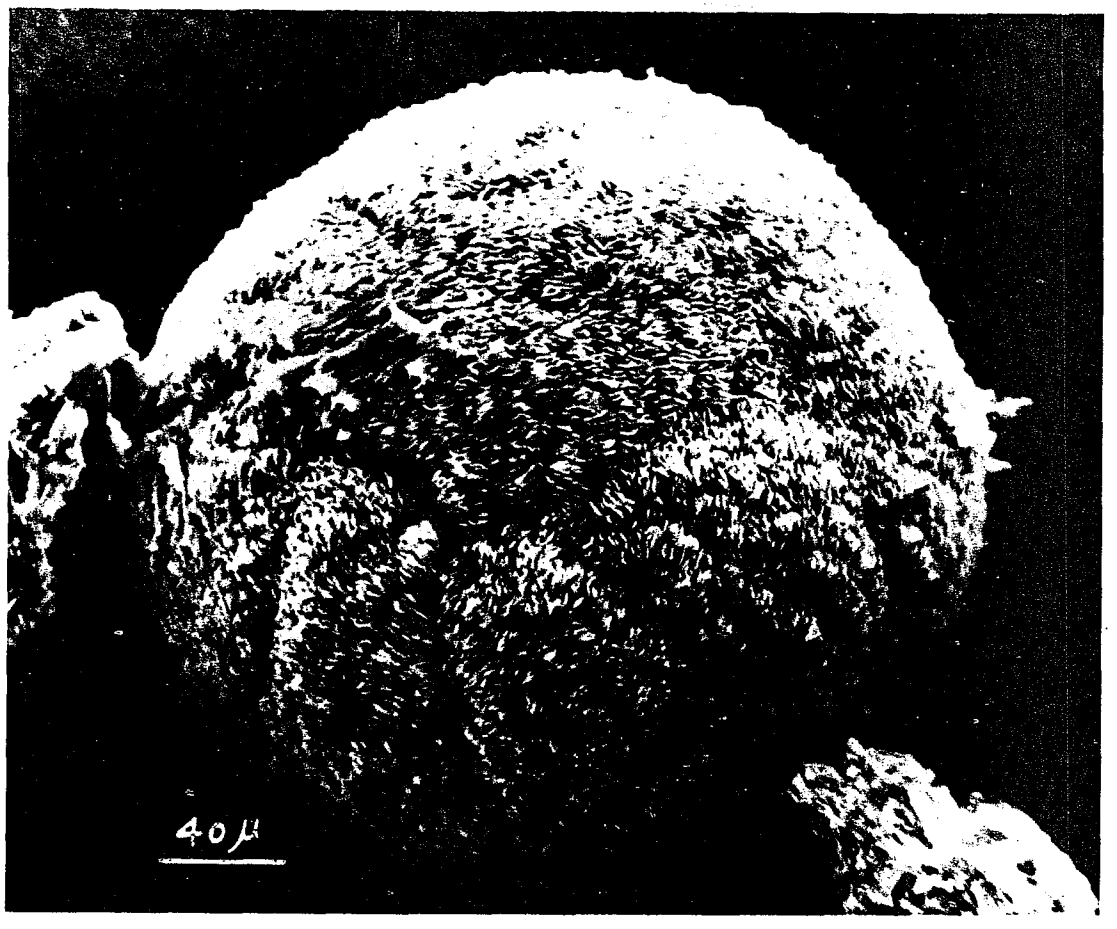

Figure 3.26 Scanning electron micrograph of TPI with $\overline{M}_v=2.6\times10^5$ crystallized from 1% amyl acetate solution at 25°C for 4 days, treated with OsO_4.

Figure 3.27 Same as Figure 3.26, but a higher magnification.

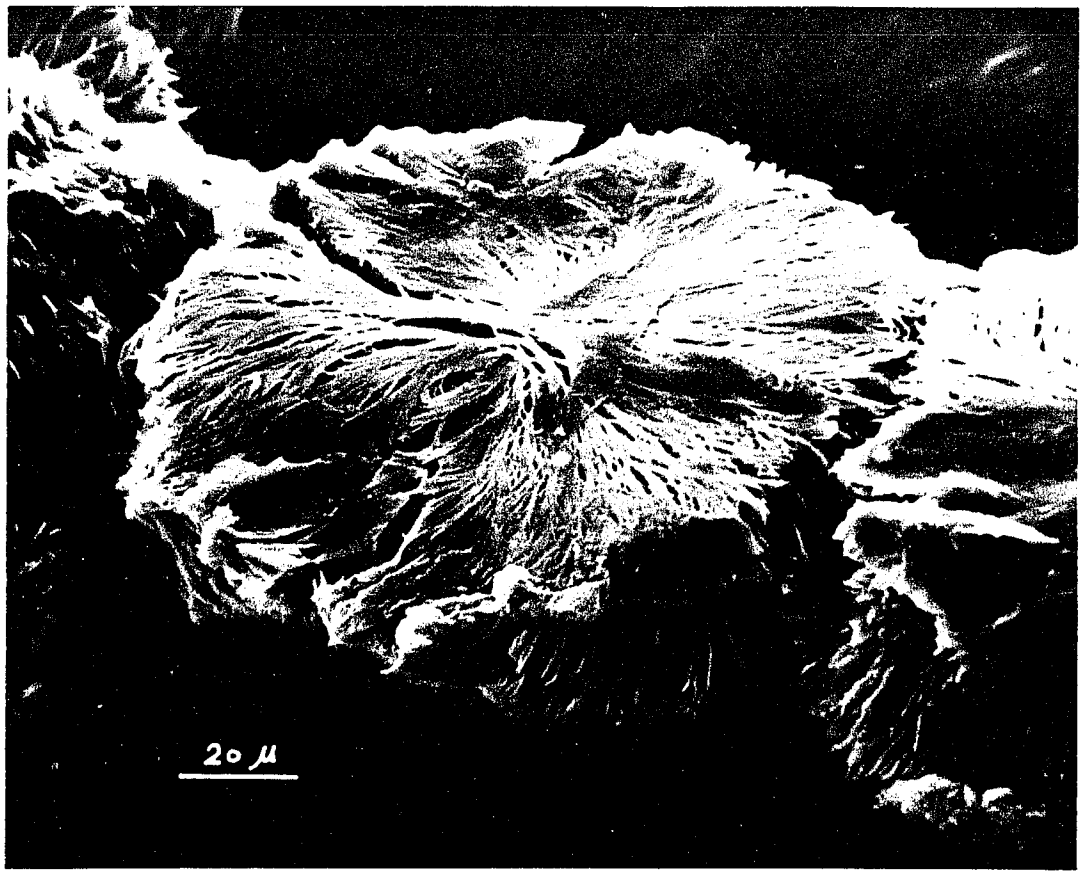

Figure 3.28 Scanning electron micrograph of unfractionated TPI crystallized from 1% amyl acetate solution at 30°C for 4 days, treated in suspension with OsO_4.

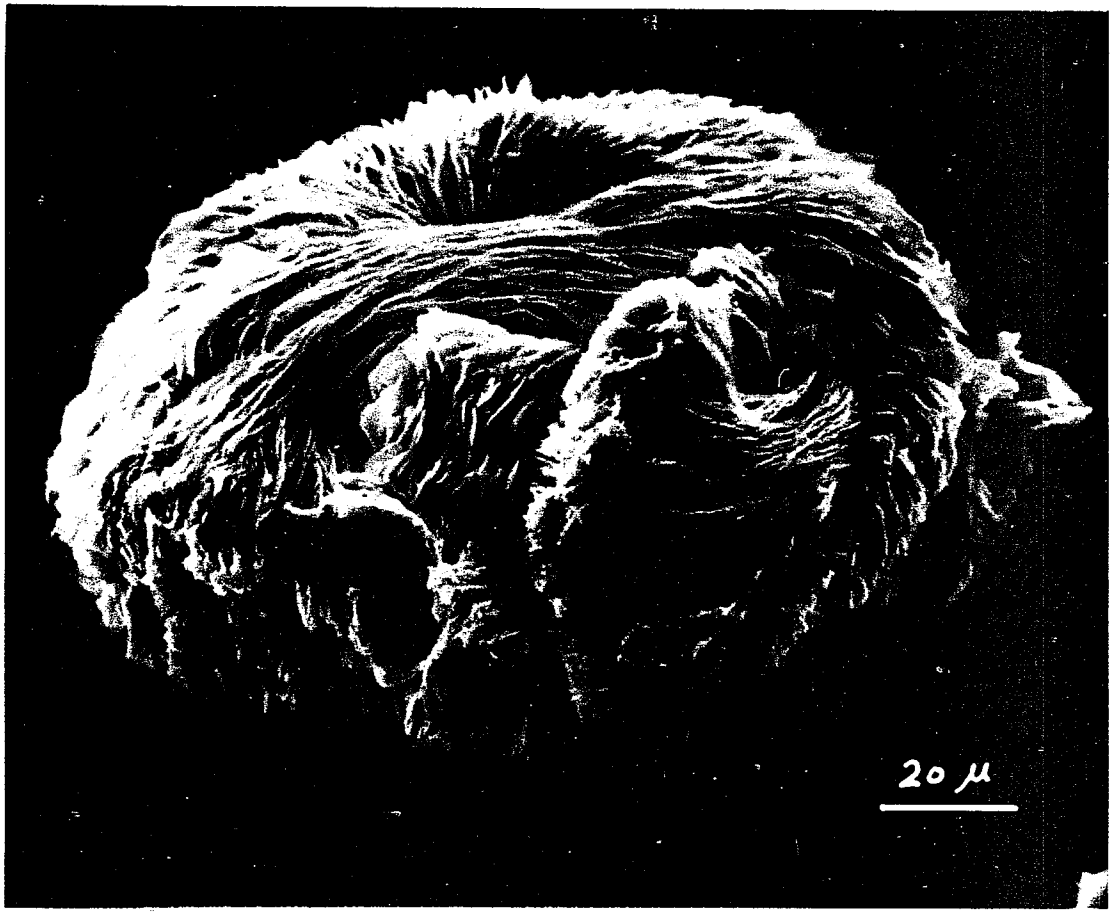

Figure 3.29 Scanning electron micrograph of unfractionated TPI crystallized from 1% amyl acetate solution at 30°C for 4 days, treated in suspension with OsO_4.

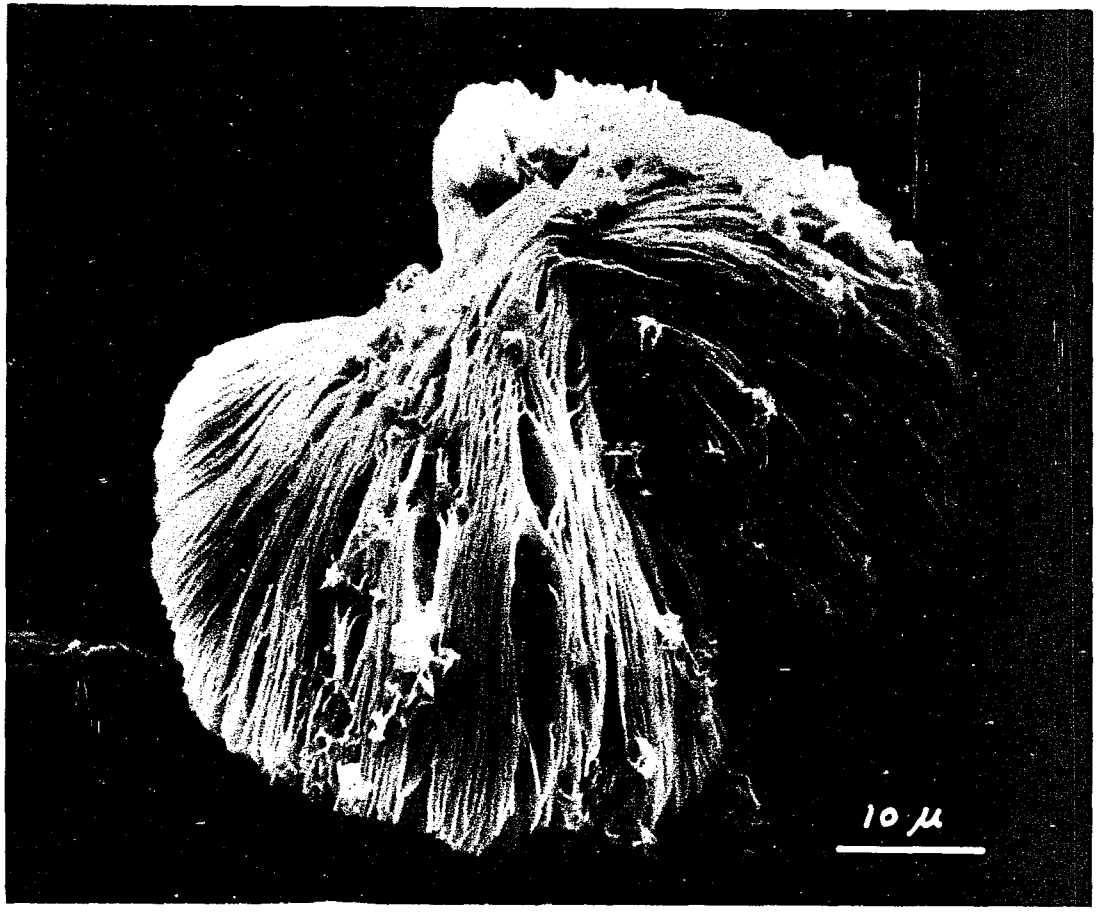

Figure 3.30 Scanning electron micrograph of TPI with $\overline{M}_v=2.6\times10^5$ precooling crystallized (T_R=31.7℃) from 1% amyl acetate solution at 30℃ for 4 days, treated in suspension with OsO_4.

Figure 3.31 Scanning electron micrograph of TPI with $\bar{M}_v=2.6\times10^5$ precooling crystallized (T_R=31.7°C) from 1% amyl acetate solution at 30°C for 4 days, treated in suspension with OsO_4.

Figure 3.32 Same as Figure 3.31, but a higher magnification.

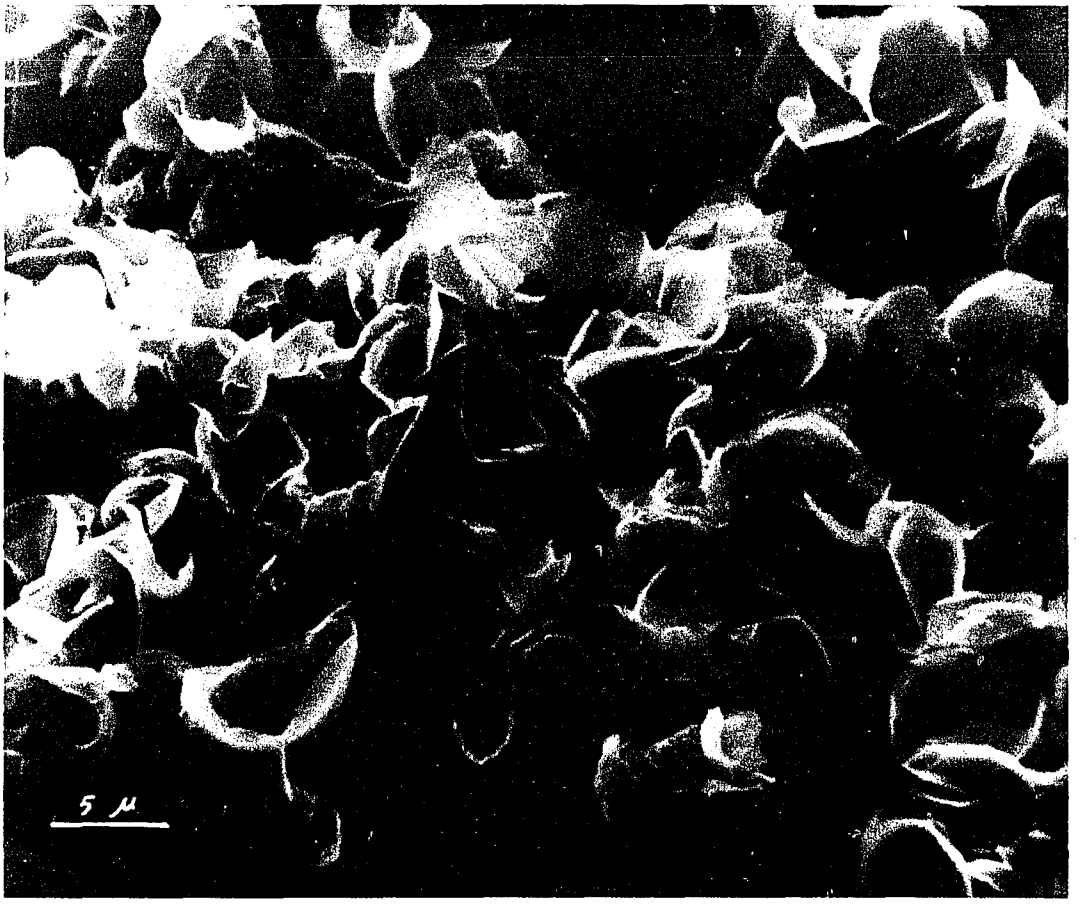

Figure 3.33 Scanning electron micrograph of TPI with $\bar{M}_v=2.6\times10^5$ crystallized from 1% amyl acetate solution at 0°C followed by annealing at 30°C, treated in suspension with OsO_4.

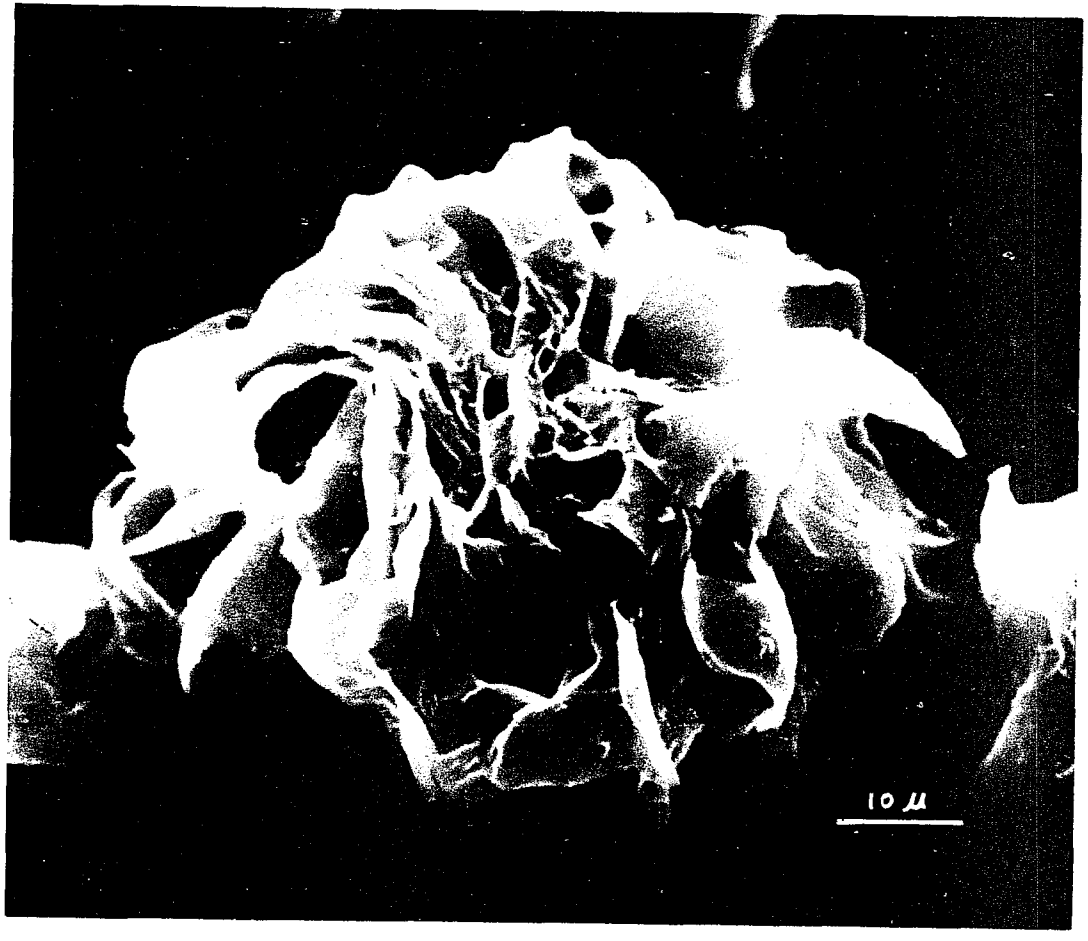

Figure 3.34 Scanning electron micrograph of balata crystallized from 1% amyl acetate solution at 0°C followed by annealing at 30°C, treated in suspension with OsO_4.

in various orientation are observed in Figure 3.32.

When a crystallization temperature of 10°C is used, overgrown curved lamellas and lamellar stacks with a small number of layers (<10) and few, if any, interconnections or branching are the morphologies found for all three of the fractions used. If the TPI is crystallized at 0°C, or is crystallized at 0°C (24 h) followed by slowly heating to 20 or 30°C (the 0/20 or 0/30 procedure), overgrown curved lamellas are the only crystal morphology found regardless of the molecular weight. A representative scanning electron micrograph for the $\bar{M}_v=2.6\times10^5$ preparation is shown in Figure 3.33. When the same crystallization procedures are used for the naturally occurring TPI (balata and gutta percha) different crystalline morphology, curved lamellar aggregates, are seen, one of which is shown in Figure 3.34.

3.2 Epoxidation of TPI Crystals in Suspension

3.2.1 Calculation of <A>, <B> and Fe from ^{13}C NMR Analysis

TPI lamellas and more complex lamellar structures in suspension are expected to react mainly at the surfaces, leading to the formation of (AB)x type segmented block copolymers. The sequences in the block copolymer are sketched in Figure 3.35.

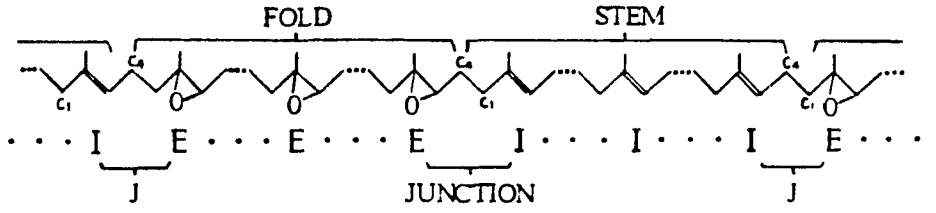

Figure 3.35 The Sequences of Block Copolymer by Epoxidation of TPI Lamellas in Suspension

If reaction at the surface is complete, the average unreacted sequences (I units in Fig.3.35) of monomer units, <A>, characterizes the average number of monomer units in a chain traverse through the crystal core and the average reacted sequences (E units in Fig.3.35) of monomer units, <B>, characterizes an average number of monomer units in the folds, in noncrystallizing chain ends and in interlamellar traverses.

Using the ^{13}C NMR assignments given in Table 2.1, equations for calculating <A>, <B> and the fraction of double bonds reacted, Fe, are as follows:

from the C1 resonances,

$$\langle A \rangle = \frac{2[II(I \text{ or } E)]}{[IEE] + [EII]} + 1 \qquad (3.1)$$

$$\langle B \rangle = \frac{2[EE(E \text{ or } I)]}{[IEE] + [EII]} + 1 \qquad (3.2)$$

from the C4 resonances:

$$\langle A \rangle = \frac{[(E \text{ or } I)II] + [EEI]}{[IIE]} \qquad (3.3)$$

$$\langle B \rangle = \frac{[(I \text{ or } E)EE]}{[IIE]} + 1 \qquad (3.4)$$

$$Fe = \frac{[EE(E \text{ or } I)] + [IEE]}{[II(I \text{ or } E)] + [IEE] + [EII] + [EE(E \text{ or } I)]}$$

or

$$Fe = \frac{\langle B \rangle}{\langle A \rangle + \langle B \rangle} \qquad (3.5)$$

where the square brackets signify areas under the particular resonance. The difference in calculating $\langle A \rangle$ and $\langle B \rangle$ from the C1 and C4 resonances is due to the incomplete separation of C4 EEI and (E or I)II resonances. The data given below are averages of the results for the C1 and C4 carbons. The precision limits of the determinations are $\pm$ 5%.

3.2.2 Effects of Reaction Medium, MCPBA Concentration and Reaction Time

The effects of the reaction medium on the epoxidation of lamellar TPI samples in suspension will be considered first. Unfractionated TPI, crystallized from amyl acetate solution at 0°C and then heated slowly to 30°C in the crystallization liquid, were epoxidized in 15 different reaction mediums mainly at two reaction times. The molar ratio of MCPBA to double bonds in the sample, [M]/[D], was 1 and the concentration was 5.5g/l. ^{13}C NMR results in terms of <A> and <B> are given in Figure 3.36 for the reaction in each liquid with the liquids being grouped according to their functionality. Starting from the left to the right, the points given correspond to: n-butanol, octanol, 2-ethoxyethanol, methanol, ethanol, 3-pentanone, 2-pentanone, methyl ethyl ketone, acetone, 4-methyl-2-pentanone, methyl acetate, ethyl acetate, propyl acetate, amyl acetate and butyl acetate. <B> changes from 4 to 16 and Fe (not shown in Figure 3.36) changes from 0.23 to 0.50 with a change of medium at constant reaction time (14 days), whereas <A> fluctuates by ±12%. When acetate esters are used, a longer reaction time (21-28 days) leads to increases in <B> as shown and increases in Fe up to 0.60 with <A> fluctuating by ±6%. The non-crystalline content of this sample, as measured by density, was 0.37. For all of the acetate esters used Fe exceeds the non-crystalline content after 14 days reaction. The dissolution temperatures of a TPI lamellar sample suspension epoxidized to 35% were measured in nine liquids using a heating rate of 1°C per hour. The results for seven of these are included in Figure 3.36. The sample was insoluble in the other two liquids, methanol and n-butanol, at all temperatures up to the boiling point. It can be observed that as the dissolution temperature for the epoxidized lamellas decreases, <B>, as obtained by reaction carried out in that liquid, increases. The dissolution temperatures of the epoxi-

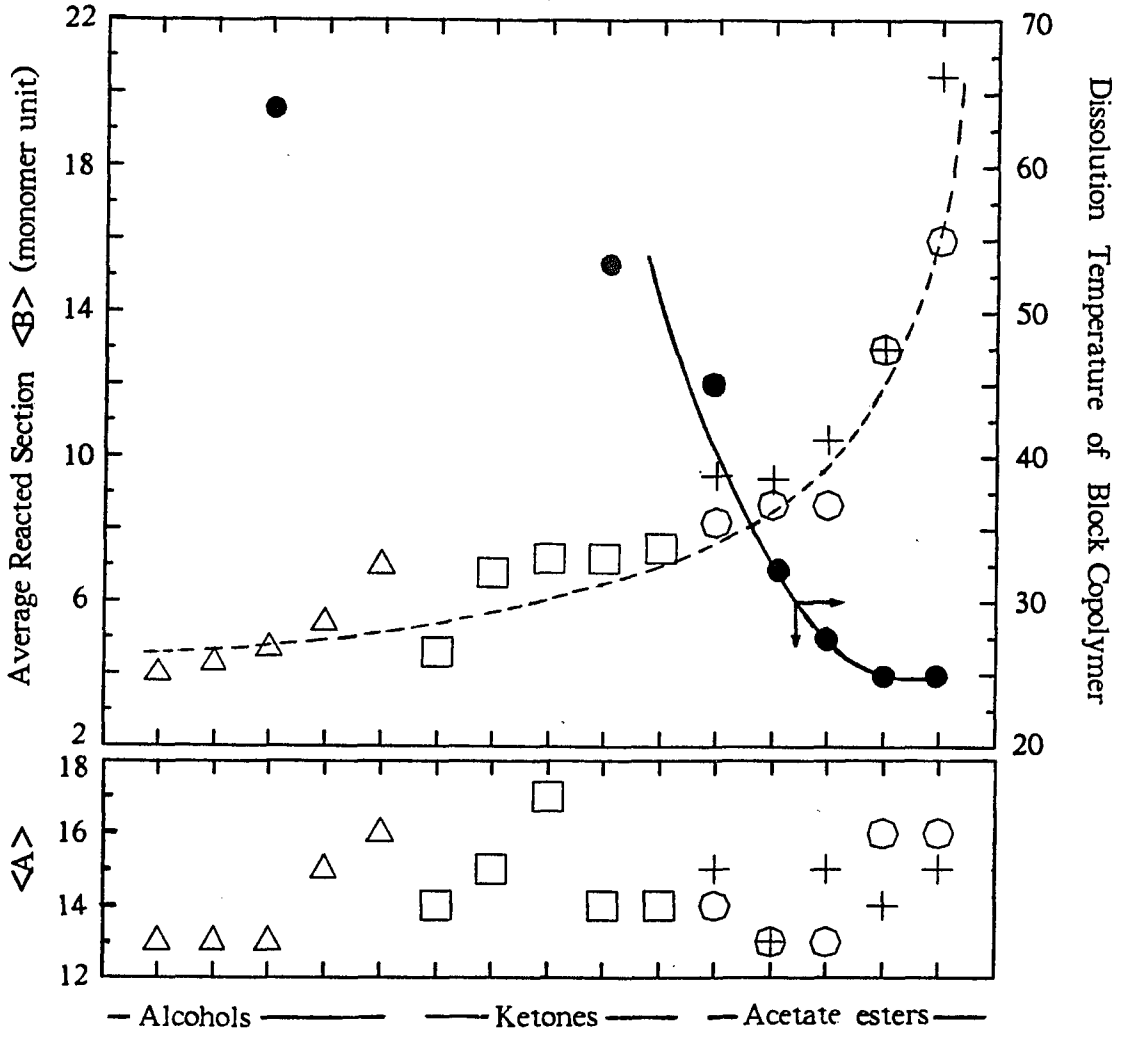

Figure 3.36 Effects of Reaction Medium on Epoxidation of TPI Lamellas

Table 3.1 <A>, <B> and Fe of Epoxidized β-TPI Lamellas at Different [M]/[D] Ratios[a]

Reaction Medium	[M]/[D][b]	Time(day)	Fe	<B>	<A>
Acetone	1	14	0.34	7.2	14
	3	10	0.36	8.2	15
		20	0.42	10.5	15
	4	10	0.41	10.0	15
n-butanol	1	14	0.23	4.0	13
	3	10	0.36	8.9	16
		13	0.38	9.5	15
		17	0.38	9.0	15
		20	0.38	9.3	15

a/ unfractionated TPI crystallized from amyl acetate at 0°C and heated to 30°C in the suspension liquid followed by suspension and epoxidation at 0°C.

b/ the concentrations at [M]/[D]=1,3 and 4 were 5.5g/l, 7.6g/l and 10.1g/l, respectively.

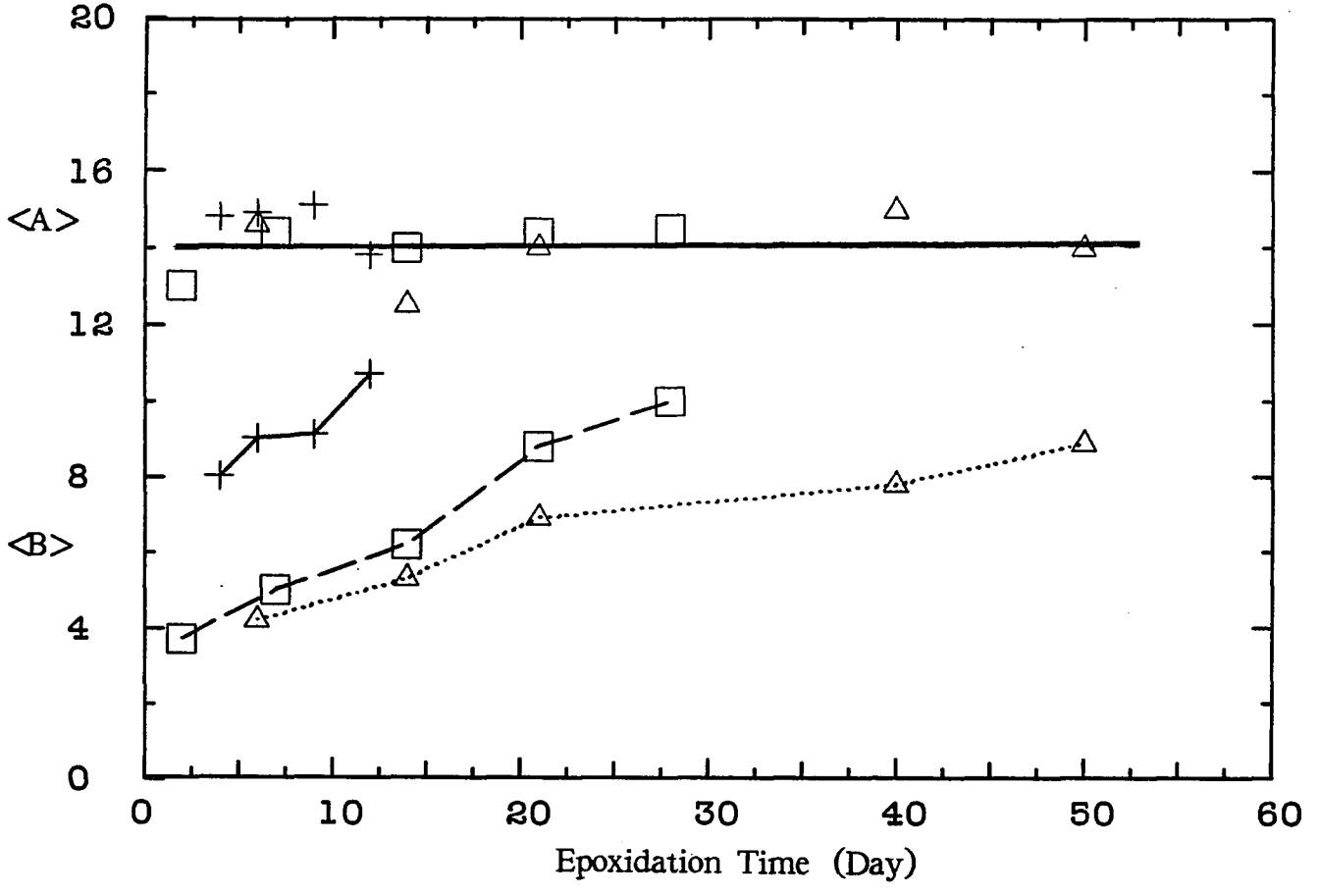

Figure 3.37 Effects of MCPBA Concentration on Epoxidation of TPI Lamellas

△:[M]/[D]=1; □:[M]/[D]=2; +:[M]/[D]=4

Reaction carried out in 2-ethoxythanol; sample crystallized at 20°C with $\bar{M}_v$=2.6×10^5

Table 3.2 The Heat of Fusion of β-TPI and Epoxidized-TPI Lamellas at Different Reaction Levels by DSC

Reaction Medium	Sample	1-Wc[a]	Fe	ΔH_f (J/g)[b]
2-ethoxyethanol	β-single lamellas Tc=20°C	0.38	0	74 ±2
			0.26	72 ±2
			0.40	62 ±3
2-ethoxyethanol	β-curved overgrown lamellas Tc=0/30	0.39	0	75 ±1
			0.34	72 ±1
			0.40	71 ±1
			0.48	65 ±1
n-butanol	β-curved overgrown lamellas Tc=0/30 unfractionated	0.37	0	76 ±3
			0.38	76 ±2 [c]

a: fraction of noncrystalline portion by density using ρ_c =1.02.

b: mean of at least 4 measurements; weight correction for the O atoms of the oxirane according to Fe.

c: average of 5 preparations at the same reaction conditions to a similar reaction level in different time (10-20 days).

dized sample are also found to be lower than the dissolution temperatures of TPI lamellas determined in the same liquid.

The quantity of MCPBA used was found to affect the epoxidation reaction. At lower [M]/[D] in media that are poor solvents the reaction was incomplete, leading to lower <A> and <B>. Reaction results at higher [M]/[D] in three of these liquids are shown in Table 3.1 and in Figure 3.37. <B> and also Fe increase with reaction time while <A> remains constant when using either acetone or 2-ethoxyethanol as suspension liquid. <B> remains constant after 13 days, however, when the reactions are carried out in n-butanol; also in this liquid Fe reached and did not exceed the density value for the non-crystalline content.

Heat of fusion measurements were carried out on unepoxidized and epoxidized lamellas as listed in Table 3.2. The heat of fusion values, ΔH_f are averages of at least four parallel measurements. Preparations reacted in 2-ethoxyethanol show a gradual decrease in ΔH_f with increasing Fe until the latter parameter reaches 1-Wc whereupon ΔH_f drops more strongly. ΔH_f remains constant when n-butanol is used as the reaction medium.

3.2.3 Completion of The Epoxidation Reaction

The fraction of reaction, Fe, for β-TPI single lamellas epoxidized in n-butanol using [M]/[D]=3 is plotted versus reaction time as shown in Figure 3.38. The reaction levels off after 8 days. The Fe value at this level is found to be in a good agreement with the noncrystalline content determined by density and FTIR. Epoxidation in n-butanol at [M]/[D]=3

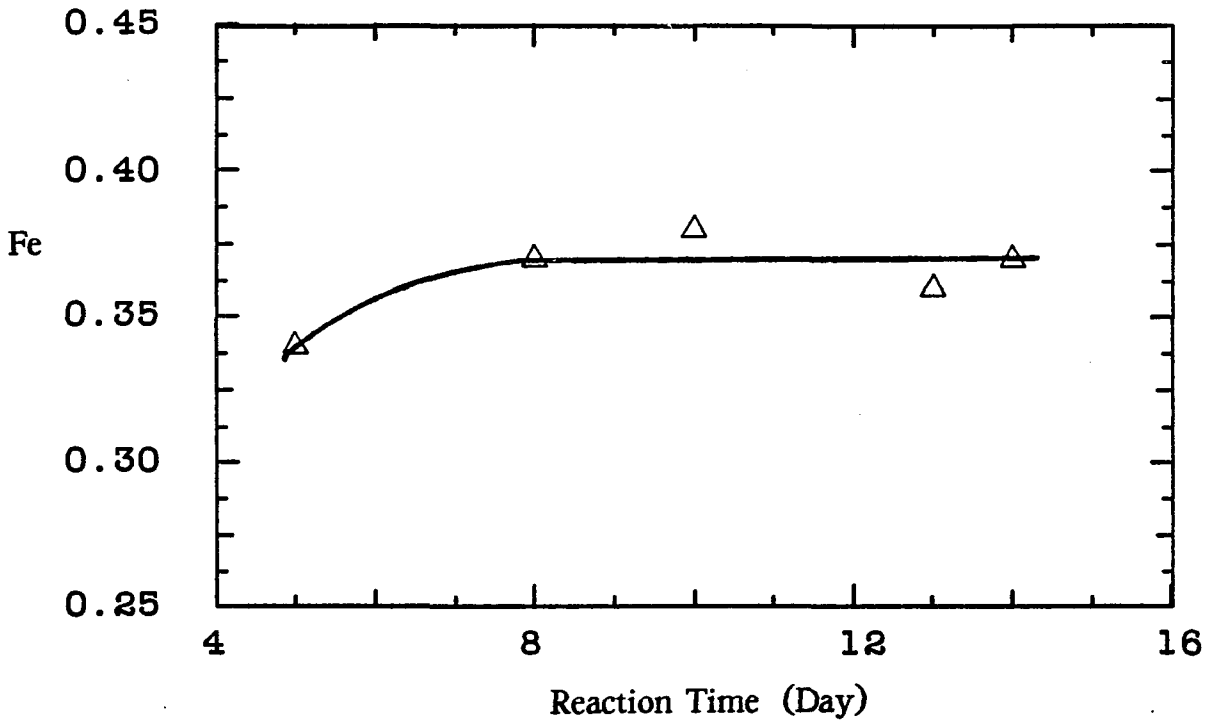

Figure 3.38 Epoxidation of TPI Lamellas at Different Reaction Time

Reaction carried out in n-butanol using [M]/[D]=3 and Co=7.6g/l

was found to be the best conditions for completion of the reaction in a reasonable time and for the avoidance of crystal core penetration and crosslinking. That the suspension liquid itself does not have reaction with and/or degradation effects on the epoxidation reagent to decrease the concentration present has been tested by the experiment of which a MCPBA/n-butanol solution with no crystals present was placed in a 0°C bath for 14 days; TPI sample was then suspended and epoxidized in this "aged" solution; the same reaction level as that from "fresh" solution was still obtained and a large amount of excessive MCPBA was also detected, suggesting that there are no unwanted effects on the epoxidation reaction from the reaction medium.

Complete reaction of the amorphous portion of the lamellas was also evident by examining the FTIR spectra of the lamellas obtained before and after epoxidation[110], as shown in Figure 3.39. Curve (a) of Fig.3.39 is the IR spectrum of β-TPI curved overgrown lamellas before reaction; the spectrum of this sample after epoxidation for 10 days is shown as curve (b) in which the amorphous band at 843cm^{-1} due to C-H out of plane deformation[111] disappears; curve (c) shows a 100% crystalline spectrum obtained by subtracting an amorphous spectrum taken at 65°[111] from the sample spectrum (curve a); and curve (d) is a spectrum of the epoxidized surface obtained by subtracting the 100% crystalline spectrum (curve c) from the epoxidized sample spectrum (curve b). The band at 1663cm^{-1}, attributed to C=C stretching, has been eliminated by such a subtraction. These results clearly suggest that all the double bonds in the amorphous region are reacted under the reaction conditions used.

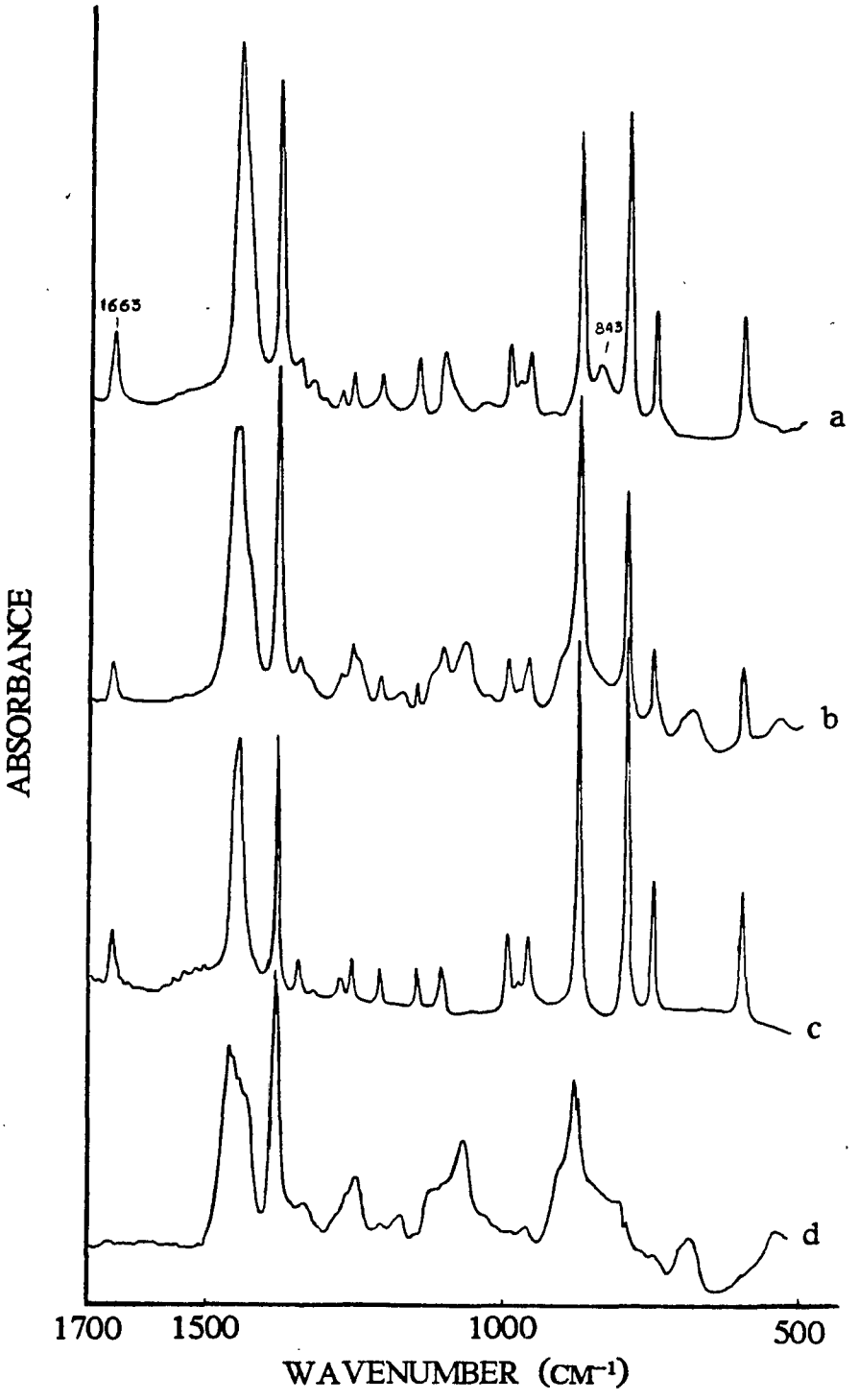

Figure 3.39 FTIR Spectra of β-TPI Lamellas before and after Epoxidation in Suspension

(a) β-TPI lamellas; (b) epoxidized β-TPI lamellas;

(c) 100% crystalline portion; (d) epoxidized surface.

3.3 Quantitative Characterization of the Amorphous and Crystalline Components in TPI Structures from Solution

With the choice of the optimum epoxidation conditions, ^{13}C NMR analysis is used to investigate the effects of molecular weight and crystallization conditions, and therefore the morphology, on the crystalline stem length and the noncrystalline traverse length for TPI structures crystallized from solution. From the preliminary studies given in Section 3.2, the epoxidation medium chosen was n-butanol; the amount of MCPBA was [M]/[D]=3 and the concentration 7.6g/l.

The preparations studied include: (1) single lamellas in the β-crystalline form prepared by the precooling method at crystallization temperatures of 20 and 30°C in amyl acetate (see Figure 3.1(a) for morphology), (2) overgrown curved β lamellar structures crystallized from amyl acetate by cooling directly to 0°C; these were then heated slowly in the crystallization liquid (0.06°C per minute) to 20, 30 and 32°C and annealed for various time periods (see Figure 3.33), (3) α lamellas (two preparations) crystallized by precooling in hexane solution at 25°C (see Figure 3.1(b)), (4) β curved aggregates formed using naturally occurring TPI by the 0/30 procedure (see Figure 3.34) and (5) α sheafs/spherulites crystallized from amyl acetate at 25°C (see, e.g., Figures 3.25 and 3.26). For the latter preparations it was necessary to employ a longer reaction time in order to obtain constant values. All preparations were epoxidized in suspension and the products subjected to ^{13}C NMR measurements.

Totally thirty-four different preparations were investigated. Five of these were studied in triplicate, twenty in duplicate and nine as single determinations. The result for each sample was a mean of data for the

C1 and C4 carbons. The precision for the duplicate and triplicate determinations as well as each C1/C4 pair was within ±5% for both <A> and <B>. All of the data are given in Appendix I.

The results of ^{13}C NMR analysis in terms of the averages obtained for <A>, <B> and Fe for the five types of preparations are given in Table 3.3. Most of these results, plotted in terms of <A> and <B> vs. molecular weight, are given in Figures 3.40 and 3.41. All the samples studied show a decrease in the average stem length, <A>, with increasing molecular weight, as can be seen in Figure 3.40. However, many of these are within the precision limits expected for these measurements except for the overgrown curved β lamellar sample cooled to 0°C and annealed to 20°C for 40 hours for which it corresponds to a 1.1 nm (2.3 monomer units) change from the lowest to the highest molecular weight fractions. For a corresponding molecular weight fraction, the <A> values are in the order: single β lamellas $\simeq$ single α lamellas > overgrown curved β lamellas annealed at 30°C $\simeq$ β curved aggregates of natural TPI > α spherulites > β curved lamellas annealed at 20°C. The change observed in <A> with a change in the morphology is largest at the high molecular weight fractions and corresponds to 1.4 nm (2.9 monomer unit). The <A> values of structures crystallized at 0°C are around 13 monomer units for all fractions (not recorded in Table 3.3); after slowly annealing to 20°C and keeping the suspension at this temperature for 40 hours, <A> increases to 15.7 for the lowest molecular weight fraction with $\bar{M}_v=5\times10^4$; but this increase in <A> decreases with increasing molecular weight. When the sample are annealed to 30°C, a similar increase in <A> is obtained for all fractions.

It is seen in Table 3.3 and Figure 3.41 that for all the samples studied

Table 3.3 <A>, <B> and Fe of TPI Structures by ^{13}C NMR

Crystn. method	Tc °C	Concn. w/v	Morphology	$\bar{M}_v$ $\times 10^{-5}$	<A>	<B>	Fe
precooling	20	0.1	β-single lamellas	0.5	16.5	8.1	0.33
				1.4	16.5	8.8	0.35
				2.6	15.5	9.0	0.37
				5.9	15.8	9.1	0.37
precooling	30	0.1	β-single lamellas	1.4	16.8	8.4	0.33
				2.6	16.6	9.0	0.35
				5.9	16.3	8.9	0.36
precooling in hexane	25	0.1	α-single lamellas	2.6	15.9	8.6	0.35
direct & annealed	0/20	1	β-curved overgrown lamellas	0.5	15.7	8.0	0.34
				1.4	15.2	8.5	0.36
				2.6	14.6	10.8	0.43
				5.9	13.8	13.3	0.49
				7.0	13.4	12.2	0.48
direct & annealed	0/30	1	β-curved overgrown lamellas	0.5	16.6	8.0	0.33
				1.4	15.8	8.3	0.35
				2.6	15.6	9.6	0.38
				5.9	15.3	10.6	0.41
				7.0	15.6	10.9	0.41
direct	25	1	α-sheafs/ spherulites	1.4	14.7	7.9	0.35
				2.6	14.6	9.8	0.40
				5.9	14.2	10.5	0.42
direct & annealed	0/30	1	β-curved aggregates natural TPI	3.0	15.5	9.4	0.38

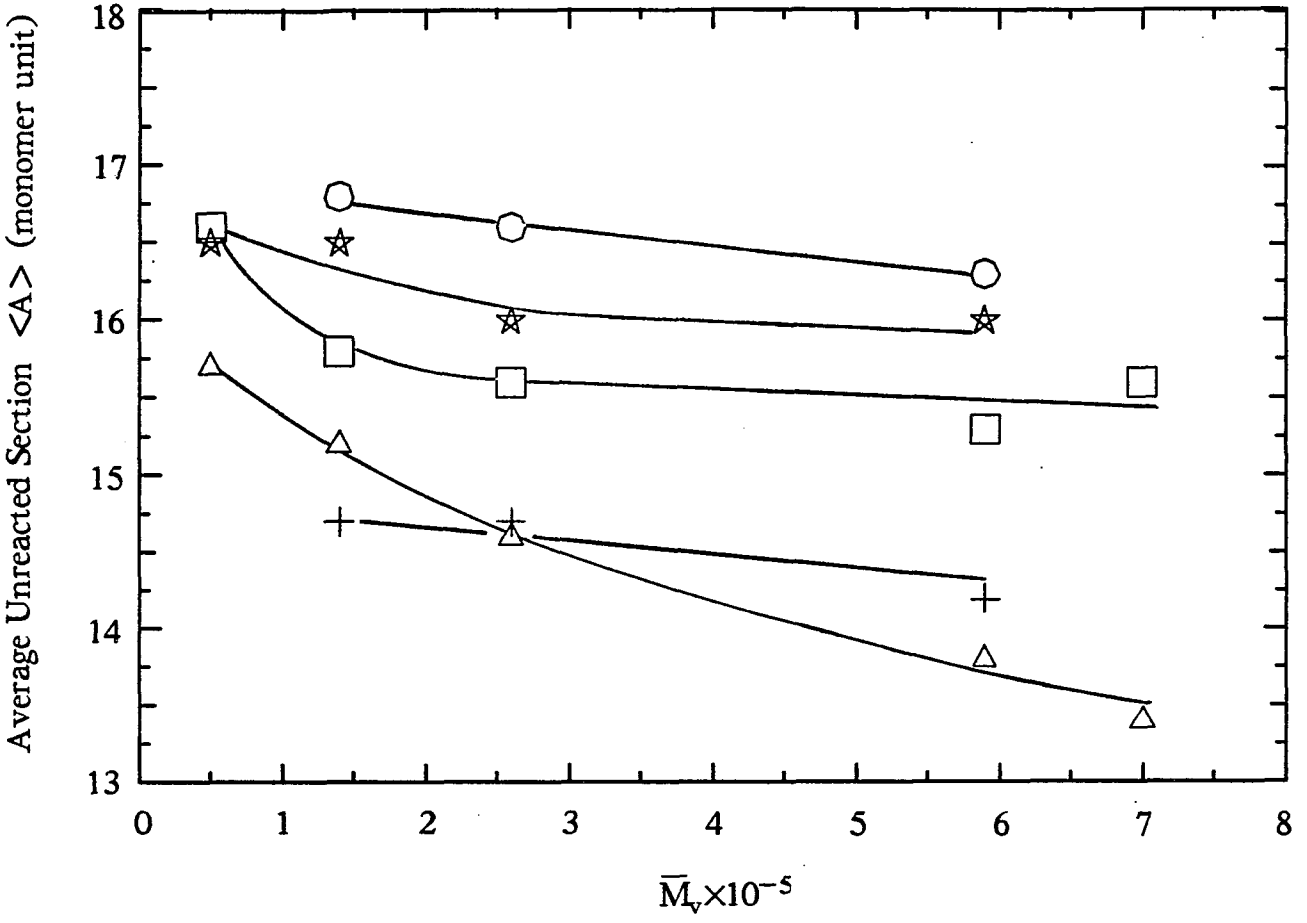

Figure 3.40 The Unreacted Block Length <A> versus Molecular Weight for Single and Multilamellas TPI Structures

(☆) β-single lamellas Tc=20°C; (○) Same but Tc=30°C; (△) overgrown curved β-lamellas Tc=0/20; (□) same but Tc=0/30; (+) α-sheaves/spherulites Tc=25°C.

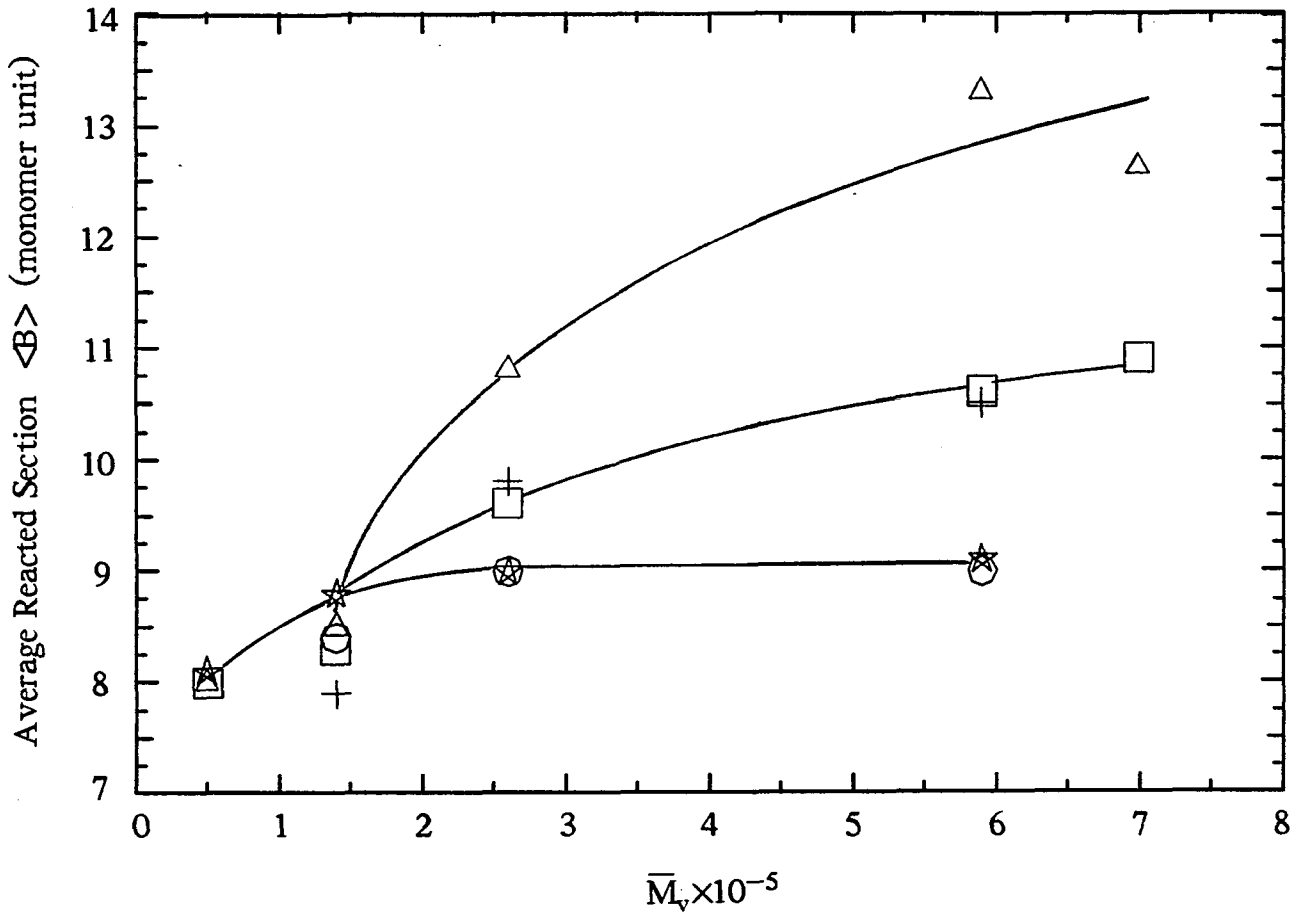

Figure 3.41 The Reacted Block Length <B> versus Molecular Weight for Single and multilamellar TPI Structures

same legend as Figure 3.40

<B> shows a value of 8.3 ±0.3 at the lower molecular weights but then exhibits wide divergences at larger molecular weight values. With increasing molecular weight the <B> values for single lamellas samples show about a 10% change initially then levelling off; while for the sample cooled to 0°C and annealed to 20°C, as much as 50-60% change occurs with a 14-fold molecular weight increase and a 35% change for the 0/30 preparations. It is also evident that at higher molecular weights (> 2.6×10^5) all multilamellar structures show larger <B> values than the single lamellas from similar fractions.

The effects of longer annealing times, higher annealing temperature and higher crystallization concentrations on the overgrown curved β lamellas are shown in Table 3.4. Increasing the annealing time at 20°C and at 30°C from 40 hours to one week caused no significant change in <A> for samples with $\bar{M}_v$ from 1.4×10^5 to 5.9×10^5. With this change in annealing time a significant decrease in <B> by 1.8 units occurs for the sample with $\bar{M}_v$ of 5.9×10^5 annealed at 20°C. The results of the following treatments did not differ significantly from those for the samples annealed at 30°C for 40 hours: i) annealing for two weeks at 30°C ($\bar{M}_v=5.9\times10^5$), ii) annealed at 20°C for 40 hours followed by an increase to 30°C for one week ($\bar{M}_v=2.6\times10^5$), iii) annealed at 32°C, which is only 2° below its T_R, for 40 hours ($\bar{M}_v=2.6\times10^5$) and iv) change of the crystallization concentration to 3, 4 and 5% (w/v) with crystallization at 0°C and annealing at 30°C for 40 hours ($\bar{M}_v=2.6\times10^5$). The morphology of the higher concentration preparations is very similar to that of 1% ones.

In Table 3.5, the noncrystalline contents of TPI preparations by both density and FTIR measurements are given and are compared with the fractions of epoxidation of these samples by ^{13}C NMR analysis. For all the

Table 3.4 Effects of Annealing Treatments and Crystallization Concentration on TPI Structures

Crystn. method	Tc °C	Concn. w/v	Morphology	$\bar{M}_v$ $\times 10^{-5}$	<A>	<B>	Fe
direct & annealed	0/20 at 20°C 1 wk	1	β-curved overgrown lamellas	1.4 2.6 5.9	15.5 14.4 13.2	8.0 10.8 11.5	0.34 0.43 0.47
direct & annealed	0/30 at 30°C 1 wk	1	β-curved overgrown lamellas	1.4 2.6 5.9	15.6 16.1 14.8	7.7 9.8 10.8	0.33 0.38 0.42
direct & annealed	0/30 at 30°C 2 wk	1	β-curved overgrown lamellas	5.9	14.5	10.9	0.43
direct & annealed	0/20 (40 h) 20/30 (1 wk)	1	β-curved overgrown lamellas	2.6	15.2	9.8	0.39
direct & annealed	0/32	1	β-curved overgrown lamellas	2.6	15.7	9.8	0.38
direct & annealed	0/30	3 4 5	β-curved overgrown lamellas	2.6 2.6 2.6	15.1 15.2 15.2	9.7 10.3 10.4	0.39 0.40 0.41

Table 3.5 Fraction of Noncrystalline Portion of TPI Structures by ^{13}C NMR, FTIR and Density

Tc (°C)	$\bar{M}_v$ $\times 10^{-5}$	Fe (^{13}C NMR)	1-Wc [a] (FTIR)	1-Wc [b] (Density)
20	0.5	0.33	0.33	0.33
	1.4	0.35	0.35	0.35
	2.6	0.37	0.37	0.38
	5.9	0.37	0.37	0.39
30	1.4	0.33		0.31
	2.6	0.35	0.36	0.36
	5.9	0.36	0.37	0.35
0/20	0.5	0.34	0.34	0.35
	1.4	0.36	0.36	0.37
	2.6	0.43	0.43	0.40
	5.9	0.49	0.50	0.47
	7.0	0.48	0.45	
0/30	0.5	0.33	0.35	0.32
	1.4	0.35	0.35	0.32
	2.6	0.38	0.38	0.39
	5.9	0.41	0.42	0.40
	7.0	0.41	0.42	0.39
0/20	1.4	0.34	0.36	0.37
at 20°C	2.6	0.43	0.42	0.41
1 wk	5.9	0.47	0.47	0.44
0/30	1.4	0.35	0.35	0.35
at 30°C	2.6	0.38	0.39	0.38
1 wk	5.9	0.41	0.42	0.40

a: average of at least two parallel measurements for each preparation; average deviation error ±0.01.

b: also mean of at least two measurements; sample used without pressured; a.d.e. ±0.01; ρ_c =1.02 as calculated from unit cell parameters in ref.[37].

22 samples, differing in molecular weight and/or crystallization conditions, values of 1-Wc are very close to the values of Fe. The Fe values range from 0.33 to 0.49 and those from both infrared and density agree within 0.03, suggesting that the surface reaction is complete without further unwanted effects. Samples used for the density measurement were unpressed dried mats. These mats are dense solid pieces for all the samples listed. The reason for using unpressed samples is that an unexpected drop in density, yielding a 0.04 to 0.08 drop in the crystallinity, has been found for the samples that have been pressed at 3×10^5Pa attempting to eliminate air[112]. The density results of pressed and unpressed samples are given in Table 3.6.

Table 3.6 Densities of TPI lamellas for Pressed and Unpressed Samples

Crystn. method	$\bar{M}_v$ $\times 10^{-5}$	Density [a] (pressed)	1-Wc [b] (pressed)	Density (unpressed)	1-Wc [b] (unpressed)
precooling	1.4	0.967	0.43	0.977	0.35
Tc=20°C	2.6	0.964	0.46	0.973	0.38
	5.9	0.966	0.44	0.972	0.39
direct &	1.4	0.970	0.41	0.976	0.35
annealed	2.6	0.965	0.45	0.972	0.39
0/30	5.9	0.967	0.44	0.971	0.40

a: samples pressured at 3×10^5Pa.

b: ρ_c = 1.02 as calculated from unit cell parameters in ref.[37].

4. Discussion

4.1 The Morphology

In the present study, it is found that at moderate crystallization temperature (20°C) the morphology of trans-1,4 polyisoprene directly crystallized from 1% amyl acetate solution changes with molecular weight ($\bar{M}_v$) in the 1.4–5.9×10^5 range and with crystallization time. The change with molecular weight is from stacks of overgrown lamellas that are curved and interpenetrating to rounded structures made up of ribbons to spherulites containing twisted and curved lamellas. The large structures observed at short crystallization times for the two fractions with the lower molecular weights apparently start as lamellar stacks and become large due to the presence of relatively few nuclei, since the size of the polymer crystals depends on the number of nuclei in the system at given crystallization conditions. These large structures could possibly grow from nuclei previously formed and not destroyed by the thermal treatment before crystallization; however, if this was the case similar structures would be expected at lower crystallization temperatures and/or for the higher molecular weight fraction and these are not found. Another possibility is that preferential nucleation of the high molecular weight portion in the fractions occurs before the temperature lowers from Td to 20°C or at early time at 20°C, leading to the large structures. For the high molecular weight fraction, this temperature would be low enough for most of the molecules to nucleate, leading to smaller sized structures due to more nuclei present at the early time. The preferential nucleation of macromolecules with higher molecular weight can be related to the

phenomenon of molecular segregation during crystallization observed in a number of studies on other polymer systems. Studies of such segregation[113,114]on isothermal crystallization of linear polyethylene from dilute solution showed that the precipitated crystals clearly contained the larger molecules, while the filtrate was enriched in shorter molecules. A similar segregation was also proven for crystallization from the melt[115]. Therefore the formation of lamellar stacks observed at longer crystallization times at Tc of 20°C and the absence of such structures at higher crystallization temperatures (25°C and above) could be interpreted in terms of preferential nucleation of larger molecules in the sample. In the former case, subsequent nucleation of the lower molecular weight portion yields a large number of nuclei, resulting in numerous smaller lamellar stacks; while in the latter case, fewer nuclei can be formed at the higher temperatures, leading to larger sized and more completely grown structures.

An optical microscopy investigation of the morphology of naturally occurring trans-1,4 polyisoprene (gutta percha) using three fractions with $\bar{M}_w$=3.6×10^4, 1.6×10^5 and 3.3×10^5 and direct crystallization temperatures of -15 to +32°C was carried out earlier by Kuo and Woodward[47]. Similar TPI sheaves obtained at 20°C were observed, but the lamellar interpenetration and the high degree of curvature clearly in evidence by scanning electron microscopy in this study were not apparent in that work due possibly to the lower contrast and magnification as well as possible motion of the structures in the suspension liquid. Definite morphological differences in these two works do appear for crystallization at 10°C and 0°C in amyl acetate. In the previous study, lamellar stacks, spherulites and "cup-shaped" aggregates of curved lamellas were evident

for gutta percha with $\bar{M}_w=1.6\times10^5$ and 3.3×10^5; whereas in the present investigation using synthetic TPI, crystallization at 10°C and 0°C leads to simpler lamellar stacks with a few layers (at 10°C) and monolayered overgrown curved lamellas (at 0°C) for all the fractions used. These differences could be due to differences in thermal history or the polymer structure. However, different morphologies do appear for the synthetic and the natural TPI with similar molecular weight crystallized under the same conditions in this study (see Figures 3.33 and 3.34), with the latter being similar to that found in the previous work. Therefore, the morphological differences resulted from the two materials are likely due to the difference in the end groups[116] in the macromolecules of these materials and/or slight difference in the trans content (by about 1%)[47]. Previously, spherulites of α-TPI, similar in overall shape to those appearing at 20°C in the current work, were obtained from dibutyl ether at 0°C ($\bar{M}_w=3.3\times10^5$).

The lamellar layers making up the TPI structures are thicker than a single lamella and therefore are overgrown, as is also evident from the formation of mosaic cracks on the surfaces of the layers upon ultrasonically vibrated (Figure 3.12) and the appearance of sublayers on the nitric acid-etched edges of the lamellar structures (Figure 3.13). The overgrown habit of TPI is also found by using transmission electron microscopy for single TPI lamellas grown by the seeding technique, presumably by screw dislocation growth[41]. Interpenetration and branching have been observed in melt-crystallized samples of polyethylene[117,118] and are believed to occur at screw dislocations[119]. In the present work, interpenetrations not only occur at or near the center of the solution-grown TPI lamellar stacks, accounting for the large curvature of the layer on one

side, but also take place more or less randomly along the length of them. The interpenetration and branching act in opposition to one another. Interpenetration keeps adjacent layers together and roughly parallel. Branching causes the stack to thicken at the growing ends and leads to curvature there. When growth is prevented in one direction, such as would occur for structures growing against the container wall, interpenetration could take place more readily. This apparently occurs, particularly at lower concentrations (0.1%) as seen in Figure 3.20. The tendency for the lamellar stacks and the larger rounded objects associated with them to fracture sideways across the center portion when subjected to ultrasonic vibration suggests that this region is under stress, is highly defective, or both. The high curvature of the inner lamellas observable in these structures would be expected to lead to high stresses at the center.

The spherulitic structures found for TPI with $\bar{M}_v=5.9\times10^5$ at a crystallization temperature of 20°C appear to be less tightly packed due to branching and twisting and are made up of ribbons smaller in width than for the structures found for lower molecular weight fractions. The resistance of these spherulitic structures to ultrasonic vibration suggests that due to the differences in construction the center portion is less defective than that of the lamellar stacks.

For the samples crystallized from amyl acetate at 30°C in this work, two types of structures appear; larger, flatter ones apparently grow at the glass surfaces while smaller, more highly curved ones crystallized from solution.

The structures grown at 0°C and annealed to 30°C in this study are curved (dished) overgrown lamellas. The formation of lamellar curvature has been found for a number of polymers crystallized at larger su-

percooling temperatures, such as poly(4-methyl-1-pentene)[120,121], poly(oxymethylene)[18] and poly(chlorotrifluoroethylene)[122], and "cup-shaped" trans-1,4 polyisoprene lamellas[47]. The nonplanar character of the curved lamellas has been explained to be due to the inherent distortion of the subcell in their constituent domains resulting from the bulkiness of the chain folds[121].

In summary, when synthetic trans-1,4 polyisoprene is crystallized from amyl acetate solution, the lamellar morphologies change with molecular weight, crystallization temperatures and time. From higher to lower crystallization temperatures (30° → 0°C), the lamellar morphologies change from complex cylindrical structures to larger rounded objects to lamellar stacks to overgrown curved lamellas, mainly due to the number of nuclei present in the crystallization systems. At the moderate crystallization temperature of 20°C a mixture of two different morphologies is always obtained, most likely due to the effect of segregation of molecules with different molecular weight in the sample. Higher molecular weight molecules nucleate preferentially leading to larger structures, while the lower molecular weight ones nucleate subsequently yielding smaller (perhaps incompletely grown) structures. On the organization of these structures, the lamellar layers formed by overgrowth of a large number of superposed lamellas is the lamellar feature that can be clearly observed. Scanning electron microscopy revealed features, such as lamellar interpenetration and curvature, branching, and twisting, either not seen or not seen clearly with optical microscopy. Constituted via interpenetrating and branching of the lamellar layers, stacks, rounded objects and spherulites are formed.

4.2 The Effects of Reaction and the Epoxidation Mechanism

It was found in this study that when TPI lamellar structures in suspension are epoxidized, both the average reacted block length, <B>, and the fraction reacted, Fe, depend on the liquid medium used. When acetate esters are used, Fe exceeds the noncrystalline fraction calculated from density measurements, suggesting that penetration of the crystalline core of the lamellas occurs. Since <A> keeps relatively constant while <B> and Fe increase, this penetration must take place principally from the lateral surfaces. The double bonds in the chains at the lateral surfaces are expected to react immediately. As the double bonds on the lateral chains reacted to form oxirane rings, two possible forces would promote the isolation of these chains from the sides of lattice: one is the attractive force between the newly formed functional groups and the liquid molecules if a relatively better suspension medium was used, another is the repellency between the oxirane units and the TPI units due to the structural change of lattice elements. If the attractive forces between the epoxidized chains and the liquid medium exceed those between epoxidized-TPI and TPI units and if the folding is mainly to nearby sites along an exposed fold plane, the reacted lateral chains could separate or loosen from the rest of the crystal and allow reaction of the next row of chain formerly inside the crystalline core. This would give a mixture of block copolymer and completely epoxidized TPI chain sequences. As the amount of completely reacted chain sequences increase, <B> would increase but <A> would not change. This proposed process is sketched in Figure 4.1.

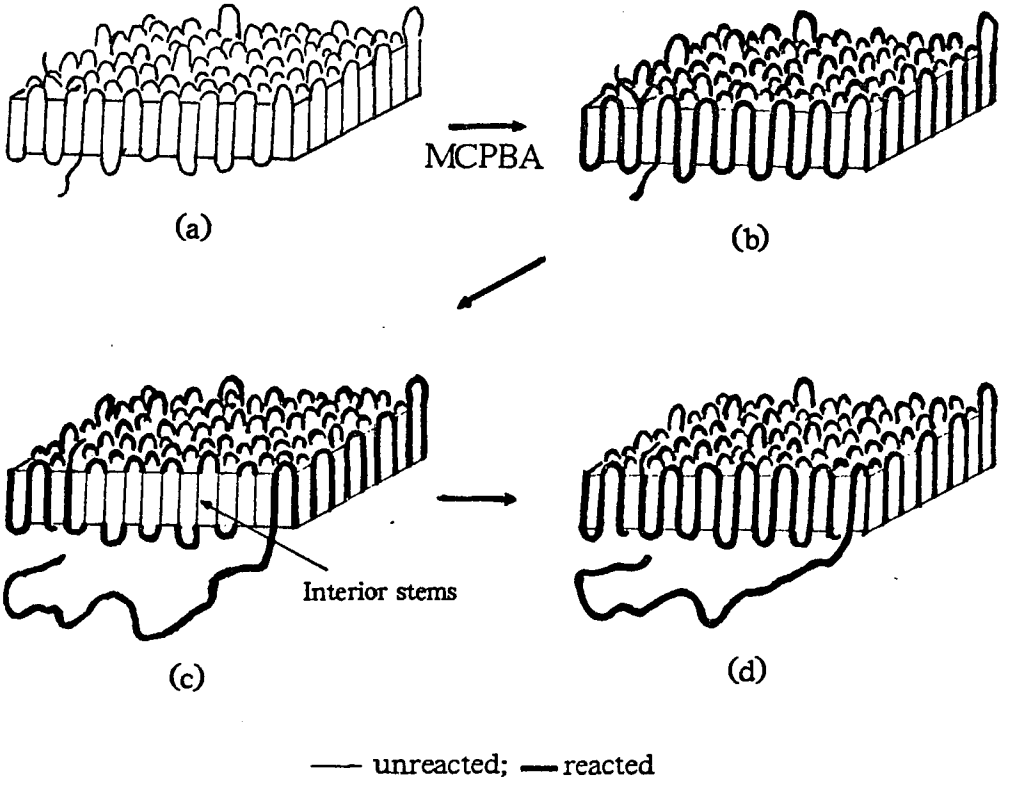

Figure 4.1 The Mechanism of Suspension Medium Effect on Epoxidation

(a) before reaction; (b) fold and lateral surfaces reacted;
(c) separation or loosening of reacted chain due to medium effect, exposing interior stem;
(d) interior stem reacted, leading to <B> and Fe increases.

The results of dissolution temperature experiments for a 65/35 TPI-epoxidized TPI block copolymer in various liquids (see Figure 3.36) support this mechanism. It was found that all of the acetate esters used have lower dissolution temperatures for the epoxidized lamellas than for the unreacted lamellas and as the dissolution temperature decreases, <B> and Fe obtained in that medium increase. Even in liquids with relatively high dissolution temperatures, such as acetone and 2-ethoxyethanol, a separation or loosening occurs at higher [M]/[D] and longer time (see Figure 3.37 and Table 3.1).

The DSC results shown in Table 3.2 are another indication that epoxidized chains separate from the lateral surfaces causing additional reaction. Although the heat of fusion could be affected by the fold thickness[4], it is unlikely that this occurs in this study, because the average unreacted block length did not decrease as Fe increased. Since the value of ΔH_f is proportional to the amount of crystalline content per unit weight of the total system, the decrease in ΔH_f implies a decrease of crystallinity occurring due to conversion of the TPI units in crystal traverses to noncrystallizing epoxidized units as the reaction proceeds.

The electron microscopy studies carried out earlier[41] on α-TPI lamellas epoxidized in amyl acetate showed considerable erosion at the sides as well as some holes in the interior part after reaction. The dissolution temperature for epoxidized TPI in amyl acetate is low and therefore appreciable loss of the lamellar side portion would be expected. The amount of reaction taking place during hydrochlorination of α- TPI lamellas and lamellar structures was found to depend on the reaction medium used[123]. Penetration from the lateral surfaces was also reported in a study of chlorination of polyethylene lamellas[124]. The electron mi-

croscopy observation found that the damage upon washing were along the lamellar edges.

Since the lamellar edges are growth planes and the adjacent chain segments on the edges of crystalline stem are part of the same molecule if assuming dominant adjacent reentry, penetration reaction from the side due to the lateral chain separation favors the presence of chain folding at the crystal surface to nearby sites.An illustration of the lamella assuming random chain reentry is shown in Figure 4.2. The presence of large amount of folding to sites not in adjacent rows is expected to hold the outside lateral crystal traverses in place and therefore lead to less penetration from these surfaces. The proposed mechanism shown in Figure 4.1 therefore probably described the chemically nondestructive modification on the crystalline regions of polymer lamellas in general. In order to obtain quantitative information concerning the lamellar structures using nondestructive chemical methods, a proper reaction medium and the reaction conditions should be carefully chosen.

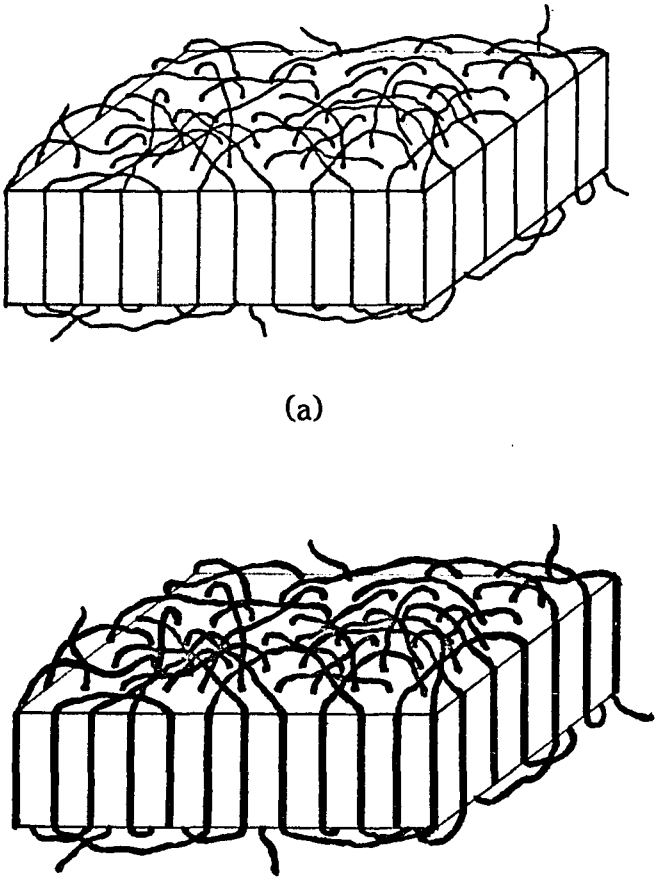

Figure 4.2 Epoxidation of TPI Lamella Assuming Random Chain Reentry

(a) before reaction;

(b) fold and lateral surfaces reacted; the lateral traverses are held so that less interior stem reaction occurs.

4.3 Quantitative Investigations of Chain Folding and Crystalline Stem Length

The attainment of constant values for Fe with reaction time and the agreement of these fractions with the noncrystalline contents from other independent measurements for the various TPI structures suggest that the epoxidation reaction at the fold surfaces is complete and that no significant penetration of the crystal core takes place. Under these conditions the values of <A> and <B> obtained by ^{13}C NMR analysis can be equated with characteristics of the original lamellar structures. <A> is directly related to the average crystalline stem length and therefore to the average thickness of the crystalline core. <B> characterizes all of the lamellar features available for reaction which includes fold surfaces, lateral surfaces, noncrystallizing chain ends and interlamellar traverses. From the dimensions of the lamellas investigated herein, the lateral surface area is estimated to be 2% or less of the total and therefore this effect can be ignored. For the single β lamellas, <B> and Fe show increases with increasing molecular weight over the lower part of the range studied (see Figure 3.40). Similar changes were observed by density measurements for α-TPI lamellas with $\bar{M}_n$ below 10^5 and were attributed previously to the presence of very short noncrystallizing chain ends[47]. <B> for β-TPI single lamellas becomes constant at 9 for higher molecular weight fractions and therefore this value is equated to the average fold length. Comparing the <B> values for all single lamellar preparations listed in Table 3.3, it is found that a 10°C change in crystallization temperature causes little or no change in the average fold length and

that α and β TPI lamellas have similar values for this parameter. The average fold length from this work is about two times that reported for α-TPI lamellas from hydrochlorination/^{13}C NMR results[123] and exceeds by 16% a value resulting from use of the epoxidation/^{13}C NMR method[107]. The Fe values reported in the hydrochlorination study were about 40% lower than the noncrystalline content from density. In light of the present study and current results using the hydrochlorination method[125], it is believed that complete reaction was not obtained in the earlier hydrochlorination work. The α-TPI lamella sample studied in the epoxidation/^{13}C NMR work[107] was epoxidized in amyl acetate at low ratio of [M]/[D] (0.8) and low concentration (2g/l)[126]. The deviation of experimental results from this work would be expected due to the effects of suspension medium and MCPBA concentration on epoxidation as discussed in Section 4.2.

In a recent comparable study of chain folding in trans-1,4 polybutadiene, TPBD, containing 1% cis units and having $\bar{M}_v$ of 2×10^4, <B> ranged in value from 5 to 9, depending mainly on the crystallization temperature, Tc[127]. The change in fold length with Tc was attributed to the rejection of cis and accompanying trans units from the crystal core during the crystallization process; the amount of trans unit rejection was expected to increase with increasing crystalline stem length, <A>, accounting for the increase in <B> with increasing Tc. A statistical treatment assuming a mixture of relatively short folds having a length B' with folds containing rejected units and having a variable length up to a value of <A> -1 was developed to calculate the crystallinity[128]; agreement with experiment was found for B' = 3-4. The average fold length for TPI single lamellas given in the present study is, therefore, two-fold or more

larger than that for TPBD. This cannot be due to the presence of cis units in TPI since no such units were detectable in the synthetic fractions used.

The chain coil dimension, and therefore the flexibility, of a linear polymer molecule can be described in terms of mean square end-to-end distance $\langle r^2 \rangle$ which could be expressed as $\langle r^2 \rangle_o$ in the unperturbed state. If the chain were freely jointed, $\langle r^2 \rangle_o$ would be equal to nl^2 of which n is the number of skeletal bonds and l^2 is their mean square length. The characteristic ratio, $\frac{\langle r^2 \rangle_o}{nl^2}$, thus represents the factor by which the actual, unperturbed dimensions of the chain coil depart from those of freely jointed chain. It is found that the characteristic ratio for TPI (7.4) is 1.3 times larger than for TPBD (5.8) as obtained from solution properties measurements for randomly coiled chains[129,130]. This difference in characteristic ratio was attributed principally to the suppression of gauche states ($\pm$ 120°) about CH_2–CH_2 bonds in TPI due to the presence of the methyl group[130]. The chains in the crystal core are farther apart for TPI than for TPBD, due again to the presence of the methyl group in the former. Both this and the gauche suppression effect can cause the difference in fold length for the two polymers.

A molecular model of a TPI lamella with a β-form crystal core was built to determine the minimum number of monomer units necessary for adjacent folding. The unit cell and the chain conformation and arrangement in the crystal cell are shown in Figure 4.3. When a molecular chain comes out from one site of the crystal core and folds back to an adjacent site, there would be three possible sites to reenter, i.e. the immediate sites along 010, 120 and 100 plane as shown in Figure 4.3(b). How-

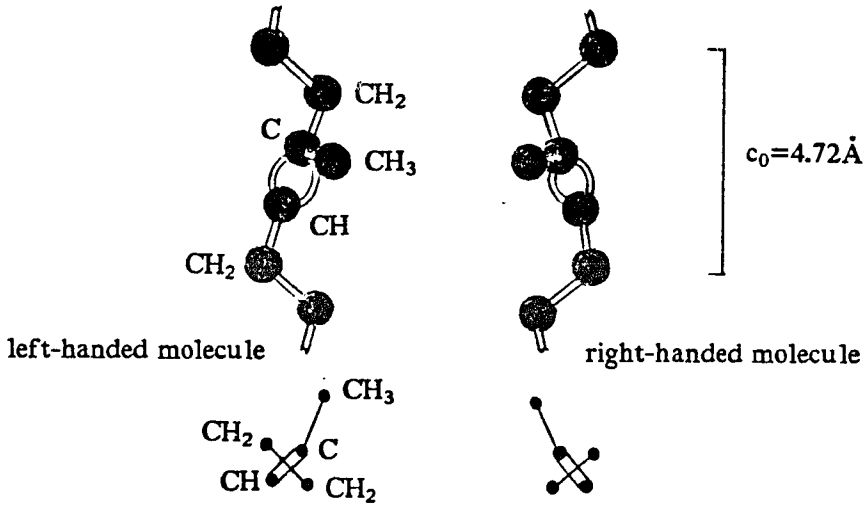

(a)

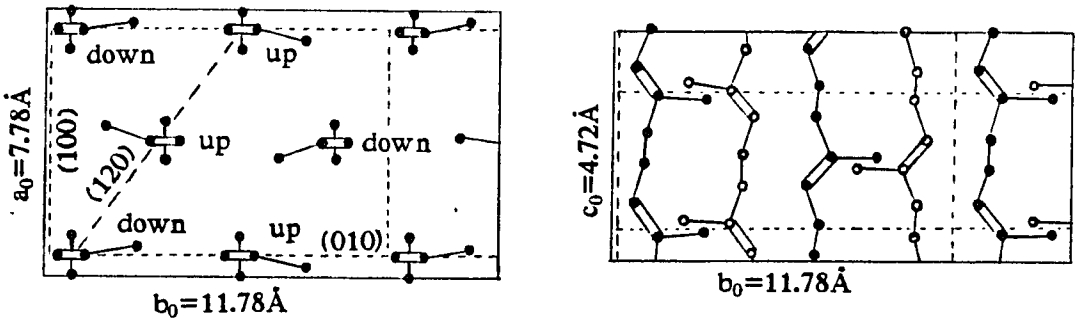

(b) (c)

Figure 4.3 Molecular Structure of β-form TPI Crystal*

(a) chain conformation in an unit cell;

(b) chain arrangement viewed along c axis;

(c) chain arrangement viewed along a axis.

* quoted from ref.[36]

ever, the molecular model shows that reentry along 100 plane is configurationally forbidden (folding along this plane will result in a head-to-head or tail-to-tail chain sequence). When the chain reenters along 010 or 120 planes, the minimum number of monomer units needed for a tightest fold is three.

Therefore, the <B> value of 9 found for TPI single lamellas in this work is considerably larger than that needed for the regularly adjacent reentry folded model. Since the proposed epoxidation mechanism for TPI lamellas discussed in Section 4.2 favors the presence of chain folding at nearby sites, the large value of <B> suggests that a significant amount of nonadjacent but nearby and/or an adjacent reentry with loose folds occurs for the TPI lamellas. These possible chain folding models are sketched in Figure 4.4. Another possibility accounting for the large <B> values could be attributed to the contribution of a physically adsorbed noncrystalline layer on the lamellar surface[82] upon crystallization, the model of which is shown in Figure 4.5. For the lamellar structure proposed, the molecules physically adsorbed on the lamellar surfaces would be expected to react completely with epoxidation reagent and contribute to <B>, leading to a larger <B> value. But this seems to be unlikely in the present study since if this was the case, the fold tightening which leads to the decrease in <B> accompanied by a similar increase in <A> after the annealing treatment would not have occurred, as to be discussed below.

Multilamellar TPI structures in the α and in the β crystalline forms were investigated in the present study. Due to the overgrown nature of these structures, it is possible that a number of interlamellar linkages exist. Each of these, as fully reacted, would count as one fold and contri-

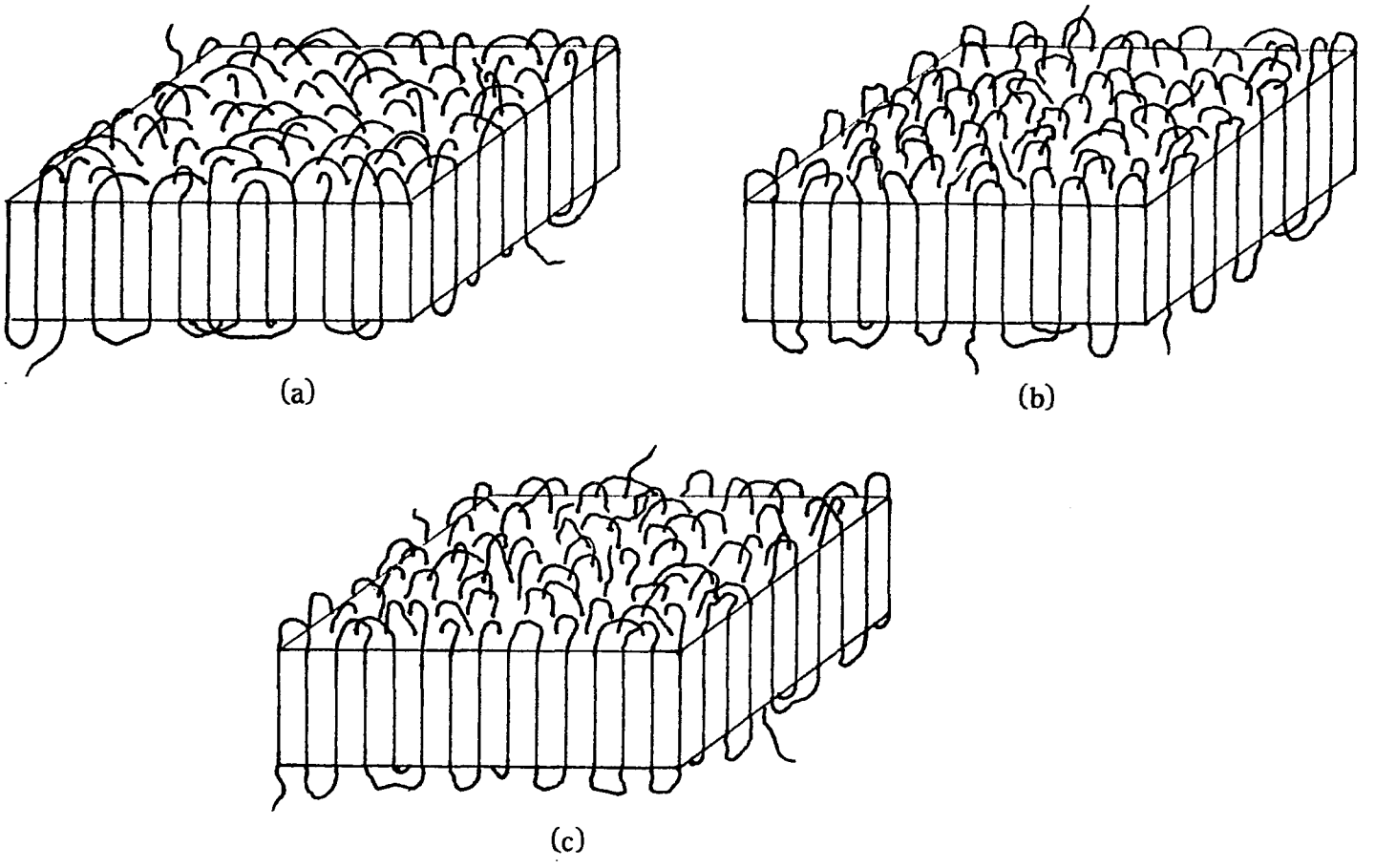

Figure 4.4 Models of Possible Chain Folding Manner for TPI Lamella
(a) dominant nonadjacent but nearby reentry
(b) adjacent reentry with loose folds
(c) a combination of (a) and (b)

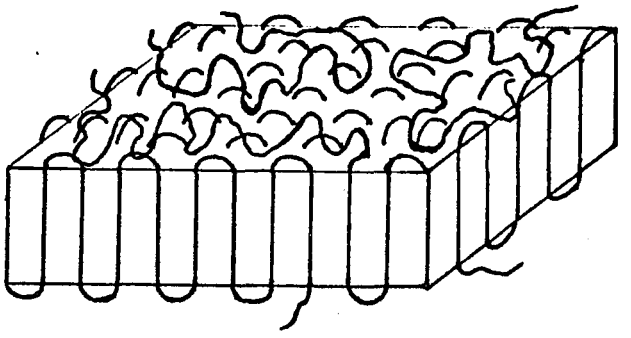

(a)

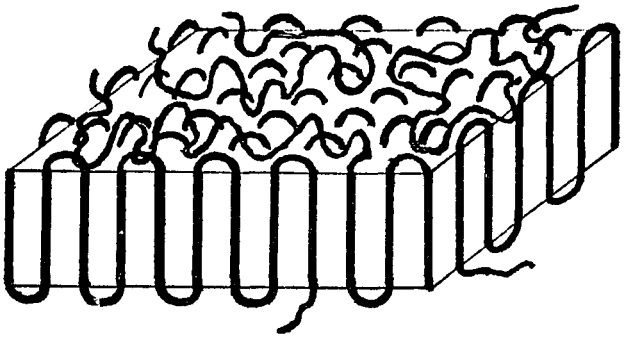

(b)

—— unreacted ▬ reacted

Figure 4.5 Epoxidation of TPI Lamella Assuming Adjacent Reentry with Physically Adsorbed Molecules on the Surface*

(a) before reaction;

(b) fold and the adsorbed molecules on the surfaces reacted leading to larger <B> value.

* sketched after Hoffman[82].

bute to <B>. It is found in Tables 3.3 and 3.4 that the <B> values depend upon molecular weight and on the details of crystallization and annealing; they exceed those found for single lamellas by as much as 60% at the largest molecular weight used. This change could be due to larger length of folds and/or to the presence of interlamellar linkages. The decrease in <B> with an increase in the annealing temperature from 20° to 30°C, with the process being carried out in the crystallization liquid, is accompanied by a similar increase in <A> (compare the 0/20 and 0/30 preparations and the 0/20 and then 20/30 preparation in Table 3.3 and 3.4). These results suggest that significant fold tightening occurs during the annealing process, and that the thickening of lamellas occurs in the direction of crystalline traverses. However, the agreement in <B> values for preparations annealed at 30°C for various time periods up to two weeks with that annealed at 32°C suggests that the folds have reached an optimum value. This fold length should be similar to that measured for single lamellas and any excess in <B> value should be due to interlamellar traverses longer than the average fold length. This conclusion is supported by the <B> value differences between α-sheafs/spherulites and α single lamellas. There is a difference in the concentrations used for single lamella preparations (0.1%) and multilamellar structures (1%), which could contribute to the difference in <B> values measured. However, no effects of concentration on <A> or <B> was found in this work in the 1 to 5% range. A recent study of TPBD structures also showed no concentration effects in the 0.05 to 5% region[127].

Since interlamellar traverses are present in the amorphous phase between lamellas, as stated above, each of them would be counted as one fold when epoxidized and would contribute to the <B> value. The shor-

test interlamellar linkage would be between adjacent sites on two adjacent lamellas, and, on average, should be equal in length to one extended fold, or at least equal to the sum of two amorphous surface layers. However, the chain entry from one lamella to another does not have to be in adjacent sites, and there would be space between two surface layers of adjacent lamellas; the average length of the interlamellar traverses would be thus expected to be larger than the minimum average fold length by a significant amount.

To estimate the average thickness of the amorphous interlayers, an equation derived by Woodward et al.[104] to calculate the crystalline core thickness, Lc, of TPBD lamellas can be used:

$$Lc = \frac{\rho_a \, Wc \, L}{\rho_a \, Wc + \rho_c(1-Wc)} \qquad (4.1)$$

where L is the total thickness of a lamella, assuming that the crystalline core with thickness Lc is sandwiched between two noncrystalline surface layers. It was also assumed that Lc is directly proportional to the crystallinity Wc and inversely proportional to ρ_c and that the thickness of the two amorphous layers, or the minimum thickness of the amorphous interlayers between lamellas, La, is directly proportional to (1-Wc) and inversely proportional to ρ_a. La can then be calculated by:

$$L - Lc = La = \frac{Lc \, \rho_c \, (1-Wc)}{\rho_a \, Wc} \qquad (4.2)$$

Table 4.1 shows La values for some multilamellar preparations using

Table 4.1 Estimation of the Average Thickness of Amorphous Interlamellar Layers *

Preparation	$\bar{M}_v \times 10^{-5}$	La (monomer unit)
overgrown curved β-lamellas annealed at 20°C	1.4	10
	2.6	12
	5.9	15
overgrown curved β-lamellas annealed at 30°C	1.4	9
	2.6	11
	5.9	12
α-sheafs/spherulites	1.4	9
	2.6	11
	5.9	12

* using eq. (4.2); (1-Wc) values used coming from Table 3.5, and Lc values from <A> of Table 3.3; ρ_a = 0.905 quoted from ref. [44]; ρ_c = 1.05 for α-form and ρ_c = 1.02 for β-form quoted from ref. [38] and [37], respectively.

1-Wc from density and <A> from ^{13}C NMR. All the estimated thickness of amorphous interlamellar layers are larger than 9, suggesting, at least qualitatively, that the average length of interlamellar traverses should be larger than the fold length for the TPI lamellas.

Therefore, in light of the above discussion the <B> excess from that of single lamellas for the overgrown curved β-lamellas annealed at 30°C and for α-sheafs/spherulites can be used to calculate the fraction of monomer units in interlamellar traverses longer than the fold length, Fe(traverse), as follows:

$$Fe(traverse) = \frac{2(\langle B\rangle - \langle B\rangle_o)}{(\langle B\rangle + \langle B\rangle_o)} \qquad (4.3)$$

where $\langle B\rangle_o$ is the value for single lamellas prepared from the same polymer. The values obtained are given in Table 4.2. The fraction of non-crystalline monomer units in interlamellar traverses increases with molecular weight. This is believed to be due to an increase in the number of these traverses at the expense of chain folds with increasing molecular weight. This result is in qualitative agreement with thermal analysis results for melt crystallized polyethylene.[131] In order to estimate the actual average length of the interlamellar traverses, the fraction of these traverses, Ft, must be known. This latter parameter can be obtained by equations deduced from a statistical calculation.[132] According to the analysis of Guttman et al.[133], the situation of a chain entering the amorphous interlayer from the crystalline core of a lamella to either form a tie chain (and thereby entering another lamella) or to form a fold (reentering the same lamella) is analogous to the "gambler's ruin" problem. The probability of forming a tie chain or forming a fold is $\frac{1}{Z+1}$

Table 4.2 Fraction of Noncrystalline TPI Units in Interlamellar Traverses *

Preparation	$\bar{M}_v \times 10^{-5}$	Fraction (Ft)
overgrown curved β-lamellas annealed at 30°C	1.4	0
	2.6	0.05
	5.9	0.2
α-sheafs/spherulites	2.6	0.1

* obtained using eq.(4.3); $\langle B \rangle_o$ and $\langle B \rangle$ used as given in Table 3.3 for single lamellas and multilamellas of corresponding molecular weight fraction and crystallization temperature.

and $\frac{Z}{Z+1}$, respectively, where Z is the number of statistical steps in a straight run of total length La between two lamellas. By assuming that the statistical step length is equal to the repeat unit length projected along the chain axis, Ls, one obtains La = ZLs. The probability of forming a tie chain thus can be related to the unit cell parameters and to experimental values of densities, lamellar thickness and molecular weight to obtain equations for calculating Ft. Carrying out this calculation using input parameters for the TPI sample prepared from fraction with $\bar{M}_v=5.9\times10^5$ by cooling to 0°C and annealing at 30°C gives Ft of 0.07.

Since the experimental value <B> includes contributions from both folds and interlamellar traverses, i.e. :

$$<B> = Ft\ <B>t + (1-Ft)<B>o \qquad (4.4)$$

the average length of an interlamellar traverse, <B>t, can be estimated for a known Ft. <B>t estimated for the above sample is 30 monomer units. However, this statistical method predicts that Ft decreases with an increase in the noncrystalline content, or La. This is unlikely since the noncrystalline content increases with molecular weight and therefore Ft increases with increasing noncrystalline content in this work.

Based on the above discussions, an illustration of chain structure for TPI multilamellas can be sketched as shown in Figure 4.6.

It can be concluded from the present study that the fraction of double bonds reacted on lamellas grown in amyl acetate and resuspended in n-butanol, as obtained by ^{13}C NMR, is very close to the noncrystalline content from both infrared and density measurements for various TPI lamellar structures. This agreement suggests that the two-phase model[62]

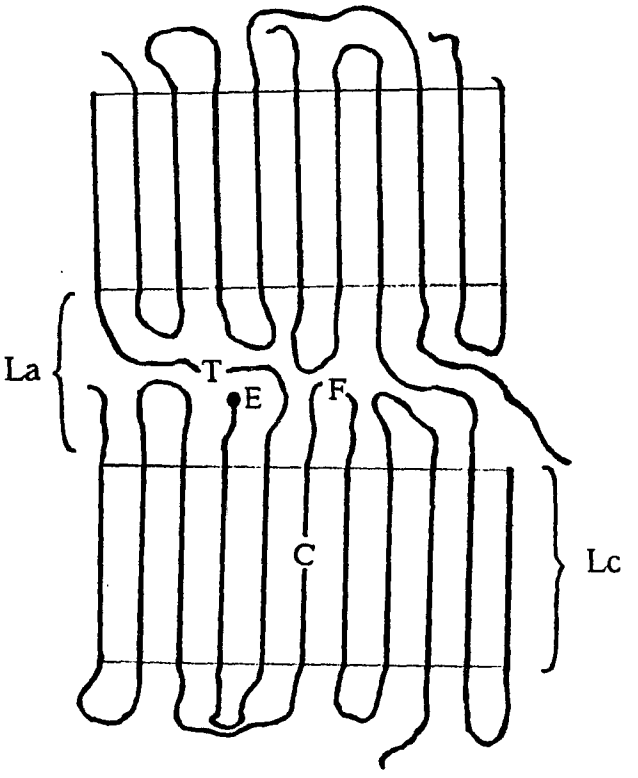

Figure 4.6 Illustration of Chain Structures for TPI Multilamellas

C: crystalline traverse; F: fold;

T: interlamellar traverse; E: noncrystalline chain end;

Lc: crystalline core thickness;

La: noncrystalline layer thickness.

is valid for these structures.

The explanation for the decrease in density for TPI mats upon application of pressure (see Table 3.6) is not yet clear at the present time. A possible explanation could be that pressing introduces collapse of some of the crystalline stems. Evidence for the increase in noncrystalline content due to lamellar collapse and rearrangements upon drying has been reported for polyethylene lamellas[134].

5. Conclusions

The results of this study lead to the following conclusions:

(1) The fine structural appearance of trans-1,4 polyisoprene crystallized from solution can be preserved by treating the samples in suspension with OsO_4. Scanning electron microscopy studies provide a clearly visible observation of these structures.

(2) The morphologies of TPI crystals vary with molecular weight, crystallization temperature and time. The observation of the structural features, such as lamellar layers, curvature, interpenetration and branching, provides useful information for understanding the organization and construction of these TPI crystals.

(3) The extent of epoxidation reaction for the TPI lamellas is dependent on the liquid medium used due to possible penetration from the lateral surfaces. The proposed epoxidation mechanism favors a nearby chain folding reentry .

(4) Optimum conditions for quantitative reaction of the double bond at the lamellar surfaces were found. Segmented block copolymers containing unreacted TPI sections and epoxidized TPI sections can be prepared using n-butanol as the reaction medium.

(5) The resulting block copolymer chain sequences can be quantitatively characterized by ^{13}C NMR analysis in terms of <A>, <B> and Fe to determine the average length of crystal stem and folds, and the amorphous content of the TPI structures.

(6) The average number of monomer unit per fold for the TPI lamellas grown in this study is 9, suggesting a fold with a significant amount of nonadjacent but nearby and/or loose adjacent reentry.

(7) Tie-molecules are detected in the multilamellar TPI structures. The amount of these interlamellar traverses increases with increasing molecular weight.

(8) The fraction of reacted double bonds determined by ^{13}C NMR is in good agreement with the noncrystalline content obtained from infrared measurements and from density determinations for the TPI lamellar structures.

Appendix I Table of ^{13}C NMR measurement results

Crystn. method	Tc °C	Concn. w/v	Morphology	$\bar{M}_v$ $\times 10^{-5}$	Epox. Time(da)	C1 <A>	C1 <B>	C1 Fe	C4 <A>	C4 <B>	C4 Fe
precool 2 days in AA	20	0.1	β-single rectangular	0.5	13	16.2	8.1	0.33	16.7	8.1	0.33
					average: <A>=16.5, <B>=8.1, Fe=0.33						
				1.4	10	16.0	9.0	0.36	16.5	9.1	0.36
					13	16.1	8.3	0.34	17.3	8.6	0.33
					average: <A>=16.5, <B>=8.8, Fe=0.35						
				2.6	10	15.0	9.4	0.39	15.3	8.9	0.38
					13	16.1	8.6	0.35	16.3	8.8	0.35
					14	15.0	9.1	0.38	15.2	9.0	0.37
					average: <A>=15.5, <B>=9.0, Fe=0.37						
				5.9	10	15.2	9.0	0.37	15.9	9.2	0.37
					13	16.1	9.0	0.36	16.3	8.8	0.35
					14	15.4	9.3	0.38	15.8	9.4	0.37
					average: <A>=15.8, <B>=9.1, Fe=0.37						
precool 4 days	30	0.1	β-single rectangular	1.4	10	16.7	8.3	0.33	17.3	8.2	0.32
					13	16.5	8.5	0.34	16.8	8.4	0.33
					average: <A>=16.8, <B>=8.4, Fe=0.33						
				2.6	10	16.1	8.7	0.35	17.2	9.1	0.35
					13	16.7	9.2	0.36	17.2	9.1	0.35
					13	15.9	9.0	0.36	16.6	9.2	0.36
					average: <A>=16.6, <B>=9.0, Fe=0.35						
				5.9	10	16.1	8.9	0.36	16.0	8.6	0.35
					13	16.3	8.8	0.35	16.5	8.9	0.35
					13	16.0	9.1	0.36	16.8	9.3	0.36
					average: <A>=16.3, <B>=8.9, Fe=0.36						

Appendix I table continued:

Crystn. method	Tc °C	Concn. w/v	Morphology	$\bar{M}_v$ $\times 10^{-5}$	Epox. Time(da)	C1			C4		
						<A>	<B>	Fe	<A>	<B>	Fe
precool 2 days in hexane	25	0.1	α-single ellipsoidal	2.6	11	16.2	8.6	0.35	16.1	8.5	0.35
					13	15.7	8.5	0.35	15.7	8.8	0.36
					average: <A>=15.9, <B>=8.6, Fe=0.35						
direct & annealed	0/20	1	β-curved overgrown lamellas	0.5	13	15.7	8.0	0.34	15.6	8.0	0.34
					average: <A>=15.7, <B>=8.0, Fe=0.34						
				1.4	10	14.9	8.7	0.37	15.2	8.7	0.37
					13	14.6	7.8	0.35	16.2	8.6	0.35
					average: <A>=15.2, <B>=8.5, Fe=0.36						
				2.6	10	14.7	10.8	0.42	14.9	10.8	0.42
					13	14.3	10.8	0.43	14.3	10.7	0.43
					average: <A>=14.6, <B>=10.8, Fe=0.43						
				5.9	10	14.1	13.4	0.49	14.0	13.3	0.49
					13	13.4	13.3	0.50	13.6	13.2	0.49
					average: <A>=13.8, <B>=13.3, Fe=0.49						
				7.0	11	13.5	12.1	0.47	13.7	12.0	0.47
					14	13.2	12.4	0.48	13.3	12.1	0.48
					average: <A>=13.4, <B>=12.2, Fe=0.48						
direct & annealed	0/20 at 20° 1 wk	1	β-curved overgrown lamellas	1.4	12	15.4	7.9	0.34	15.9	7.9	0.33
					13	15.0	8.2	0.35	15.8	8.1	0.34
					average: <A>=15.5, <B>=8.0, Fe=0.34						
				2.6	12	14.3	10.4	0.42	15.0	10.6	0.42
					13	14.2	11.1	0.44	13.9	10.9	0.44
					average: <A>=14.4, <B>=10.8, Fe=0.43						
				5.9	12	13.2	11.0	0.45	13.4	11.1	0.45
					13	13.0	11.9	0.48	13.2	11.9	0.47

Appendix I table continued:

Crystn. method	Tc °C	Concn. w/v	Morphology	$\bar{M}_v$ $\times 10^{-5}$	Epox. Time(da)	C1 <A>	C1 <B>	C1 Fe	C4 <A>	C4 <B>	C4 Fe
					average: <A>=13.2, <B>=11.5, Fe=0.47						
direct & annealed	0/30	1	β-curved overgrown lamellas	0.5	13	16.3	8.0	0.33	16.8	7.9	0.32
					average: <A>=16.6, <B>=8.0, Fe=0.33						
				1.4	10	14.9	7.8	0.34	15.4	8.3	0.35
					13	15.8	8.1	0.34	16.9	9.0	0.35
					average: <A>=15.8, <B>=8.3, Fe=0.35						
				2.6	10	15.8	9.6	0.38	15.5	9.4	0.38
					13	15.4	9.7	0.39	15.5	9.7	0.39
					average: <A>=15.6, <B>=9.6, Fe=0.38						
				5.9	10	14.6	10.1	0.41	15.6	10.6	0.40
					13	14.9	10.4	0.41	16.1	11.1	0.41
					average: <A>=15.3, <B>=10.6, Fe=0.41						
				7.0	11	15.6	10.7	0.41	15.8	10.9	0.41
					14	15.4	10.9	0.41	15.5	10.9	0.41
					average: <A>=15.6, <B>=10.9, Fe=0.41						
	0/30 at 30° 1 wk	1	β-curved overgrown lamellas	1.4	12	15.3	7.6	0.33	15.8	7.7	0.33
					average: <A>=15.6, <B>=7.7, Fe=0.33						
				2.6	12	15.9	9.6	0.38	16.3	9.9	0.38
					average: <A>=16.1, <B>=9.8, Fe=0.38						
				5.9	12	14.9	10.8	0.42	14.6	10.7	0.42
					average: <A>=14.8, <B>=10.8, Fe=0.42						
	at 30° 2 wks			5.9	13	14.7	11.0	0.43	14.3	11.1	0.44
					13	14.5	10.8	0.43	14.6	10.6	0.42
					average: <A>=14.5, <B>=10.9, Fe=0.43						

Appendix I table continued:

Crystn. method	Tc °C	Concn. w/v	Morphology	$\bar{M}_v$ $\times 10^{-5}$	Epox. Time(da)	C1 <A>	C1 <B>	C1 Fe	C4 <A>	C4 <B>	C4 Fe
direct & annealed	0/32	1	β-curved overgrown lamellas	2.6	12	15.8	9.5	0.37	15.7	9.5	0.38
					14	15.7	10.1	0.39	15.4	10.0	0.39
					average: <A>=15.7, <B>=9.8, Fe=0.38						
	0/20 20/30 at 30° 1 wk			2.6	12	15.5	9.8	0.39	15.2	9.8	0.39
					14	15.0	9.8	0.40	14.9	9.8	0.40
					average: <A>=15.2, <B>=9.8, Fe=0.39						
direct & annealed	0/30	3	β-curved overgrown lamellas	2.6	11	15.0	9.6	0.39	15.2	9.7	0.39
					average: <A>=15.1, <B>=9.7, Fe=0.39						
		4		2.6	12	15.1	10.2	0.40	15.2	10.3	0.40
					average: <A>=15.2, <B>=10.3, Fe=0.40						
		5		2.6	12	15.1	10.3	0.41	15.3	10.3	0.41
					average: <A>=15.2, <B>=10.4, Fe=0.41						
direct & annealed	0/30	1	β-curved aggregates (natural TPI)	3.0	11	15.5	9.1	0.37	15.8	9.1	0.37
					12	15.2	9.6	0.39	15.1	9.6	0.39
					17	15.4	9.3	0.38	15.8	9.4	0.37
					average: <A>=15.5, <B>=9.4, Fe=0.38						
direct	25	1	α-sheafs/ spherulites	1.4	18	14.7	7.9	0.35	14.7	7.8	0.35
					22	14.4	7.8	0.35	15.1	8.0	0.35
					average: <A>=14.7, <B>=7.9, Fe=0.35						
				2.6	18	14.4	9.7	0.40	14.8	9.8	0.40
					22	14.5	9.9	0.41	14.5	9.9	0.41
					average: <A>=14.6, <B>=9.8, Fe=0.40						
				5.9	18	14.3	10.6	0.43	14.4	10.5	0.42
					22	14.2	10.5	0.42	14.0	10.5	0.43
					average: <A>=14.2, <B>=10.5, Fe=0.42						

7. References

[1] Morawetz, H. "Polymers: The Origins and Growth of a Science", Ch. 9, John Wiley, New York (1985).

[2] Meyer, K. H., "Natural and Synthetic High Polymers", 2nd Ed., Interscience, New York (1950).

[3] Geil, P. H. "Polymer Single Crystals", Interscience, New York (1963).

[4] Wunderlich, B. "Macromolecular Physics", Vol. 1, Academic Press, New York (1973).

[5] Keller, A. in "Growth and Perfection of Crystals", Doremus, R. H. et al. Ed., pp.499, Wiley, New York (1958).

[6] Keller, A. Rep. Prog. Phys., 31(Part 2), 623 (1968).

[7] Keith, H. D. in "Physics and Chemistry of the Organic Solid State", (Fox, D. et al. Ed.), pp. 461, Interscience, New York (1963).

[8] Rees, D. V.; Bassett, D. C. J. Mater. Sci., 6, 1021 (1971).

[9] Fava, R. A. J. Polym. Sci., D: Macromolecular Reviews, 5, 1 (1971).

[10] Khoury, F.; Passaglia, E. in "Treatise on Solid State Chemistry", (Hannay, N. B. Ed.), Vol. 3, pp. 335, Plenum Press, New York (1976).

[11] Keller, A. Phil. Mag., 2, 1171 (1957).

[12] Blundell, D. J.; Keller, A.; Kovacs, A. J. J. Polym. Sci., Phys. *B* 4, 481 (1966).

[13] Blundell, D. J.; Keller, A.; J. Macromol. Sci., Phys. *B* 2, 301 (1968); *ibid.* *B* 2, 337 (1968).

[14] Keller, A. Kolloid Z. Z. Polymere, 219, 118 (1967).

[15] Barnes, W. J.; Price, F. P. Polymer (London), 5, 283 (1964).

[16] Keller, A. Polymer, 3, 393 (1962).

[17] Reneker, D. H.; Geil, P. H. J. Appl. Phys., 31, 1916 (1960).

[18] Khoury, F.; Barnes, J. D. J. Res. Nat. Bur. Std. (U.S.), 78*A*, 95 (1974).

[19] Geil, P. H.; Reneker, D. H. J. Polym. Sci., 51, 569 (1961).

[20] Bassett, D. C.; Keller, A. Phil. Mag. 7, 1553 (1962).

[21] Wunderlich, B.; Sullivan, P. J. Polym. Sci., 61, 195 (1962).

[22] Bassett, D. C.; Keller, A.; Mitsuhashi, S. J. Polym. Sci., *A* 1, 763 (1963).

[23] Bunn, C. W.; Alcock, T. C. Trans. Faraday Soc., 41, 317 (1945).

[24] Keller, A.; Waring, J. R. S. J. Polym. Sci., 17, 447 (1955).

[25] Keith, H. D.; Padden, F. J.,Jr. J. Appl. Phys. 34, 2409 (1963).

[26] Keith, H. D.; Padden, F. J.,Jr. J. Appl. Phys. 35, 1270 (1964).

[27] Keith, H. D.; Padden, F. J.,Jr. J. Appl. Phys. 35, 1286 (1964).

[28] Keith, H. D.; Padden, F. J.,Jr. J. Polym. Sci., Part A, 2, 4339 (1964).

[29] Go, S.; Prudhomme, R.; Stein, R. S.; Mandelkern, L. J. Polym. Sci.,

Polym. Phys. Ed., 12, 1185 (1974).

[30] Mandelkern, L.; Go, S.; Peiffer, D.; Stein, R. S. *ibid.*, 15,1187 (1977).

[31] Maxfield, J.; Mandelkern, L. Macromols., 10, 1141 (1977).

[32] Bassett, D. C. Phil. Mag., 6, 1053 (1961).

[33] Khoury, F. J. Res. Nat. Bur. Std. (U.S.), 70A , 29 (1966).

[34] Olley, R. H.; Hodge, A. M; Bassett, D. C. J. Polym. Sci., Polym. Phys. Ed., 17, 627 (1979).

[35] Olley, R. H.; Bassett, D. C. Polymer, 23, 1707 (1982).

[36] Bunn, C. W. Proc. Roy. Soc. London, Ser. A 180, 40 (1942).

[37] Fisher, D. Proc. Phys. Soc. London, 66, 7 (1953).

[38] Takahashi, Y.; Sato, T.; Tadokoro, H.; Tanaka, Y. J. Polym. Sci., Polym. Phys. Ed., 11, 233 (1973).

[39] Schlesinger, W.; Leeper, H. M. J. Polym. Sci., 11, 203 (1953).

[40] Keller, A.; Martuscelli, E. Makromol. Chem. 151, 189 (1972).

[41] Anandakumaran, K.; Herman, W.; Woodward, A. E. Macromols., 16, 563 (1983).

[42] Communication with Dr. Chaturedi, P. N. whose paper will appear in J. Mater. Sci., Lett. Ed.

[43] Mandelkern, L.; Quinn, F. A. Jr.; Roberts, D. E. J. Am. Chem. Soc., 78, 926 (1956).

[44] Cooper, W.; Vaughan, G. Polymer, 4, 329 (1963).

[45] Lovering, E. G. J. Polym. Sci. Part A, 30, 329 (1970).

[46] Davies, C. K. L.; Long, O. E. J. Mater. Sci., 12, 2165 (1977); 14, 2529 (1979).

[47] Kuo, C.; Woodward, A. E. Macromols., 17, 1034 (1984).

[48] Fischer, E. W. Z. Naturforsch, 12*a*, 753 (1957).

[49] Till, P. H. Jr. Polym. Sci., 24, 301 (1957).

[50] Storcks, K. H. J. Am. Chem. Soc., 60, 1753 (1938).

[51] Jackson, J. B.; Flory, P. J.; Chiang, R. Trans. Faraday Soc., 59, 1906 (1963).

[52] Sharma, R. K.; Mandelkern, L. Macromols., 2, 266 (1969).

[53] Fischer, E. W.; Peterlin, A. Makromol. Chem., 74, 1 (1964).

[54] McCall, D. W.; Anderson, E. W. J. Polym. Sci., *A* 1, 1175 (1963).

[55] Fischer, E. W.; Goddar, H.; Schmidt, G. F. J. Polym. Sci., *B* 5, 619 (1967).

[56] Statton, W. O.; Geil, P. H. J. Appl. Polym. Sci., 3, 357 (1960).

[57] Keller, A. Faraday Discuss. Chem. Soc., 68, 145 (1979).

[58] Keller, A. Kolloid Z. Z. Polymere, 197, 98 (1964).

[59] Holland, V. P.; Lindenmeyer, P. H. J. Appl. Phys., 36, 3049 (1965).

[60] Hoffman, J. D.; Lauritzen, J. I.; Passaglia, E.; Ross, G. S.; Frolin, L. J.; Weeks, J. J. Kolloid Z. Z. Polymere, 231, 564 (1969).

[61] Flory, P. J. J. Am. Chem. Soc., 84, 2857 (1962).

[62] Fischer, E. W.; Schmidt, G. Angew. Chem., 74, 551 (1962).

[63] Bassett, D. C.; Frank, F. C.; Keller, A. Phil. Mag., 8, 1739 (1963).

[64] Bank, M. I.; Krimm, S. J. Polym. Sci., Part A-2, 7, 1785 (1969); J. Appl. Phys., 39, 4951 (1968).

[65] Ching, J.; Krimm, S. J. Appl. Phys., 46, 4181 (1975).

[66] Jing, X.; Krimm, S. J. Polym. Sci., Polym. Phys. Ed., 20, 1155 (1982).

[67] Sadler, D. M; Keller, A. Polymer, 17, 37 (1976).

[68] Sadler, D. M; Keller, A. Macromols., 10, 1128 (1977).

[69] Sadler, D. M; Keller, A. Science, 203, 263 (1979).

[70] Williams, T.; Blundell, D. J.; Keller, A.; Ward, I. M. J. Polym. Sci., Part A-2, 6, 1613 (1968).

[71] Williams, T.; Keller, A.; Ward, I. M. *ibid.*, 6, 1621 (1968).

[72] Flory, P. J. "Statistical Mechanics of Chain Molecules", Wiley & Sons, (1969).

[73] Yoon, D. Y.; Flory, P. J. Faraday Discuss. Chem. Soc., 68, 288 (1979).

[74] Fischer, E. W.; Stamm, M; Dettenmaier, M; Herchenroder, P. Polymer preprints, 20, 219 (1979).

[75] Schelten, J.; Ballard, D. G. H.; Wignall, G. D.; Longman, G.; Schmatz, W. Polymer, 17, 751 (1976).

[76] Summerfield, G. C.; King, J. S.; Ullman, R. J. Appl. Cryst., 11, 548 (1978).

[77] Mandelkern, L. J. Polym. Sci., C, 50, 457 (1975).

[78] Mandelkern, L. Progr. Polym. Sci., 2, 165 (1970); Faraday Discuss. Chem. Soc., 68, 310 (1979).

[79] Keller, A.; Martucelli, E.; Priest, D. J.; Udagawa, Y. J. Polym. Sci., A 2, 1807 (1971).

[80] Roe, R. J.; Bair, H. E. Macromols., 3, 454 (1970).

[81] Keller, A. J. Polym. Sci., Symposium, 51, 7 (1975).

[82] Hoffman, J. D.; Davis, G. T. J. Res. Natl. Bur. Stand. Sec. A, 79, 613 (1975).

[83] Mandelkern, L. J. Polym. Sci., Symposium, 54, 85 (1976).

[84] Keith, H. D.; Padden, F. J. Jr. J. Polym. Sci., 41, 525 (1959).

[85] Keith, H. D.; Padden, F. J. Jr.; Vadimsky, R. G. J. Polym. Sci., A-2, 4, 267 (1966).

[86] Davis, H. A. J. Polym. Sci., A-2, 4, 1009 (1966).

[87] Clark, E. S. SPE J., 23(7), 46 (1967).

[88] Hase, Y.; Geil, D. H. J. Macromol. Sci., Phys. B 7, 1 (1973).

[89] Rybnibar, F.; Geil, D. H. J. Macromol. Sci., Phys. B 7, 1 (1973).

[90] Slichter, W. D. J. Appl. Phys., 31, 1865 (1961).

[91] Miller, R. L. "Crystalline Olefin Polymers", Wiley, New York (1965).

[92] Geil, P. H. Polym. Rev. 5 (1963).

[93] Hoffman, J. D.; Davis, G. T. in "Treatise on Solid State Chemistry", Vol.3, Ch. 7, Hannay, N. B. Ed., Plenum Press (1976).

[94] Jackson, J. F.; Mandelkern, L. Macromols., 1, 546 (1968).

[95] Bair, H. E.; Salovey, R. J. Macromol. Sci., *B* 3, 3 (1969).

[96] Ergoz, E.; Mandelkern, L. J. Polym. Sci., *B* 10, 631 (1972).

[97] Keller, A.; Priest, D. J. J. Macromol. Sci., *B* 2, 479 (1968).

[98] Keller, A. J. Polym. Sci., Polym. Phys. Ed., 13, 2259 (1975).

[99] Woodward, A. E. in "Modification of Polymers", Carraher, C. E. Jr.,; Moore, J. A. Ed., Plenum Publishing, pp.141 (1983).

[100] Stellman, J. M; Woodward, A. E. J. Polym. Sci., Part B, 7, 755 (1969).

[101] Stellman, J. M; Woodward, A. E. J. Polym. Sci., Part A-2, 9, 59 (1971).

[102] Hendrix, C.; Whiting, D. A.; Woodward, A. E. Macromols., 4, 571 (1971).

[103] Wichacheewa, P.; Woodward, A. E. J. Polym. Sci., Polym. Phys. Ed., 16, 1849 (1978).

[104] Tseng, S.; Herman, W.; Woodward, A. E.; Newman, B. A. Macromols., 15, 338 (1982).

[105] Tseng, S.; Woodward, A. E. Macromols., 15, 343 (1982).

[106] Schilling, F. C.; Bovey, F. A.; Tseng, S.; Woodward, A. E. Macromols., 16, 808 (1983).

[107] Schilling, F. C.; Bovey, F. A.; Anandakumaran, K.; Woodward, A. E. Macromols., 18, 2688 (1985).

[108] Anandakumaran, K.; Kuo, C.; Mukherji, S.; Woodward, A. E. J. Polym. Sci., Polym. Phys. Ed., 20, 1669 (1982).

[109] Eirich, F. R. "Science and Technology of Rubber", Academic Press, New York (1978).

[110] Gavish, M; Corrigan J.; Woodward, A. E., submitted for publication.

[111] Gavish, M; Brennan P.; Woodward A. E. submitted for publication.

[112] Zemel, I. unpublished results.

[113] Kawai, T.; Keller, A. J. Polym. Sci. B, 2, 333 (1964).

[114] Peterlin, A.; Meinel, G. J. Appl. Phys., 35, 3221 (1964); J. Polym. Sci. B, 2, 751 (1964).

[115] Bank, M. I.; Krimm, S. J. Polym. Sci. B, 8, 143 (1970).

[116] MacGregor, E. A.; Greenwood, C. T. "Polymer in Nature", John Wiley & son, New York (1980).

[117] Bassett, D. C.; Hodge, A. M. Polymer, 19, 469 (1978).

[118] Bassett, D. C.; Hodge, A. M. Proc. R. Soc. London, *A* 359,121 (1978); *ibid.* *A* 377, 25, 39, 61 (1981).

[119] Keith, H. D.; Padden, F. J., Jr. Polymer, 25, 28 (1984).

[120] Woodward, A. E. Polymer, 5, 293 (1964).

[121] Khoury, F.; Barnes, J. D. J. Res. Natl. Bur. Stand., Sect. A 76, 225

(1972).

[122] Barnes, J. D.; Khoury, F. J. Res. Natl. Bur. Stand., Sect. A 78, 363 (1974).

[123] Tischer, F.; Woodward, A. E. Macromols. 19, 1328 (1986).

[124] Chang, B. H.; Siegmann, A.; Hilter, A. J. Polym. Sci., Polym. Phys. Ed., 22, 255 (1984).

[125] Corrigan, J. P.; Woodward, A. E. unpublished results.

[126] Anandakumaran, K. Ph. D. Dissertation, The City University of New York (1983).

[127] Wang, P.; Woodward, A. E. Macromols., in press.

[128] Wang, P.; Woodward, A. E. Macromols., in press.

[129] Wagner, H.; Flory, P. J. J. Am. Chem. Soc., 74, 195 (1952).

[130] Mark, J. E.; J. Am. Chem. Soc., 89, 6829 (1967).

[131] Mehta, A.; Wunderlich, B. J. Makromol. Chem., 175, 977 (1974).

[132] Gedde, U. W.; Jansson, J.-F. Polymer, 26, 1469 (1985).

[133] Guttman, C. M.; DiMarzio, E. A.; Hoffman, J. D. Polymer, 22, 1466 (1981).

[134] Fanconi, B.; Sarazin, D. Polym. Prepr. (Am. Chem. Soc., Div. Polym. Chem.) vol. 25(2), 173 (1984).